942

RADIOMETRIC MEASUREMENTS OF THE ATTENUATION OF MILLIMETRIC RADIO WAVES BY RAIN

by

RAJAN CHADHA

A Thesis submitted for the Degree of Master of Philosophy in the University of London

Department of Electrical Engineering
Imperial College, London

CONTENTS

		Page
	Abstract	1
1.	INTRODUCTION	2
	1.1 General Nature of Problem	2
	1.2 Interest in Radiometer Measurements and Associated Problems	4
	1.3 Principle of Radiometer	7
	1.3.1 Basic Radiometric Systems	10
	1.4 Importance of Data Related to Space Communication	12
	1.5 Previous Measurements	14
2.	SCATTERING BY DISTORTED RAINDROPS	16
	2.1 Introduction	16
	2.2 Model for Calculation	19
	2.2.1 Sources of emission	19
	2.2.2 Properties of rain	19
	2.2.3 Rain temperature	24
	2.2.4 Properties of clear weather	24
	2.2.5 Solar radiation	25
	2.3 Radio Emission by Rain	26
	2.3.1 Emission by rain within the beam of aerial (no scattering)	26
	2.3.2 Emission by rain and first order scattering	31
	2.3.3 Contribution from higher order scattering	32
	2.4 Emission from the Ground; Scattering of First and Higher Orders	33
	2.5 Results	36
	2.5.1 Polarisation of emitted energy by rain (no scattering)	36
	2.5.2 Polarisation of emitted and scattered radiation by rain	40
	2.5.3 Relationship between polarised True and Apparent attenuation	41
	2.5.4 Ground emission and polarisation properties	45
	2.5.5 Rain temperature	51
	2.5.6 Effect of depth and horizontal extent of rain on scattering and polarisation of emitted energy	52
	2.5.7 Orders of scattering	55
	2.5.8 Aerial efficiency	57

		Page
3.	EXPERIMENTAL PROCEDURE FOR STUDYING SCATTERING EFFECTS BY RAIN	57
	3.1 Equipment	57
	3.1.1 Equatorial mount	57
	3.1.2 Control unit	60
	3.1.3 Aerial	61
	3.1.4 RF head structure	62
	3.1.5 The receiving system	63
	3.2 Data Recording	67
	3.3 Calibration of the System	67
	3.4 Experimentation and Analysis	69
4.	EXPERIMENTAL TECHNIQUE FOR STUDYING POLARISATION PROPERTIES	78
	4.1 Experimentation for Studying Polarisation Properties of Emitted Energy by Rain	79
	4.1.1 Mounting	79
	4.1.2 Aerial and aerial feeds	79
	4.1.3 The receiving system and calibration	80
	4.2 Experimentation and Analysis	83
5.	EXPERIMENTAL TECHNIQUE FOR STUDYING THE EFFECT OF POLARISED SCATTERED RADIATION ON PASSIVE RADIOMETER MEASUREMENTS	86
	5.1 Equipment	86
	5.1.1 Mounting and aerial	86
	5.1.2 Receiving system	87
	5.2 Recording and Calibration	89
	5.3 Experimentation and Analysis	89
6.	RAINFALL MEASUREMENTS	91
7.	LONG TERM PERFORMANCE	93
8.	A COMPLETE SURVEY OF POSSIBLE ERRORS IN THE MEASUREMENT	94
	(a) Calibration Accuracy	94
	(b) Error due to changes in Radiation Pattern	97
	(c) Contribution from Background Radiations	99
	(d) Error in Calculating Attenuation from Absorption	99
	(e) Error in the Measurement of Extinction	100

		Page
9.	EXPERIMENTAL RESULTS ON SCATTERING EFFECTS BY RAIN	102
	9.1 Experimental Results on Scattering by Rain	102
	9.1.1 Clear weather attenuation	102
	9.1.2 Attenuation on a cloudy day and effect of solar burst	103
	9.1.3 Drizzle	108
	9.1.4 Medium rain	108
	9.1.5 Heavy rain	110
	9.1.6 Sleet	121
10.	STATISTICAL ANALYSIS	121
	10.1 Cumulative distribution of Attenuation and Scattering at all possible Angles of Elevation	123
	10.2 Cumulative distribution of Various Elevation Angle	127
	10.3 Seasonal Variability	130
11.	EXPERIMENTAL RESULTS ON POLARISATION EFFECTS BY RAIN	133
12.	FURTHER WORK	137
13.	CONCLUSIONS	141
	ACKNOWLEDGEMENTS	143
	BIBLIOGRAPHY	144
APPENDIX A1	Operating characteristics of 37.0 GHz Nodding Radiometer (horizontally polarised)	
APPENDIX A2	(1) Measurement of Radiation Pattern (2) Gain Stability of System (3) Noise Temperature of Systems (4) Sensitivity (5) Effect of Water Layer Overfeeds	
APPENDIX A3	Electronic ON/OFF Attenuator Driver	
APPENDIX A4	Design Requirements of Mounting and Drive	
APPENDIX A5	Derivation of Elevation from Local Time	

ABSTRACT

After a brief discussion of the importance of attenuation by rain on planning of Earth-satellite links at frequencies above 10 GHz it is argued that the much needed information on this is obtainable economically using radiometric techniques.

It is shown in this report that there is a need to consider scattering and polarisation in estimating true attenuation on an earth-space path, using a passive radiometer above 30 GHz. That the attenuation deduced from sky noise is grossly under estimated if the said cases are neglected and is proved theoretically by considering distorted drops and varying temperature of rain with height, based on Zavody's theory.

Theoretical results are compared with experimental results for different rainfall rates obtained using a "Nodding" 37.0 GHz radiometer, and its details discussed. The results obtained during periods of wet snow are also compared and discussed. The accuracy of the measurements, including calibration of the radiometer, and the effect of changes in the radiation pattern during sun-tracking, is discussed. The effect of a water layer over the feed is included. Cumulative distribution curves for rainfall rate, true attenuation and error due to scattering over all elevation ranges and in 10 degree elevation ranges are presented. It is shown that seasonal variability effects can be avoided by simultaneously using true attenuation and scattering error.

The polarisation behaviour of the emitted and scattered energy both by rain and ground is shown theoretically and verified experimentally by operating a cross-polarised radiometer in the thermal emission mode. The construction of the cross-polarised radiometer is discussed in detail and the development of a programmable electronic ON/OFF attenuator achieved.

Polarisation behaviour of scattering is discussed and shown to exist experimentally by operating the cross-polarised radiometer in the "Nodding mode" during stormy periods. The error due to polarisation behaviour of scattering could not be predicted on a long term basis because of the limited number of recordings.

1. INTRODUCTION

1.1 General Nature of Problem

To support the increasing data handling requirements of an expanding technology and of greater number of communication channels around the world, the higher frequency spectrum needs exploiting[1][2]. The rather large band-width required for data handling forces one to consider frequencies above 10 GHz: Virtually all terrestrial systems presently in service operate in bands below 10 GHz[9]. The frequency band below 10 GHz is further under stress due to expanding satellite communication systems.

The band from 10 to 300 GHz known as "millimetre waves" offers the potential for relieving the over crowded situation below 10 GHz[9]. In addition to relieving spectrum crowding, millimetre-wave systems offer extremely wide band-width capabilities. The size and weight of the microwave components is greatly reduced. High gain, narrow-beam antenna of modest size are more practicable at higher frequencies. These factors definitely result in low cost communication per channel, eventually passed on to the consumer.

The propagation characteristics in the millimetre band are significantly different from those at lower frequencies. Millimetre waves are greatly influenced by the Troposphere in space communication application. In addition to the normal free-space loss associated with wave propagation, millimetre waves experience resonance absorption by water vapour, oxygen and other gases such as ozone, hydrogen sulphide and carbon monoxide, etc. However, because of the low molecular densities of the latter gases, only the water vapour and oxygen contribute significant effects in the 10-300 GHz band. The study of the plot of total attenuation dB/km versus frequency suggests that the first three windows in the electro-magnetic spectrum above 10 GHz where water vapour and oxygen absorption are low occurs at frequencies 19 GHz, 37 GHz

and at 95 GHz. It is in these bands that the greatest potential for communication via satellites exists.

The most significant atmospheric condition that has an adverse effect on reliable millimetre wave earth-space communication is attenuation by heavy precipitation, hail, wet snow, etc.[9]. The effects such as refractive-index variations or multipath fluctuations are not usually significant for an Earth-satellite link compared to the attenuation caused by rain at frequencies above 10 GHz.

To give an idea of the severe effect of attenuation caused by rain[25], we consider a uniform rainfall stretched along a path length of 1 km. The rain attenuation in the 37.0 GHz carrier band is 3.5 decibels and out of which 1.4 decibels is due to scattering at a uniform rainfall rate of 12.5 mmh^{-1}. If the communication system is designed to work through a uniform rainfall rate of 12.5 mmh^{-1} (fixed path length of 1 km), an increase of rainfall to 25 mmh^{-1} would require an approximately two-fold increase in transmitting power. This is an idealistic situation but for a practical Earth-space link many-fold increase in transmitting power will be required to compensate for changes in path length or rain rate, thereby posing a serious problem.

The capacity of microwave[9][1] communication systems can be further increased at the carrier frequency by transmitting orthogonally polarised waves. Unfortunately, for millimetric wave propagation during periods of intense rain, there is a transfer of some of the energy into the cross-polarised channels[24, 25, 38, 39, 49]. The amount of energy transferred depends on the rainfall rate, canting angle distribution of rain drops, path length and carrier frequency. An extensive theoretical and experimental study has been carried out by Semplak, Oguchi, Chu, Morrison, Watson and Arabai[38, 39, 40, 41, 44]. It is shown by Chu[56] that the depolarisation on an Earth-space path is less than that

on a terrestrial path for the same attenuation level, provided the incident linear polarisation from the satellite is parallel or perpendicular to the plane containing the direction of propagation and the local gravity direction. For a given rain rate and frequency the difference in attenuation between horizontal and vertical polarisations will be small, therefore in comparison with the annual statistical variation of attenuation for the same rain rate and frequency · it will be unimportant. However, study of difference in attenuation between horizontal and vertical polarisations is of crucial importance in planning frequency re-use by employing orthogonal polarisations or in polarisation-diversity communication systems. This suggests that we must focus attention on the knowledge of the magnitude of large attenuation and degrading of polarisation by rain if proper use is to be made of long distance communication via Earth-orbiting satellite. The challenge is to design around the problem in such a way as to produce a low cost communication system.

1.2 Interest in Radiometer measurements and Associated Problems

The much needed information on rain attenuation on an Earth space path could either be obtained by putting a communication satellite into orbit and studying the millimetric wave propagation during rainy periods on long term basis or by using a radiometric technique. The first proposal is definitely expensive and therefore the aim of producing a low cost communication system is defeated.

The radiometric technique is an attractive choice because of its low cost and its capability to obtain long-term statistics of atmospheric attenuation along Earth-space paths at any given elevation angle and for variety of locations. Since only a few milliwatts of oscillator power is required for the radiometer, harmonic mixing could also be used for high frequency radiometers. Radiometers can either be used in a sun-tracking mode or by monitoring the antenna noise temperature due to thermal emission of rain. The advantages

and disadvantages of the solar-tracking radiometer can be outlined as follows :-

(i) An intense radio source (e.g. Sun) is required.

(ii) High Dynamic range ($\sim$ 25 decibels) and the accuracy of measured excess of attenuation is within 3.0 percent.

(iii) An accurate knowledge of background radiations and losses in wave guide system (e.g. feeds) is not required.

(iv) A high precision tracking-system capable of following the Sun both in hour angle and declination is required. The tracking-system must be able to take into account declination changes of the Sun during the day.

(v) The measurements can be obtained only during the day and in the direction of the Sun i.e. measurements could be made only on elevations defined by the Sun.

(vi) The measurements do not refer to one fixed polarisation. The polarisation of the system keeps on changing with elevation of the Sun.

(vii) Study of seasonal effects on a fixed elevation angle defined by a planned satellite is impossible.

The advantages and disadvantages of thermal-emission technique are :-

(i) No radio-source is required.

(ii) No tracking system is required.

(iii) The measurements can be made at any elevation angle and at any location either day or night rapidly.

(iv) An accurate knowledge of the background radiation and losses in the wave guide system and their variation with temperature is required.

(v) An accurate knowledge of rain temperature and scattering is required.

(vi) It is possible to study seasonal effects on a fixed polarisation and elevation angle defined by a planned satellite.

(vii) Smaller dynamic range (~ 12 decibels) and there are questions on the accuracy such as error arising due to multiple scattering of energy from rain and ground.

In calculating attenuation from thermal emission measurements, it is in general assumed

(a) The medium is an absorber with a constant mean temperature profile.

(b) Losses due to scattering are negligible.

(c) Energy emitted and rescattered is not polarisation sensitive i.e. randomly polarised.

The radiative transfer equation[4] for unpolarised radiations reduces to a scalar equation. If the Rayleigh-Jeans approximation of Planck's law is used and the atmosphere is assumed to be in thermodynamic equilibrium, then apparent sky temperature measured with a radiometer can be used to calculate the corresponding attenuation in decibels from the expression (equation derived in next section)

$$A(db) = 10 \text{ Log}_{10} \frac{T_m}{T_m - T_{ae}} \qquad (1)$$

A = Atmospheric attenuation

T_m = Atmospheric mean absorption temperature

T_{ae} = Apparent sky temperature during rain.

Equation (1) does not give the correct attenuation if water in condensed form is present in the radio path, as part of the attenuation will be due to scattering[20][10]. It is thought to be one of the main causes of discrepancies between actual attenuation and attenuation measured by thermal emission. This suggests equation (1) must be modified to take into account scattering losses.

Zavody[5] theoretically estimated (assuming spherical drops and the laws and Parson's drop size distribution) that attenuation from thermal emission measurements will be underestimated by 3 dB in 10 dB_h at 37.04Hz if scattering losses are neglected. It is also suggested that the radiation scattered from the ground also becomes important at higher rainfall rates and cannot be neglected. We also ask ourselves a question if the emitted and scattered radiations are polarisation sensitive? A theoretical and experimental study of scattering and polarisation is discussed later in this report. The answer to the above question is important for the better performance of ground receiver station from extra attenuation margin point of view. The question also arises if the attenuations obtained from passive vertical and horizontal polarised radiometers are compatible with that of actual vertical and horizontal attenuations.

1.3 Principle of Radiometer

The principle of radiometry has been expressed in a variety of forms by Dieter, Castelli and Ushatzoff, (1965)[57] and Dicke, (1946)[15]. It can be stated in simple words as "the noise power collected by an aerial immersed in an absorbing homogeneous medium of infinite extent at temperature T equals the noise power available across a resistor maintained at the same temperature".

The thermal noise received by an aerial can be derived from Planck's radiation law (Dicke, 1946). Planck's law in terms of power P (power density w/m^2) of unpolarised radiation, radiated into solid angle $d\Omega$ steradians over a bandwidth $\Delta\nu$ can be written as

$$P = \frac{2h\,\nu^3}{c^2\left[\exp\left(\frac{\nu h}{kT}\right) - 1\right]} \quad \Delta\nu\ \Delta\Omega \ \text{watts/m}^2 \qquad (2)$$

where,

ν = frequency, cps

h = Planck's constant (6.63×10^{-34} joule sec)

k = Boltzmann's constant (1.38×10^{-23} Joule^{o} k^{-1})

c = velocity of light (3×10^{8} m/sec)

T = kinetic temperature ^{o}K

In general at millimetre wavelengths $h\nu \ll kT$, therefore $\mathrm{Exp}[h\nu/kT] - 1 \approx h\nu/kT$, which leads to the Rayleigh-Jeans approximation to Planck's radiation law, which from equation (2) is

$$P\nu,\ \nu + \Delta\nu = \frac{2kT}{\lambda^2}\,\Delta\nu\ \Delta\Omega \tag{3}$$

If we consider an aerial immersed in an absorbing medium of infinite extent. Then the energy collected by the aerial and absorbed in a matched load Z attached to the output is

$$P(\nu) = \tfrac{1}{2}\int_{4\pi} \frac{2kT(\theta,\varphi)}{\lambda^2}\ \Delta\nu\ A(\theta,\varphi)\ d\Omega \text{ watts} \tag{4}$$

where

$A(\theta,\varphi)$ = Polar diagram of the aerial (i.e. "Effective Receiving area")

$T(\theta,\varphi)$ = Radiation temperature in direction θ from the vertical and φ from an arbitrary horizontal axis

The factor $\frac{1}{2}$ appears because the above equation relates to unpolarised radiation, whereas any given aerial system can only respond to one sense of polarisation at any one instant.

If we assume $T(\theta,\varphi)$ is constant over the solid angle subtended by the beam.

$$P = \tfrac{1}{2} \cdot \frac{2kT}{\lambda^2}\,\Delta\nu \int_{4\pi} A(\theta,\varphi)\ d\Omega$$

From the theory of aerials $\int_{4\pi} A(\theta,\varphi)\ d\Omega = \lambda^2$, because of the definition of antenna gain $G(\theta,\varphi)$ and its relation to effective receiving area

$$A(\theta,\varphi) = \frac{\lambda^2}{4\pi}\ G(\theta,\varphi)$$

$$P = kT\ \Delta\nu \tag{5}$$

or $$\overline{e^2} = 4kTR\ \Delta\nu$$

This is the mean - square voltage developed across a resistor R maintained at temperature T. For a non-black body, i.e. a partially absorbing body equation (5) takes the form

$$P = k(aT)\,\Delta\nu$$

where

a = Fractional absorption of the medium

aT = Noise temperature of the absorbing medium.

The equations (2) to (5) govern the principle of radiometry.

In order to evaluate attenuation from thermal emission measurements, the equation (1) is derived by considering a black body source at temperature T_s viewed by a radiometer through a slice of medium at temperature T_m, and through which the atmospheric fractional loss is 'a'. The radiometric measured antenna temperature T_{ae} when the aerial is pointed toward the zenith, is a function of the absolute temperature of the atmosphere assumed to be at ground air temperature T_m as well as of the atmospheric fractional loss 'a' and the sky temperature itself (T_s).

Therefore, under conditions of thermodynamic equilibrium

$$T_s - a\,T_s + a\,T_m = T_{ae} \tag{6}$$

Now
$$a = \frac{P_i - P_o}{P_i} \tag{7}$$

P_i = Power into the medium

P_o = Power out of the medium

Since the atmosphere is assumed to be homogeneous, the T_m radiation to an antenna immersed in the medium will be constant. For free space $T_s = 0^{o}k$, therefore from equation (6) $a = \frac{T_{ae}}{T_m}$

From equation (7)

$\frac{P_i}{P_o} = \frac{1}{1 - a}$, substituting for 'a' from equation (6) and converting to decibels, one obtains

$$\text{Total loss A in decibels} = 10 \text{ Log}_{10} \frac{T_m}{T_m - T_{ae}} \qquad (8)$$

Equation (8), in general, is used for predicting attenuation from the observed aerial temperature T_{ae} and assumed atmospheric temperature T_m. For a measured loss and observed aerial temperature, equation (8) can be inverted to obtain T_m and will be termed as "apparent medium temperature".

1.3.1 Basic Radiometric Systems

Total Power Radiometer

An ordinary superheterodyne receiver may be used as a radiometer. If a square-law detector is used the output of such a receiver is proportional to the sum of the power received from the source and the noise power generated in the receiver. Ideally the receiver noise power is constant, and changes in output voltage represent changes in input power, the minimum detectable change depending upon the number of samples taken, i.e. upon the pre-detection and post-detection band-widths. An approximate expression for the minimum detectable change in input power, expressed as a change ΔT in effective input temperature is[13]

$$\Delta T = \frac{T_n}{(B\tau)^{\frac{1}{2}}} \qquad (9)$$

where

Tn = Effective system noise temperature

B = Pre-detection bandwidth

τ = Post-detection time constant

Unfortunately, changes in the gain and noise temperature of the receiver cause changes in output very much greater than ΔT, rendering this type of receiver useless for radio-astronomy and for probing the constituents of the atmosphere.

The Dicke Radiometer

Let NO be the receiver output power then from equation (9), the fluctuations should have a value $\Delta NO = NO(B\tau)^{-\frac{1}{2}}$.

If at a time t, the gain of changes by Δg, then

$$\frac{\Delta g}{g} \cdot < (B\tau)^{-\frac{1}{2}}$$

If B = IMC/s and τ = 1 sec., the value of $\Delta g/g$ must not exceed 10^{-3} i.e. the gain of the receiver must be stable to 1 part in 1000. Such a stability necessarily requires a stabilized power supply to better than 1 part in 10,000 and to hold the temperature constant to about $1^{o}C$.

A successful method suggested by Dicke (1946) reduces the effect of changes in the receiver gain. The essential property of the system is that the output is proportional to the difference in power from two sources, rather than being proportional to the sum of the source and receiver noise powers. This is accomplished by alternately connecting the receiver to the aerial and to a comparison load at a known temperature using a rotating switch. The important characteristic of this system is that, provided the aerial and the load both present the same impedance, the receiver noise is the same in both positions of the switch and hence changes in the gain do not appear in the record. At millimetre wavelengths, where the receiver noise is predominant, the effects of changes in the receiver gain are considerably reduced.

It is simple to show that in the case where the receiver noise $(N - 1)\ T_c$ is large compared with that of the aerial T_A or the load T_S,

the permissible fluctuations in gain are increased by the factor $(N - 1)\ T_o/(T_A - T_S)$ by comparison with total power receiver, where

N = Noise factor

T_o = Ambient temperature ^oK

As a practical example which corresponds to a millimetre wavelength operation, we take noise factor $N = 10$ ($T_o = 290.0$ K), $T_A = 100$ K, $T_S = 290$ K $= T_o$. In this case the required stability of the receiver gain is reduced by a factor of 14.0 over that required for a total power receiver. Thus instead of a gain stability of the order of 1 part in 1000, it would only be necessary to achieve a stability of about 1 part in 80. For the Dicke system, the minimum detectable change depends upon the number of noise samples taken i.e. upon the predetection bandwidth and integration time (τ). If B is the pre-detection bandwidth then B number of independent noise-pulse contribute per second in producing the detector output and after post-detection integration $B.\tau$ independent contributions are left. Therefore, the root mean-square deviation is $\frac{1}{(B\tau)^{\frac{1}{2}}}$

or

$$\frac{\Delta T}{T_n} = \frac{2}{(B\tau)^{\frac{1}{2}}} \qquad (10)$$

The factor of '2' appears because the Dicke receiver is connected to the aerial only half the times and therefore twice less sensitive compared to total power radiometer.

1.4 Importance of Data Related to Space Communication

The performance of a communication system is a function of signal to noise ratio, and the sky noise normally contributes a significant portion of the total noise at the output of the Earth-station receiver. The intensity of sky noise is normally represented in terms of an equivalent temperature of a black

body which would emit the same intensity of radiation over the same frequency range (Dicke, 1946)[15].

An Earth-station receiving system is normally specified by the ratio of aerial gain to system noise temperature under 'clear sky' conditions. At frequencies below 10 GHz an incomplete picture of the propagation path (i.e. pressure, temperature and humidity) does not matter but at higher frequencies these effects will be felt. Fluctuations in atmospheric pressure, temperature, water vapour content and the appearance of precipitation as cloud and rainfall may all contribute to system noise. This means the performance of the system will vary depending on climate and therefore some kind of extra margin in the receiving system is required for reliable communication. In other words the sky-noise increase associated with attenuation must also be considered in relation to the degradation of noise temperature of a satellite Earth-station. As an example we consider a 37 GHz receiver with a system noise temperature of 110 K on a clear day. An attenuation of 14.0 decibels will increase the antenna temperature by about 260 K (assuming effective temperature of the medium 290.0^{o}K). The system noise therefore will increase to about 110 K + 260 K = 370 K. In order to maintain "clear day" (assuming fluctuations on a clear day are negligibly small) system performance, an extra margin of 10 Log $\frac{370}{110}$ = 5.2 decibels must be included beyond that for attenuation alone of 14.0 decibels. The margin will be different for vertical or horizontal polarised receiving station if the energy emitted and scattered by rain is polarisation sensitive. Therefore the data obtained from radiometric measurement and using modified technique of calculation at 37.0 GHz will help in specifying the performance of Earth-station but as stated earlier data are also needed in accurate estimation of the rain attenuation required by design engineers.

The performance of the Earth-station can be further improved by studying the polarisation properties of the emitted and scattered radiations by rain and is undertaken in a later section. It is shown that a vertically polarised system experiences less noise along the propagation path during rainy periods compared to a horizontally polarised system. The cross-polarised radiometric measurements can also be linked to the actual Earth-satellite data and the error can be studied on a long term basis for predicting actual vertical and horizontal attenuations. The analysed data linked to meteorological conditions will give an idea about drop-size distortion and average path length. The cumulative plot of scattering and true attenuation, if used simultaneously will be independent of seasonal effects and is of particular interest to planning engineers.

1.5 Previous Measurements

Microwave radiometry came into being with the development by Dicke[15] in 1946 of the source switching type of instrument now universally known as the Dicke radiometer. This type of radiometer has remained in widespread use, being by far the most widely used for solar radio observations, and is currently being used at millimetre wavelengths for studying the transparency of the atmosphere. With the advent of microwave components at higher and higher frequencies, the radiometer is an attractive choice for studying the water vapour absorption and oxygen absorption. The clear day atmospheric attenuation measurements at wave length 3.5-2.5 mm using a radiometric technique is reported by Gibbin[46]. The measurements at lower wavelength i.e. 2 mm is also in progress by the same author.

The use of the radiometric technique in studying the effect of rain on millimetre wavelengths on an Earth-space path was initiated in the U.K. during the year 1966 under S.R.C.'s research program[3, 4, 7, 17]. A good example of the results obtainable on rain-attenuation using basic sun tracking

radiometer is the three year sample of 19 GHz and 37 GHz attenuation measurements reported by Davies[3, 7, 14]. The data were taken from 1968 to 1971 for periods when the Sun was 5^{o} above the horizon and represent about 10500 hours of recordings. The technique used for the measurement was essentially suggested by Conway[45]. It involves fast electronic switching between the feed on the Sun and the feed off the Sun. The advantage being most of the background radiations cancels out and the knowledge of losses within feeds is not required.

Wilson[10] has reported measurements of attenuation by rain at 16 and 30 GHz using a solar radiometer. The primary aim was to relate attenuation at 16 GHz to that at 30 GHz or in other words for a given 16 GHz attenuation, what is the corresponding conditional probability at 30 GHz for the same attenuation. Simultaneous measurements using Sun and sky during rainy periods were also made at 16 GHz, and the excess of attenuation measured by Sun-tracker are plotted against attenuation calculated from sky brightness (thermal emission measurements). The plotted results show a large scatter beyond 10 dB and some of the scatter are undoubtedly caused by real differences in attenuations, and was attributed to[10] scattering playing a role. This error also shows up in the data published by Altshuter and Wulfsberg[47] for 35 GHz. Although they found a high correlation coefficient (0.97 at 35 GHz) between attenuation measured with the Sun as a source and that inferred from thermal emission, but there is a considerable scatter of points for measured attenuation above 10 decibels. The good agreement of results at low measured attenuations reported by Altshuler et al.[47] is in contrast with the scatter found by Wilson. Anomalies between measured attenuation and that obtained from thermal emission was also reported by Croom et al.[48]. Until recently a theoretical study by Zavody[5, 18] suggested that possibly the anomalies are

due to non-consideration of scattering in inferred attenuation from thermal emission measurements. Therefore a detailed experimental study is undertaken by us to assess the magnitude of error due to scattering and if it is compatible with Zavody's theory.

Recently direct attenuation measurement from satellite is also compared with radiometer measurements. One of such results reported by Strickland[49] is to calibrate a 16 GHz radiometer using a 15.3 GHz ATS-5 satellite signal.

It was said earlier in the section that the polarisation properties of the emitted and scattered radiation by rain is important for polarisation diversity communication systems or for an Earth-station using orthogonal polarisation to increase communication channels. Experiments have been conducted to study the effect of rain on linear polarisation using transmitting and receiving systems both on horizontal land-based and on an Earth-space path[49]. However no attempt is made to measure the extent of polarisation behaviour of energy scattered by rain and ground.

A cross-polarised radiometer was built to measure the above effect. The experimental details are discussed later in the report.

2. SCATTERING BY DISTORTED RAINDROPS

2.1 Introduction

The apparent absorber temperature is near or below freezing for millimetric observations in North America[52] and in the U.K.[48] whereas the rain is in fact usually fairly warm (approximately 285°K in North America)near the surface of the Earth. This discrepancy is explainable in terms of scattering by raindrops[5].

It is known[53] that supercooled droplets in clouds can exist at temperature down to 233°K (- 40°C)but it would be extremely unlikely that they will be present in such a huge quantity so as to actually lower the temperature

of the rainy medium to below freezing point. Several authors (e.g. Crane[20], Wilson[10]) pointed out that if water in condensed form is present in the radio path then part of the attenuation is due to scattered energy that never reaches the aerial. This is thought to be one of the causes of discrepancies between observed attenuation and that calculated from simultaneous aerial-temperature measurements.

A theoretical study by Zavody[18] reveals that scattering by raindrops is a function of the operating frequency, drop size, the geometry of the storm, temperature profile of the rain, elevation angle of the aerial, and the kinetic temperature and microwave properties of the ground surrounding the aerial. The error in estimating attenuation owing to neglect of scattering effects increases with increasing frequency. This is expected, as the ratio of scattering to absorption increases with frequency. The error also increases with decreasing elevation angle. The analysis also suggests that the scattered contribution from the ground to the total aerial temperature plays an important role at higher rainfall rates i.e. high values of attenuation. This is due to observed aerial temperature approaching the atmospheric temperature. Even slight change of a few degrees Kelvin in the observed aerial temperature due to the scattered contribution from the ground will make a significant difference in obtaining the true attenuation. The importance of the ground contribution can be judged by considering a receiver whose aerial temperature is 272.9^{o}K from all sources of radiations including ground. This aerial temperature assuming temperature of rain and ground to be 273.0 K correspond to 34.4 dB's. If we neglect ground contribution, the aerial temperature at 247.9^{o}K corresponds to 10.4 dB's only i.e. under estimation of true attenuation by 24.0 dB's.

The basis of theoretical[18] calculation has been to solve radiative transfer equation (4) to obtain the total flux density at the receiver for each source and summing the separate contributions from radiations not scattered,

radiations scattered once, twice and so on. The resultant aerial temperature was obtained after summation of a sufficient number of contributions to obtain convergence. The calculations have been applied to highly idealized storm conditions. Zavody[5] in his analysis assumed that the rain extended uniformly from ground to a height of 3 kms or more with a drop-size distribution given by Laws and Parson[50]. The drop-size distribution does not vary appreciably with height and is assumed to have a second order effect. The assumption seems valid since the resultant changes in the aerial temperature and attenuation are in the same direction for a given rainfall rate. The raindrops were assumed to be spherical falling with their terminal velocity with respect to the ground and the temperature of the rain is uniform and constant with height.

It is important to make a correct estimate of the effective atmospheric temperature. Incorrect choice of the value of the effective temperature of the rainy medium is the most serious when the aerial temperature measured is high, i.e. when attenuation is large. For a difference between atmospheric and aerial to be 20 K, a variation in 5K around 273.0 K (atmospheric temperature) leads to a change of + .89 dB or - 1.15 dB in 11.4 dB's.

The photographic measurements of the physical shape of rain drops have been made by many investigators (30-36). These measurements indicate that drops larger than about 1 mm radius, take on the average asymmetric oblate spheroidal form with a flattened base. Some photographs are taken while the drops are suspended in the air stream of a vertical wind tunnel[30, 33, 36] or some are taken when the drops have attained their terminal velocity after falling from a height in stagnant air[31]. Some of the photographs show vibrational oscillations of water drops which cause the water drops to oscillate between oblate and prolate shape[30-35]. These oscillations may be partly due to the initial oscillation when the drops are released from a drop forming device or partly due to the turbulence from the air flow in the wind tunnel. The above

physical measurement shows that it is unreasonable to assume raindrops to be spherical.

We present a modified theoretical model which takes into account the important sources of energy that are received by an upward looking aerial during periods of rain. The calculation presented reduces to Zavody's[5] theoretical calculations if we assume spherical raindrops and the temperature of rain to be uniform and constant with height.

2.2 Model for Calculations

2.2.1 Sources of Emission

We consider a microwave radiometer observing a source of brightness 'B_s'. During periods of rain over the aerial, the energy can reach the aerial directly from the source within its beam, scattered and multiple scattered energy by rain drops, and the energy emitted and scattered by the ground. The aerial is assumed to be lossless with a very narrow beam and no side lobes.

At 37.0 GHz, attenuation and emission from cloud is much smaller compared with rain. A typical measured figure is 0.42 dB. Attenuations as high as 6.0 dBs were also measured. The cloud was visually identified as cumulus cloud. These high attenuations due to clouds were rare and therefore neglected in the theoretical treatment.

2.2.2 Properties of Rain

The rain is assumed to be homogeneous and to extend from ground level to height h. The drops are assumed to be non-spherical but axi-symmetric oblate spheroids. It is also assumed that Laws and Parson's drop-size distribution holds at all heights, and the drops fall with their terminal velocity with respect to ground given by Medhurst[19].

The theoretical calculation of the properties of oblate spheroidal

drops are extensively dealt with by Oguchi[38], Morrison[40], Cross and Chu[39]. Oguchi[38] has obtained extinction, scattering and absorption coefficient of different sizes of distorted rain drops. In the derivation, it is assumed that linear relationship between axial ratio of minor to major axis and the mean drop radius (Figure 1), and drops to be axi-symmetric. The coefficients tabulated by Oguchi for various drop sizes were used to obtain coefficients for various rainfall rates and are given in Table 1 and Table 2 for vertical and horizontal polarisation respectively at 37.0 GHz. The complex refractive index of water was used as recommended by Saxton and Lane[58]. We will use these coefficients to study the polarisation behaviour of emitted and scattered radiation by rain.

Since the scattering is not isotropic, average normalized scattering coefficients of rain $S'_V(\theta,\Gamma)$ and $S'_H(\theta,\Gamma)$ for vertically and horizontally polarised radiation is introduced using part of the co-ordinate system shown in Figure 2. Angles θ and Γ refer to the incidence and scattering angles respectively. The average power $\overline{P_{V,H}(\theta,\Gamma)}$ scattered by rain of unit volume into unit solid angle in direction Γ towards the vertical or horizontal polarised receiver for the incident power flux density unity D is given by

$$\overline{P'_V(\theta,\Gamma)} = \frac{K_{SV}\, S'_V(\theta,\Gamma)}{4\pi} \qquad \text{vertically polarised receiver} \qquad (11)$$

$$\overline{P_H(\theta,\Gamma)} = \frac{K_{SH}\, S'_H(\theta,\Gamma)}{4\pi} \qquad \text{horizontally polarised receiver} \qquad (12)$$

The normalized scattering coefficients $S'_{V,H}(\theta,\Gamma)$ takes into account the radiation pattern of raindrops.

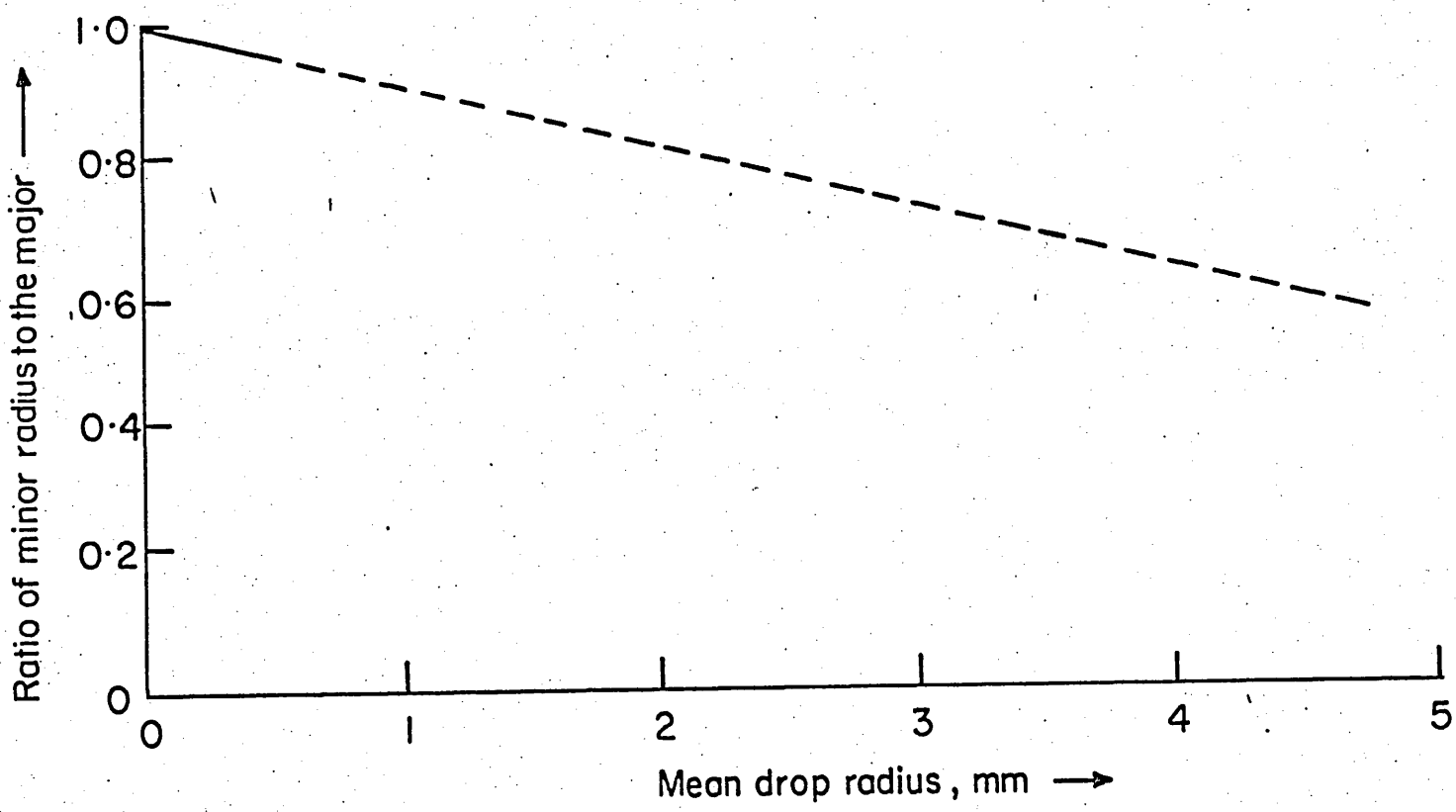


FIGURE 1

REF NO 3219/17 NEG NO

Absorption K_a, Scattering K_s and Extinction K_e

Coefficients of Rain using Distorted Rain Drops and

Laws & Parsons Drop Size Distribution in N_P km^{-1}

VERTICAL

Rainfall Rate mm h^{-1}	0.25	1.25	2.5	12.5	25.0	50.0	100.0	150.0
K_a	0.009	0.0441	0.086	0.354	0.662	1.220	2.133	2.949
K_s	0.0019	0.0178	0.043	0.302	0.613	1.199	2.332	3.377
K_e	0.0109	0.0619	0.129	0.656	1.274	2.419	4.465	6.326

TABLE 1

HORIZONTAL

Rainfall Rate mm h^{-1}	0.25	1.25	2.5	12.5	25.0	50.0	100.0	150.0
K_a	0.0094	0.0468	0.096	0.435	0.815	1.502	2.575	3.373
K_s	0.0024	0.0230	0.051	0.339	0.706	1.404	2.820	4.301
K_e	0.0118	0.0698	0.147	0.774	1.521	2.906	5.395	7.674

TABLE 2

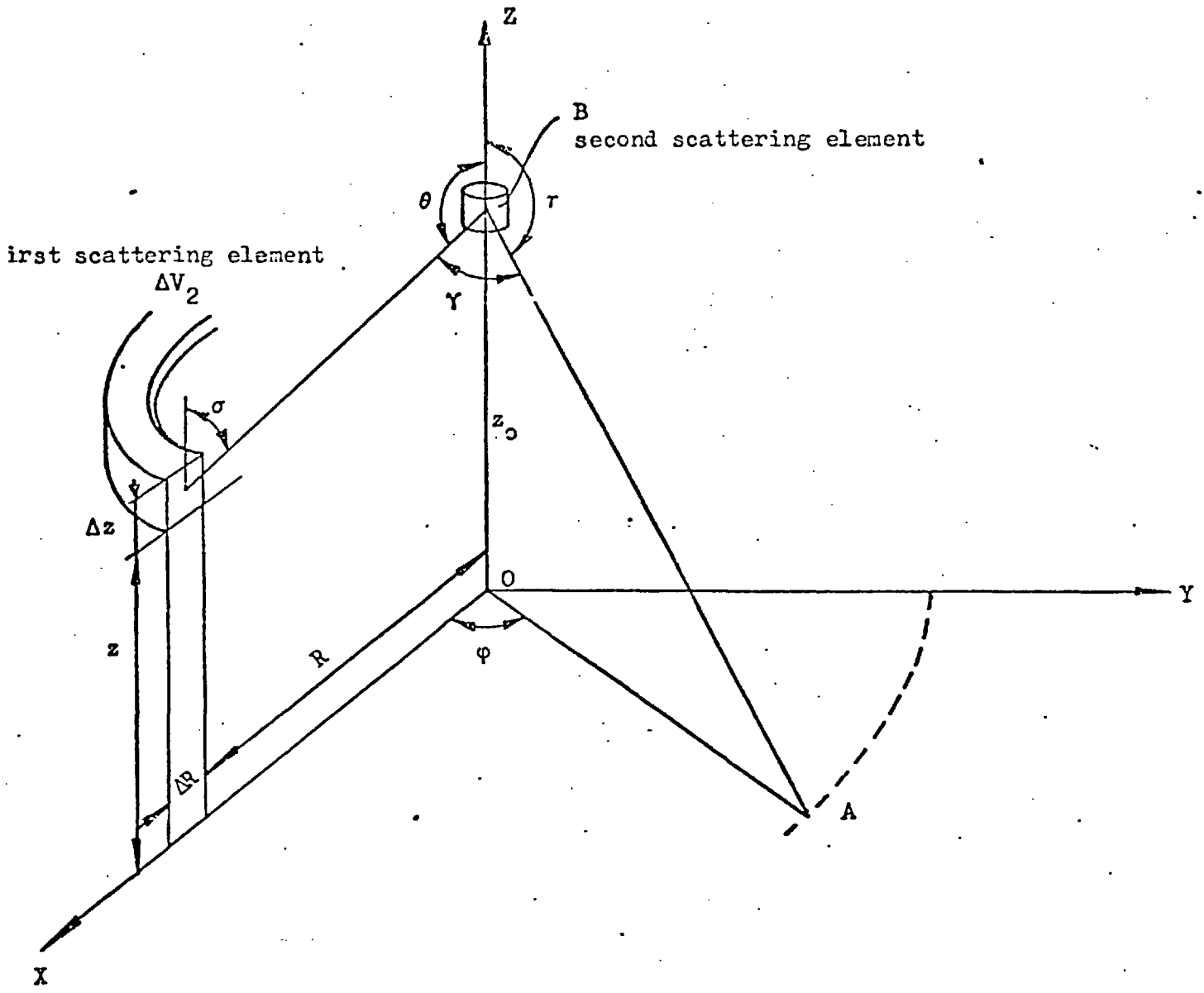

Z
B
second scattering element
θ
τ
irst scattering element
ΔV2
γ
σ
z0
Δz
0
Y
z
R
φ
ΔR
A
X

FIGURE 2

Therefore,

$K_{SV}\ S'_V(\pi, 0)$ = vertical forward scattering coefficient

$K_{SH}\ S'_H(\pi, 0)$ = horizontal forward scattering coefficient

where

$K_{SV,H}$ = vertical or horizontal scattering coefficients of rain, N_{pm}^{-1}

2.2.3 Rain Temperature

It is unlikely that the temperature of the rain will be much different from ambient theoretical estimate by Jonas[12] suggests that the temperature of rain drops is about 2 K below ambient, and decreases with height at a rate of about 5.1 K/km.

We assume an exponential temperature profile of rain with height given by the formula.

$$T(h) = T_g \exp(-Kh) \tag{13}$$

where

$T(h)$ = effective rain temperature at height h in metres

K = constant = 0.0000182

h = height in metres

2.2.4 Properties of Clear Weather

The atmosphere without the rain behaves as a medium of zero scattering coefficients at 37 GHz. The clear weather attenuation at 37.0 GHz will be a function of water content and much lower contribution to the total attenuation will come from oxygen. The attenuation due to oxygen becomes significantly high at frequencies around the above 50 GHz. A clear day attenuation of 0.33 dB per atmosphere has been measured. (Results presented in later section.)

The value of 0.0075 N_p km^{-1} at 37.0 GHz corresponds to the vertical extent of water vapour 10 kms and is used in obtaining total attenuation on a clear day. The attenuation due to both oxygen and water vapour falls off exponentially with height. Therefore the emission from the part that is situated above the rain will be neglected at 37.0 GHz, as its contribution to the total flux at ground level is negligible.

2.2.5 Solar Radiation

It is well known that the Sun is an extremely powerful source of radio noise which exhibits apparent noise temperatures of the order of 10^6K at 300 Mc/S and 7000 K at 37.0 GHz. The solid angle subtended by the Sun at the Earth is about 7×10^{-5} steradians and from this it can be seen that the solar noise picked up by an isotropic aerial on the Earth will give rise to an aerial noise temperature of $\frac{7 \times 10^{-5}}{4\pi}$ or 6×10^{-6} times the values given above for the whole area of the Sun. The noise in an isotropic aerial on the Earth at 37.0 GHz is, therefore, given by

$$T_{n_o} = \frac{T_S \times 7 \times 10^{-5}}{4\pi} = 0.039 \text{ K only}$$

where, T_S = brightness temperature of Sun

However, if a solar burst occurs, the solar flux can increase as much as 10 dB, thereby increasing T_n to 0.4 K. It can be easily shown that even if the solar flux density increases as much as 10 dB at 37.0 GHz and rain occur at the same time, for no aerial elevation the increase in aerial temperature due to scattered radiation from the Sun is no greater than 0.50 K[5]. Therefore changes in the solar flux density will not have significant effect on the thermal emission technique of obtaining attenuation on an Earth-space path using radiometers.

2.3 Radio Emission by Rain

We consider a source of brightness as being observed at B, Figure 3, through a rainy medium of vertical depth h. In the absence of rain or cloud, the brightness of the source is independent of the distance 'a' or 'b' at which it is being observed, since the power per unit solid angle is constant.

2.3.1 Emission by Rain within the Beam of Aerial (no scattering)

Assuming there is no scattering the change in brightness dB produced by a volume of length dr will then be given by

For a vertically polarised system

$$dB_V = - B_S K_{aV} dr + \frac{J_V}{4\pi} dr \qquad (14)$$

For a horizontally polarised system

$$dB_H = - B_S K_{aH} dr + \frac{J_H dr}{4\pi} \qquad (15)$$

Equations (14) and (15) can be combined together

$$dB_{V,H} = - B_S K_{aV,H} dr + \frac{J_{V,H}}{4\pi} \qquad (16)$$

According to the Rayleigh-Jeans Law (from equation 3)

$$B = \frac{2kT}{\lambda^2} \qquad (17)$$

where

B = observed brightness watts m^{-2} c.p.s.$^{-1}$ rad^{-1}

T = observed brightness temperature K

k = Boltzmann's constant

λ = wavelength in metres

$K_{aV,H}$ = total vertical or horizontal absorption coefficient of rain NP m^{-1}

$J_{V,H}$ = vertical or horizontal emission coefficient, W m^{-3} Hz^{-1}

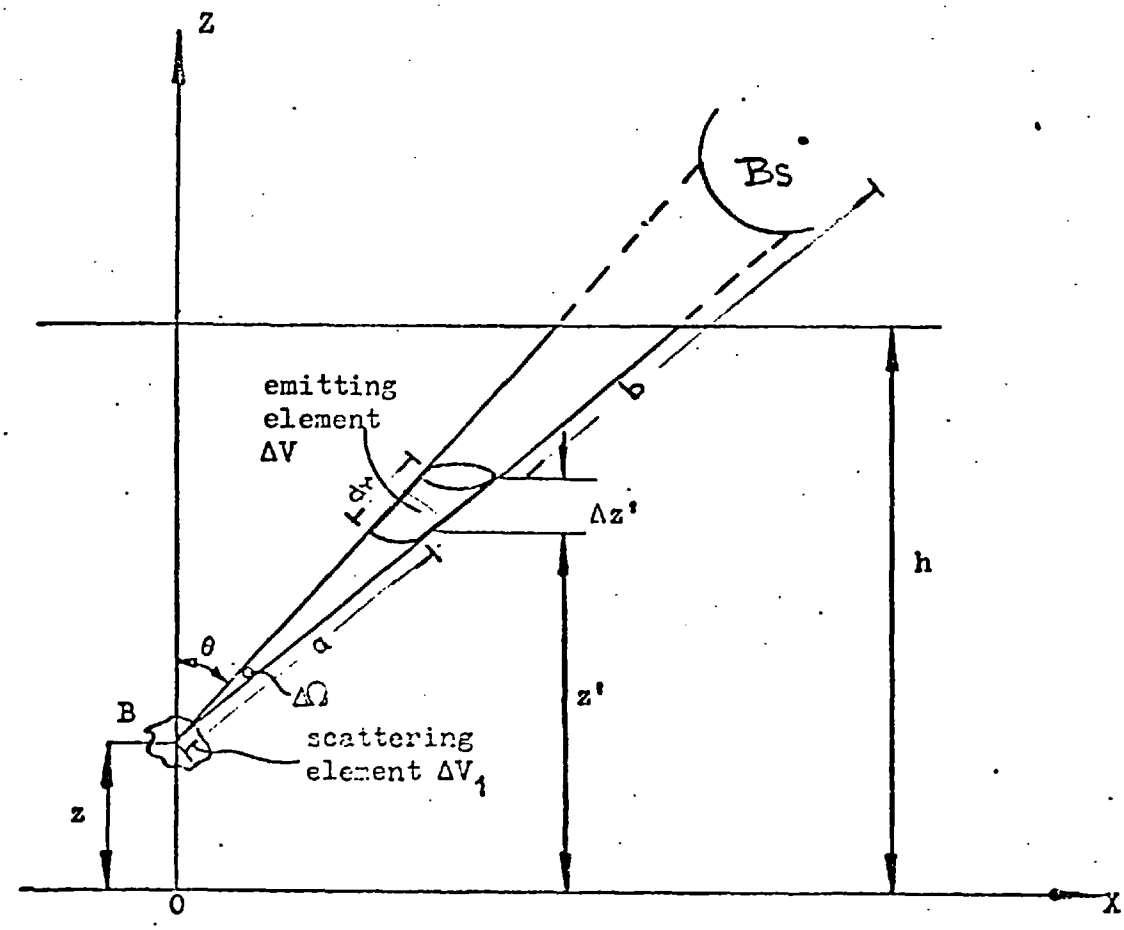

Z
Bs
emitting
element
ΔV
Δz'
h
θ
ΔΩ
B
scattering
element ΔV1
z
z'
0
X

FIGURE 3

Under conditions of local thermodynamic equilibrium, there will be no change in brightness.

$$dB_{V,H} = 0$$

From equation (16) and (17), we get

$$J_V = \frac{8\pi\ kT}{\lambda^2} K_{aV} \quad \text{watt m}^{-3}\ \text{Hz}^{-1} \tag{18}$$

$$J_H = \frac{8\pi\ kT}{\lambda^2} K_{aH} \quad \text{watt m}^{-3}\ \text{Hz}^{-1} \tag{19}$$

'T' in our case is temperature of rain. Equations (18) and (19) show that power per unit volume per unit bandwidth is different for vertical and horizontal polarisation because of K_{aV} and K_{aH}.

The power flux density per unit bandwidth emitted by an element ΔV is given by

$$\Delta W_{V,H} = \frac{J_{V,H}\ \Delta V}{4\pi\ a^2}\ e^{-(K_{eV,H}\ a)} \tag{20}$$

Now

$$\Delta V = \frac{a^2\ \Delta\Omega\ \Delta Z'}{\cos\theta}$$

so that

$$\Delta W_{V,H} = \frac{J_{V,H}\ \Delta\Omega}{4\pi\ \cos\theta}\ \exp\left[-a.\ K_{eV,H}\right]\ \Delta Z' \tag{21}$$

We assume that the temperature of the rain decreases exponentially w.r.t. ground as

$$T(h) = T_g\ e^{-Kh} \tag{22}$$

T_g = temperature measured at ground

K = constant

h = height in metres

$K_{eV,H}$ = total vertical or Horizontal Extinction Coefficient of rain $Np\,m^{-1}$.

$$\Delta W_{V,H} = \frac{8\pi\ K\ T_g\ e^{-Kh}\ \Delta\Omega\ K_{aV,H}}{4\pi\ \cos\theta\ \lambda^2} \exp\left[-(K_{eV,H}.a)\right] \Delta Z'$$

$$\Delta W_{V,H} = \frac{2k\ T_g\ \Delta\Omega}{\cos\theta\ \lambda^2} \exp\left[-(K_{eV,H}/\cos\theta + K)(Z'-Z)\right] \Delta Z'.K_{aV,H}.$$

As $K_{aV,H}$ and $K_{eV,H}$ are constant along the path.

$$W_{V,H}(Z,\theta) = \int_Z^h \Delta W = \frac{2K\ T_g\ \Delta\Omega\ K_{aV,H}}{\lambda^2(K_{eV,H} + K\cos\theta)} \left[1 - \exp\left\{-K'_{eV,H}(h - Z)/\cos\theta\right\}\right]$$

for $\theta \leq \pi/2$ (23)

or . For Aerial Elevation $\pi/2 - \Gamma$, $Z=0$

$$W(0,\Gamma)_{V,H} = \frac{2k\ T_g\ K_{a\ V,H}\ \Delta\Omega}{\lambda^2(K_{e\ V,H} + K\cos\Gamma)} \left[1 - \exp\left(-K_{e\ V,H}'\ h/\cos\Gamma\right)\right] \quad (24)$$

where .

$$K'_{eV,H} = K_{eV,H} + K\cos\Gamma$$

Therefore, the ratio of vertically polarised aerial temperature to the horizontally polarised aerial temperature is given by

$$\frac{T_{AV}^{o}(T)}{T_{AH}^{o}(T)} = \frac{\frac{W(0,\Gamma)_V}{2K\ \Delta\Omega}\lambda^2}{\frac{W(0,\Gamma)_{H,0}}{2K\ \Delta\Omega}\lambda^2} = \left(\frac{K_{eH} + K\cos\Gamma}{K_{eV} + K\cos\Gamma}\right)\left(\frac{K_{aV}}{K_{aH}}\right)\left(\frac{1 - \exp\left\{-K'_{eV}.h/\cos\Gamma\right\}}{1 - \exp\left\{-K_{eH}\ h/\cos\Gamma\right\}}\right) \quad (25)$$

At high values of rainfall rates, the ratio $\left(\frac{1 - \exp\left(-K'_{eV}.h/\cos\Gamma\right)}{1 - \exp\left(-K'_{eH}.h/\cos\Gamma\right)}\right)$ approaches unity and, therefore equation (25) reduces to

$$\frac{T_V^{o}(0,\Gamma)}{T_H^{o}(0,\Gamma)} = \frac{(K_{eH} + K\cos\Gamma)\ K_{aV}}{(K_{eV} + K\cos\Gamma)\ K_{aH}} \quad (26)$$

We can similarly derive an expression for rainfall whose temperature decreases linearly with height

$$T(h) = T_g - K'h$$

K' = Constant

T_g = Temperature at h = 0

we can write

$$\Delta W_{V,H}(Z,\theta) = 2K(T_g - K'Z')\,\Delta\Omega\,\Delta Z'\,K_{aV,H}\exp[-K_{eV,H}(Z' - Z)/\cos\theta]$$

$$W(Z,\theta)_{V,H} = \int_Z^h dW$$

$$= \frac{2K\,K_{av,H}\,\Delta\Omega}{K_{eV,H}\,\lambda^2}\left[T_g\left\{1 - \exp\left(-K_{eV,H}(h - Z)/\cos\theta\right)\right\}\right.$$

$$+ K'\frac{\cos\theta}{K_{eV,H}}\left\{\exp\left(-K_{eV,H}(h - Z)/\cos\theta\right)\left(\frac{h\,K_{eV,H}}{\cos\theta} + 1\right)\right.$$

$$\left.\left. - \frac{Z\,K_{eV,H}}{\cos\theta} - 1\right\}\right] \qquad (27)$$

For $K' = 0$, the above equation for $W(Z,\theta)$ reduces to $\left[T_g\left\{1 - \exp\left(-K_{eV,H}(h - Z)/\cos\theta\right)\right\}\right]$. This is the power flux density per unit bandwidth emitted by rain whose temperature is constant with height i.e. T_g.

/Equation (28)

$$\frac{T_{AV}^{o}(0,\Gamma)}{T_{AH}^{o}(0,\Gamma)} = \frac{K_{aH}\, K_{eH}}{K_{aH}\, K_{eV}} \left[T_g \left\{ 1 - \exp\left(- K_{eV}\, h/\cos\Gamma\right) \right\} \right.$$

$$\left. + \frac{K' \cos\Gamma}{K_{eV}} \left\{ \exp\left(- K_{eV}\, h/\cos\Gamma\right).\left(h\, \frac{K_{eV}}{\cos\Gamma} + 1\right) - 1 \right\} \right] /$$

$$T_g \left\{ 1 - \exp\left(- K_{eH}.h/\cos\Gamma\right) \right\} + \frac{K' \cos\Gamma}{K_{eV}} \cdot \left\{ \exp\left(- 1\, K_{eH}\, h/\cos\Gamma\right) \cdot \left(\frac{h\, K_{eH}}{\cos\Gamma} + 1 \right) - 1 \right\} \qquad (28)$$

The equations (27) and (28) represent the equation for the emission by rain within the beam of aerial which is not being scattered.

2.3.2 First Order-Scattering

To evaluate the effect of polarisation on scattering we consider that the radiation are incident on an element of volume ΔV_1 at B (Figure 3) we assume that the canting angle of the raindrops within the elementary volume is zero i.e. no depolarisation. This means that any horizontally polarised power flux density per unit bandwidth will be scattered as horizontally polarised and the same will be true for vertical polarisation. The power per unit bandwidth scattered in direction Γ and in unit solid angle is given by

Vertical Polarisation

$$P_V^{(1)}(Z,\Gamma) = \frac{K_{sV}\, \Delta V_1}{4\pi} \int_{4\pi} S'_V(\theta,\Gamma)\, W_V(Z,\theta)\, d\Omega \qquad (29)$$

/Horizontal Polarisation

Horizontal Polarisation

$$P^{(1)}_{H}(Z,\Gamma) = \frac{K_{sH}\,\Delta V_1}{4\pi} \int_{4\pi} S'H\,(\theta,\Gamma)\; W_H(Z,\theta)\; d\Omega \qquad (30)$$

Substituting for $W_{V,H}(Z,\theta)$ in the above equation we can write

$$P^{(1)}_{RV,H}(Z,\Gamma) = \frac{K\,T_g\,K_{aV,H}\,K_{sV,H}}{\lambda^2(K_{eV,H} + K\cos\theta)} \left[\int_0^{\pi/2} S_{V,H}(\theta,\Gamma)\,\sin\theta \left\{ 1 - \exp(KZ). \right.\right.$$

$$\left.\left. \exp\left(-\frac{K_{eV,H}}{\cos\theta}\,(h - Z) - Kh\right) \right\} d\theta + \int_{\pi/2}^{\pi} S_{V,H}(\theta,\Gamma)\,\sin\theta \left\{ 1 - \right.\right.$$

$$\left.\left. \exp(+KZ) \cdot \exp(K_{eV,H}\,Z/\cos\theta) \right\} d\theta \right] \qquad (31)$$

This is the power per unit bandwidth, due to emission by rain and first order of scattering propagation in direction Γ in unit solid angle by unit volume at height Z. The emission coefficient will be given by $J_{V,H} = 4\pi\, P^{(1)}_{RV,H}(Z,\Gamma)$. Following the procedure outlined above, we can show that the vertically polarised aerial temperature due to emission of rain and first order scattering is given by

$$T^{(1)}_{A_V}(\Gamma) = \frac{\lambda^2}{2K\cos\Gamma} \int_0^h \exp(-K_{eV}\,Z/\cos\Gamma)\; P^{(1)}_{R_V}(Z,\Gamma)\; dZ \qquad (32)$$

Similarly, the horizontal temperature is given by

$$T^{(1)}_{A_H}(\Gamma) = \frac{\lambda^2}{2K\cos\Gamma} \int_0^h \exp(-K_{eH}\,Z/\cos\Gamma)\; P^{(1)}_{R_H}(Z,\Gamma)\; dZ \qquad (33)$$

2.3.3 Higher Order Scattering

Higher order scattering was obtained by considering a volume ΔV_2 bounded by R, R + ΔR and by the horizontal planes, Z, Z + ΔZ.

This volume gives rise to scattered radiation in unit solid angle, the scattered radiation being given by $\Delta V_2 \, P^{(1)}_{R_{V,H}} (Z,\Gamma)$. The second order power per unit bandwidth scattered in direction Γ per unit volume and unit solid angle is given by

$$\Delta P^{(2)}_{V,H} (Z_o, \Gamma) = S_{V,H} (\theta,\Gamma) \, K_{sV,H} \exp \frac{(- K_{e\,V,H}\, d)}{4\pi\, d^2} \quad P^{(1)}_{R_{V,H}} (Z,\Gamma).\Delta V_2$$

where

$$d = \left\{ R^2 + (Z - Z_o)^2 \right\}^{\frac{1}{2}}$$

$$\theta = \pi - \sigma$$

$$\Delta V2 = 2\pi R \, \Delta R \Delta Z$$

The total rescattered power per unit bandwidth in direction Γ per unit volume and unit solid angle at height Z_o is given by summing all contribution from $Z - 0$ to $Z = h$ and $R \to 0$ to $R \to \infty$.

Aerial temperature due to emission by rain and second-order scattering is given by

$$T^{(2)}_{A_{V,H}} (\Gamma) = \frac{\lambda^2}{2K \cos \Gamma} \int_o^h \exp (- K_{eV,H} \, Z/\cos \Gamma) \, P^{(2)}_{R_{V,H}} (Z,\Gamma) \, dZ \qquad (34)$$

Similarly, higher order scattering can be extrapolated using following equation

$$T^{(n)}_{A_{V,H}} (\Gamma) = \frac{\lambda^2}{2K \cos \Gamma} \int_o^h \exp (- K_{eV,H} \, Z/ \cos \Gamma) \, P^{(n)}_{R_{V,H}} (Z, \Gamma) \, dZ \qquad (35)$$

2.4 Emission from the Ground; Scattering of First and Higher Orders

It has been shown that radiations scattered from ground cannot be neglected for heavy rainfall rates. The energy emitted and scattered by the

ground into the aerial will be different for horizontally or vertically polarised radiometers. The power flux density per unit bandwidth at height Z is given by

$$W_{V,H}(Z, \theta) = \frac{2K T_g}{\lambda^2} \left\{ \exp (K_{e_{V,H}} Z/\cos \theta) \right\} \Delta\Omega \qquad (36)$$

for $\theta \geq \pi/2$

The power per unit bandwidth scattered by unit volume in the direction Γ in unit solid angle is given by

$$P_{G\,V,H}^{(1)}(Z,\Gamma) = \frac{K T_G K_{S.V,H}}{\lambda^2} \int_{\pi/2}^{\pi} \exp (K_{e_{V,H}} Z/\cos \theta) S'_{V,H}(\theta,\Gamma) \sin \theta \qquad (37)$$

Aerial temperature due to emission by the ground and first order scattering is

$$T_{AG_{V,H}}^{(1)} = \frac{\lambda^2}{2K \cos \Gamma} \int_{o}^{h} \exp (- K_{e_{V,H}} Z/ \cos \Gamma) P_{G_{V,H}}^{(1)} (Z, \Gamma)\, dZ \qquad (38)$$

Since $\left(T_{A_{G,V}}^{(1)} - T_{A_{G,H}}^{(1)}\right)$ not equal to zero, therefore the scattered radiations from the ground will be polarised. However if $K_{eH}=K_{eV}$ & $S'_V(\theta,\Gamma)$ is equal to $S'_H(\theta,\Gamma)$, then $T_{A_{G,V}}^{(1)} = T_{A_{G,H}}^{(1)}$. The higher order contribution can be obtained using the procedure outlined above.

The total contribution to the vertically polarised aerial temperature due to rain and ground is given by

$$T_{AV}(\Gamma) = T_{AV}^{o} (\Gamma) + (T_{A_V}^{(1)} + T_{A_{G,V}}^{(1)}) + (T_{A_V}^{(2)} + T_{A_{G,V}}^{(2)}) + \ldots\ldots\ldots \qquad (39)$$

Similarly, for a horizontally-polarised system

$$T_{AH}(\Gamma) = T_{AH}^{o} (\Gamma) + (T_{A_H}^{(1)} + T_{A_{G,H}}^{(1)}) + \ldots\ldots\ldots\ldots\ldots\ldots \qquad (40)$$

$T_{AV}(\Gamma)$ and $T_{AH}(\Gamma)$ are called 'Apparent Temperatures' and $\alpha_{AV}(\Gamma)$, $\alpha_{AH}(\Gamma)$ being corresponding 'Apparent Attenuations'.

The true Vertical Aerial temperature, T_{TV}, is given by

$$T_{TV} = T_m - \frac{T_m}{10^{\frac{0.434}{\cos \Gamma}\left\{ \int_o^h K_{eV}\, dh + \int_o^{ho} K_{air}\, dh \right\}}} \tag{41}$$

The corresponding True Vertical attenuation, $\alpha_{T,V}(\Gamma)$, is

$$\alpha_{TV}(\Gamma) = \frac{4.34}{\cos \Gamma} \left[\int_o^h (K_{aV} + K_{sV})\, dh + \int_o^{ho} K_{air}\, dh \right] \tag{42}$$

The true Horizontal aerial temperature $T_{T_H}(\Gamma)$ is given by

$$T_{TH} = T_m - \frac{T_m}{10^{\frac{0.434}{\cos \Gamma}\left\{ \int_o^h K_{eH}\, dh + \int_o^{ho} K_{air}\, dh \right\}}} \tag{43}$$

The corresponding True Horizontal attenuation, α_{TH}, is

$$\alpha_{TH}(\Gamma) = \frac{4.34}{\cos \Gamma} \left[\int_o^h (K_{aH} + K_{sH})\, dh + \int_o^{ho} K_{air}\, dh \right] \tag{44}$$

∴ Error due to scattering for a vertically polarised aerial

$$= S_V = (\alpha_{TV} - \alpha_{AV}) \text{ db's} \tag{45}$$

Error due to scattering for a Horizontally polarised aerial -

$$S_H = (\alpha_{TH} - \alpha_{AH}) \text{ db's} \tag{46}$$

where

K_{air} = Absorption coefficient of clear air $N_p\ m^{-1}$

h = height of rain (metres)

h_o = height of atmosphere (metres)

2.5 Results

The four parameters namely T_{TH}, T_{TV}, T_{AH} and T_{AV} involved in equations (39) to (43) show that if we have to describe completely the polarisation properties of emitted and scattered radiations then we must devise an experiment capable of measuring all the said parameters simultaneously or in short duration. The experimental procedure and results are discussed in a later section. A Fortran program was developed to solve the various equations by feeding the coefficients of rain, height of rain, temperature of rain at the surface, temperature of the ground. The program evaluates T_{TH}, T_{TV}, T_{AH} and T_{AV} for different rainfall rates. It also evaluates separately polarisation dependence of radiation scattered from the ground. The final results are in decibels and in 18^o steps of elevation. The accuracy of calculated results is expected to be 0.1^oK.

2.5.1 Polarisation of Emitted Energy by Rain (no scattering)

The power flux density per unit bandwidth for zero order scattering for horizontal and vertical polarisation is represented by equation (24) and is solved to obtain the difference 'T_{AH}-T_{AV}' as a function of rainfall rate assuming horizontal extent of rain 10 kms and aerial looking into a storm at 18^o from the vertical. Figure (4) shows such a plot for different vertical path lengths, a difference of 6.5^oK can exist between apparent horizontal and vertical aerial temperature for a vertical depth of 3 kms and rainfall rate 10 mm h^{-1}.

The general behaviour of the curve shows that for a given path length, the difference ΔT increases with lower rainfall rates reaches a

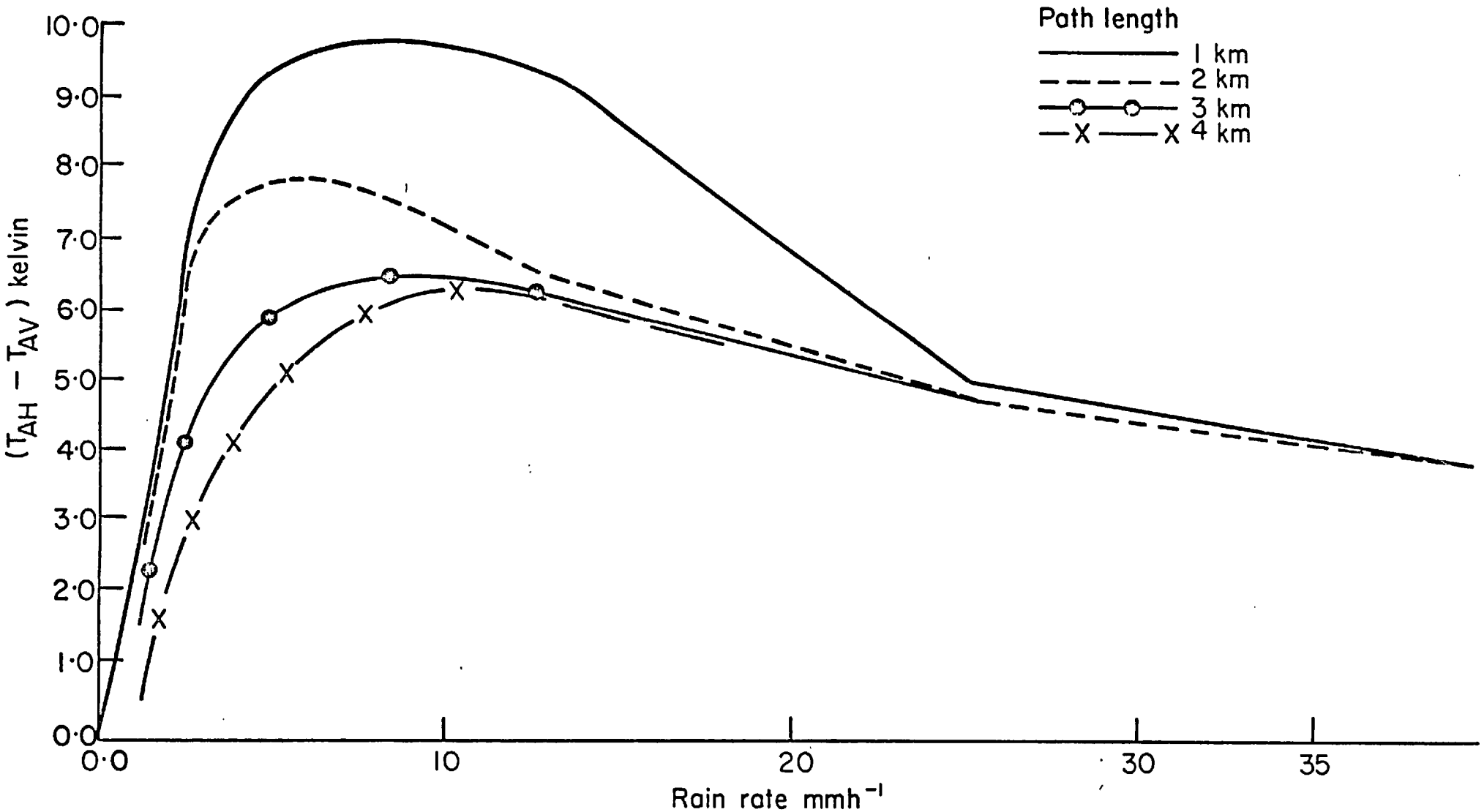


FIGURE 4

REF NO 2249/18 NEG NO

maximum value and then starts decreasing with further increase of rainfall rates. At heavy rain ΔT is independent of changes in path length and rainfall. At lower rainfall rate the behaviour of the plot is mainly governed by the term $[1 - \exp(- K_{eV,H}.h/\cos \Gamma]$(equation 24). The term increases with lower rainfall rates to attain unit value faster for horizontal polarisation compared to vertical polarisation, thus explaining the increase of ΔT at lower rainfall. At higher rainfall rate the term attains its maximum value of unity and the difference ΔT is created mainly by vertical and horizontal coefficients of rain. The ratio of absorption to the extinction coefficient decreases faster for horizontal polarisation compared to vertical polarisation of rain due to the presence of polarised scattering. At heavy rainfall rates, the difference between ratio of two polarisations becomes constant, making ΔT independent of path length and rainfall changes. Physically this case refers to the situation where observed aerial temperature has attained the actual temperature of rain.

The effect of variation of vertical depth on the peak value of ΔT is also depicted in Figure (4). As the propagation distance becomes longer the saturation of the exponential term* occurs at much lower value of ΔT thereby decreasing the peak value. The value of 'h' for a given rainfall, for which ΔT is a maximum that can be estimated by differentiating $(T_{AH}-T_{AV})$ w.r.t. h and is given as follows.

$$T_{AH} - T_{AV} = \frac{K_{aH}\, T_g}{(K_{eH} + K \cos \Gamma)} \quad [1 - \exp(- K_{eH}.h/\cos \Gamma)] - \frac{K_{aV}}{(K_{eV} + K \cos \Gamma)}$$

$$[1 - \exp(- K_{eV}.h/\cos \Gamma)] \qquad (47)$$

---

* The term is analogous to vertical or horizontal fractional absorption.

Differentiating w.r.t. 'h', $K_{aH,V}$, K_{eH}, being constant with 'h'

$$\frac{d(T_{AH} - T_{AV})}{dh} = \left[\frac{K_{aH}\, T_g}{(K_{eH} + K \cos \Gamma)} \cdot \frac{K_{eH}}{\cos \Gamma} \exp\left(-\frac{K_{eH} \cdot h}{\cos \Gamma}\right) - \frac{K_{aV}\, T_g}{(K_{eV} + K \cos \Gamma)} \left(\frac{K_{eV}}{\cos \Gamma}\right), \exp\left(-\frac{K_{eV} \cdot h}{\cos \Gamma}\right) \right] \quad (48)$$

Putting $\frac{d}{dh}\ (T_{AH} - T_{AV}) = 0$ for maxima. (49)

$$\frac{K_{aV} \cdot K_{eV}}{K_{aH} \cdot K_{eH}} \left(\frac{K_{eH} + K \cos \Gamma}{K_{eV} + K \cos \Gamma}\right) = \exp\left[-\frac{(K_{eH} - K_{eV})}{\cos \Gamma} .h\right]$$

or

$$h_{max} = \frac{\cos \Gamma}{K_{eV} - K_{eH}} \log e \left[\frac{K_{aV} \cdot K_{eV}}{K_{aH} \cdot K_{eH}} \left(\frac{K_{eH} + K \cos \Gamma}{K_{eV} + K \cos \Gamma}\right)\right] \quad (50)$$

For a rainfall of 12.5 mm h^{-1}, $h_{max} = 0.4$ kms for $\Gamma = 18^{\circ}$

Equation (48) is differentiated again w.r.t. 'h' to establish that h_{max} is given by equation (50).

$$\frac{d^2(T_{AH} - T_{AV})}{dh^2} = \left[- \frac{K_{aH} \cdot T_g \cdot K_{eH}^2}{(K_{eH} + K \cos \Gamma) \cdot \cos^2 \Gamma} \exp\left(-\frac{K_{eH} \cdot h}{\cos \Gamma}\right) + \frac{K_{aV} \cdot T_g\, K_{eV}^2}{(K_{eV} + K \cos \Gamma)\, \cos^2 \Gamma} \exp\left(-\frac{K_{eV} \cdot h}{\cos \Gamma}\right) \right]$$

Substituting for $\exp\left(-\frac{K_{eV} \cdot h}{\cos \Gamma}\right)$ from equation (49), we get

/Equation (51)

$$\frac{d^2(T_{AH} - T_{AV})}{dh^2} = \left[\frac{K_{aH} \cdot T_g \cdot K_{eV} \cdot K_{eH}}{\cos^2 \Gamma (K_{eH} + K \cos \Gamma)} \exp - \frac{K_{eH} \cdot h}{\cos \Gamma} - \right.$$

$$\left. \frac{K_{aH} T_g K_{eH}^2}{(K_{eH} + K \cos \Gamma)\cos^2 \Gamma} \exp - \frac{K_{eH} \cdot h}{\cos \Gamma} \right]$$

$$= \frac{T_g K_{aH} K_{eH}}{\cos^2 \Gamma (K_{eH} + K \cos \Gamma)} \left[K_{eV} - K_{eH} \right] \exp - \frac{K_{eH} \cdot h}{\cos \Gamma} \qquad (51)$$

Because of the shape of raindrops $K_{eV} < K_{eH}$. Therefore $\frac{d^2(T_{AH} - T_{AV})}{dh^2}$ is always negative or in other words h_{max} is the path length giving a maximum value of ΔT for a given rainfall rate.

It is clear from equation (50) that h_{max} is a function of coefficients of rain and therefore will vary with rainfall rate. Value of h_{max} decreases with increasing rain rate. A rainfall of 100 mm h^{-1} will correspond to 0.04 km whereas 1.25 mm h^{-1} will correspond to 1.65 km. This suggests that a rainy medium can be broken up into an infinite number of horizontal layers and at high values of attenuation during rainfall, only the lower and hotter portion of the rain contributes effectively to the brightness since the lower drops absorb the radiation from the upper drops and replace it with their own.

The above effect would not have been apparent under the spherical drop assumption since the difference ΔT equals zero thereby reducing to Zavody's results.

2.5.2 Polarisation of Emitted and Scattered Radiation by Rain

Taking account of all the ways, described previously, in which energy can reach an upward looking radiometer aerial, the difference of

true horizontal and vertical, apparent horizontal and vertical were computed and plotted against rainfall rate (Figure 5). The plot shows that error in assuming $\alpha_{TV} = \alpha_{TH} = \alpha_{AV} = \alpha_{AH}$ is considerable. For 10 mm h^{-1} the difference of apparent attenuations between polarisations can be as high as 2.8 decibels. Part of this is due to difference between vertical and horizontal scattering and found to be just over 56% at 10 mm h^{-1}, and only 36% at 2.5 mm h^{-1} of the total. Therefore as expected at low rainfall rates the polarisation properties of the emitted energy are governed by absorption because of low scattering. The results correspond to an aerial elevation of 18.0 degrees.

The difference between apparent vertical and horizontal, decreases with increase of elevation angle. It occurs because of the lower contribution from emitted and scattered energy by the rain and from the ground. The ratio of energy scattered out of the beam to the energy scattered into the beam decreases with increase of elevation angle. The difference is minimum at zenith and maximum for zero elevation.

The difference of true horizontal and vertical attenuation is also plotted on the same graph (Figure 5). The true difference increases faster than apparent difference. The true difference between horizontal and vertical is 3.9 dB's at 10 mm h^{-1} and increases with rainfall rate. This suggests that the relative differences between true and apparent i.e. error due to scattering is also polarisation sensitive and increases with rainfall rate. As much as 1.1 dB (at 10 mm h^{-1}) difference can exist between horizontal and vertical scattering error.

2.5.3 Relationship between Polarised True and Apparent Attenuation

The error in assuming true and apparent attenuation to be the same for either of the polarisations i.e. vertical or horizontal can be

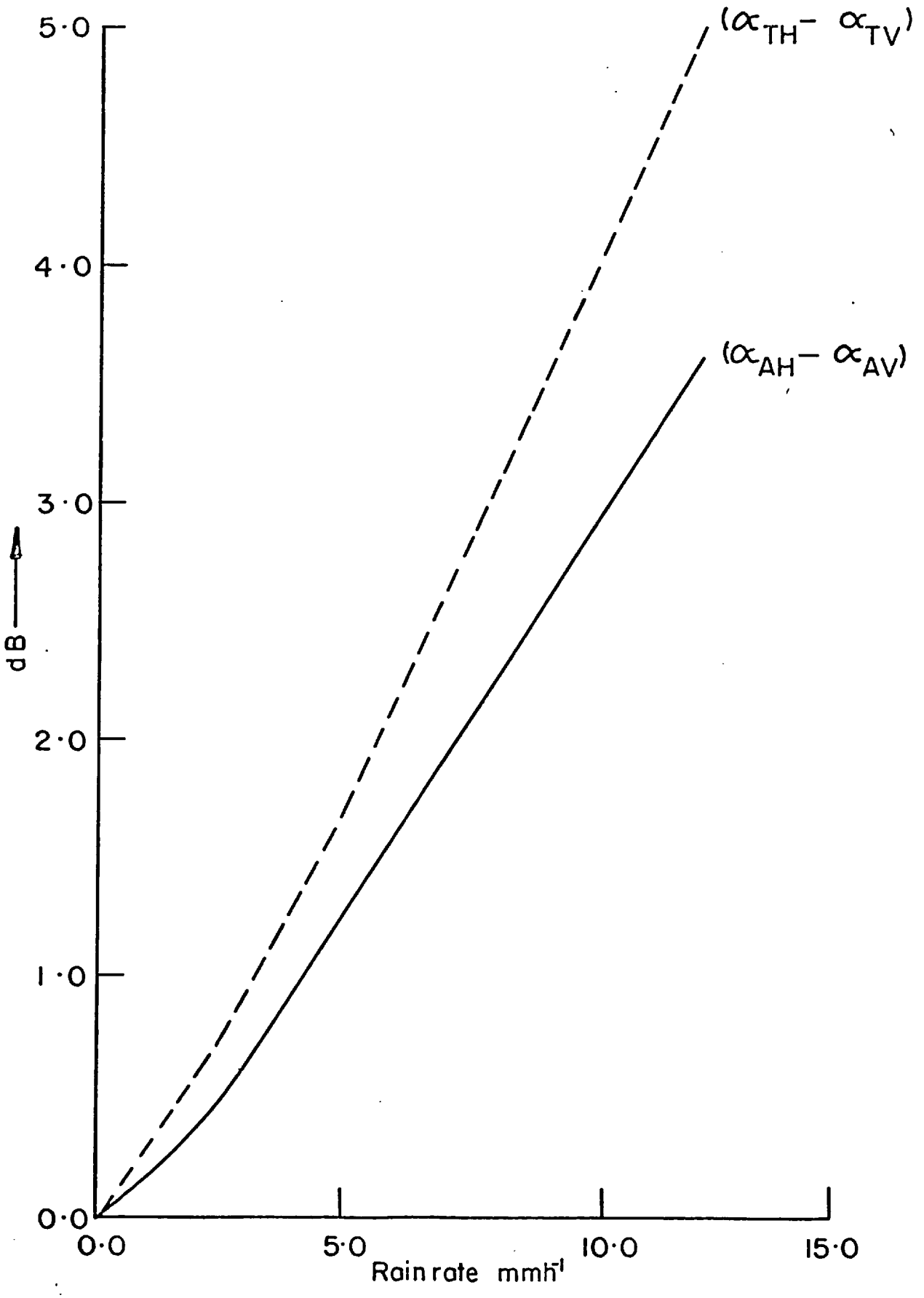

5·0
4·0
3·0
2·0
1·0
0·0
dB
$(\alpha_{TH} - \alpha_{TV})$
$(\alpha_{AH} - \alpha_{AV})$
0·0
5·0
10·0
15·0
Rain rate mmh⁻¹

FIGURE 5

considerable : it increases with rainfall rate and frequency. This is expected because the scattering and absorption coefficient increases with frequency and rainfall rate. Table (1, 2) show that at 37 GHz for rain of 125 mm h^{-1}, the ratio of scattering coefficient to the absorption coefficient for vertical and horizontal polarisation is 0.85 and 0.78 respectively.

True attenuation as a function of apparent attenuation for both polarisations (including ground contribution) is plotted in Figure (6) for a rain of depth 3 kms and horizontal extent 10 kms, aerial elevation being 18^{o}. The plotted result show that error due to scattering for vertical polarisation can differ by 1.2 decibels from horizontal scattering error at 9.0 decibels of apparent attenuation, the vertical and horizontal error for the same apparent attenuation being 3.25 dB and 4.45 dB respectively. It is also apparent from the derived equations that the error for vertical or horizontal polarisations increases as the elevation angle is decreased. This occurs because the ratio of energy scattered out of the beam to the energy scattered into the beam is smallest when the aerial is pointing at zenith. The relative difference of error between vertical and horizontal also decreases with increase of elevation angle.

For extremely low values of attenuations all the curves have same slope, where, the attenuation is primarily due to clear air or partial clouds.

$$\frac{\alpha_{TV}(\Gamma)}{\alpha_{aV}(\Gamma)} = \frac{\alpha_{TH}(\Gamma)}{\alpha_{aH}(\Gamma)} = 1 \qquad (52)$$

Therefore four parameters, namely true vertical attenuation corresponding to apparent vertical attenuation and true horizontal attenuation corresponding

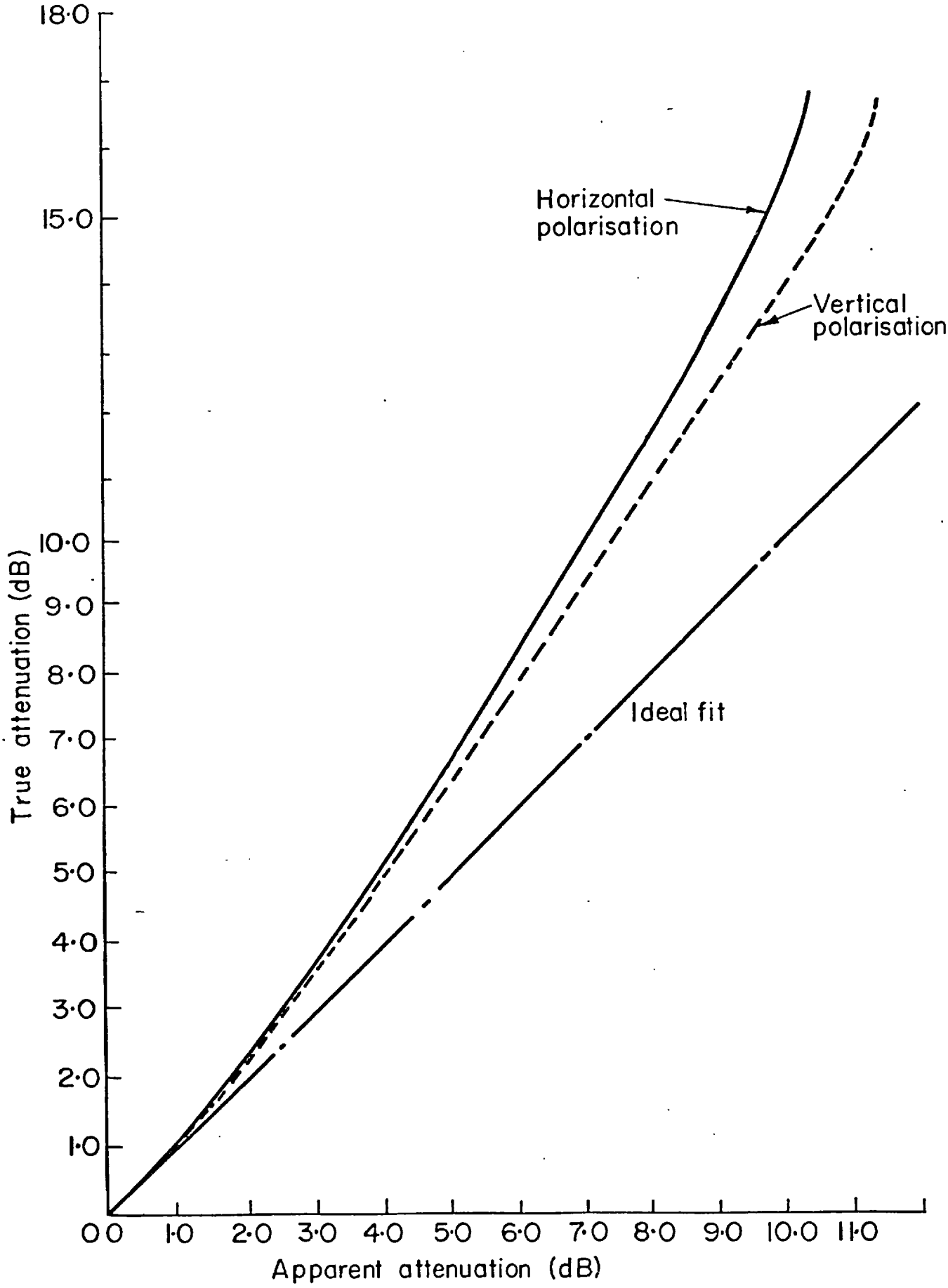

18·0
15·0
10·0
9·0
8·0
7·0
6·0
5·0
4·0
3·0
2·0
1·0
0 0
1·0
2·0
3·0
4·0
5·0
6·0
7·0
8·0
9·0
10·0
11·0
True attenuation (dB)
Apparent attenuation (dB)
Horizontal polarisation
Vertical polarisation
Ideal fit

FIGURE 6

to apparent horizontal attenuation are required to define completely attenuation on an Earth-space path from radiometric measurements.

Under un-polarised assumption the results deduced from sky temperature can be low by as much as 3 decibels in 10 decibels. Changes in the drop-size distribution with height and clear air attenuation are assumed to have a negligible effect.

If the drop-size distribution is not constant with height, but the number of small drops increases with height at the expense of larger ones, then for moderate rainfall both attenuations for either polarisations will be slightly greater than those calculated for the specified rainfall. The horizontal error will also be greater than the vertical error. But the above will not be true for heavy rainfall because most of the contribution to the aerial comes from lower parts of rain layer and the results could be significantly in error, specifically the difference between horizontal and vertical error. The influence of changes in other parameters e.g. temperature of the rain and ground is discussed in the sections below.

2.5.4 Ground Emission and Polarisation Properties

The ground can be assumed to be a black body at temperature T_g. The assumption will hold as long as the ground does not behave as a large reflecting surface because the absorption coefficient of a smooth surface is a function of power reflection coefficient. For a practical case the surface surrounding the aerial is generally rough, and the amount of radiation arriving at the aerial via the surface will depend on the roughness. A surface that is rough compared to $\lambda/2$ does not produce specular reflection[54] and therefore power reflection coefficient has got no meaning at millimetre wavelengths. Measurements at millimetre wavelengths

indicate that when ground is covered by vegetation, its emissivity is very high for vertical or horizontal polarisation (55). Therefore a considerable amount of energy emitted by the ground is scattered into the aerial by the falling rain drops. The ground contribution to the aerial increases with increase of rain rate and decrease of aerial elevation. It is greatest at the low angles of aerial elevation, where the amount of rain near ground level and in the beam is a maximum. The ground contribution to the vertical and horizontal polarised aerial is plotted in Figure (7). The plotted results correspond to the rain model discussed earlier and 18^{o} elevation. The contribution from the ground can be as high as 46.0 K and 46.9 K for vertical and horizontal polarisations at 37.0 GHz. The maximum difference between vertical and horizontal is 2.75 K for 1.5 mm h^{-1} and less than 1.0 K for rainfall rates greater than 8.0 mm h^{-1}. The low difference between polarisations signifies that the scattering is closer to isotropic.

The effect of variations of ground temperature on vertical and horizontal apparent attenuations and to what extent the ground contributes to total attenuation is important. The contribution from the ground and rain is tabulated in the accompanying Table (3). The attenuations were calculated by assuming 273.0 K and 295.0 K respectively. During heavy shower a slight change of aerial temperature leads to an enormous change in attenuation due to saturation i.e. an aerial temperature close to actual temperature of rain. Therefore an accurate estimate from the ground becomes extremely important to give correct value of attenuation from radiometric measurements. The percentage contribution to the total attenuation from the ground at 12.5 mm h^{-1} (assuming the temperature of the rain and ground to be 273.0 K) towards vertical and horizontal aerial is 46.76% & 54.8% respectively. But if the temperature of the rain and ground is increased to 295.0 K, the same percentage is reduced to 38.1% and 40.8% respectively. It is interesting to note that the percentage difference between

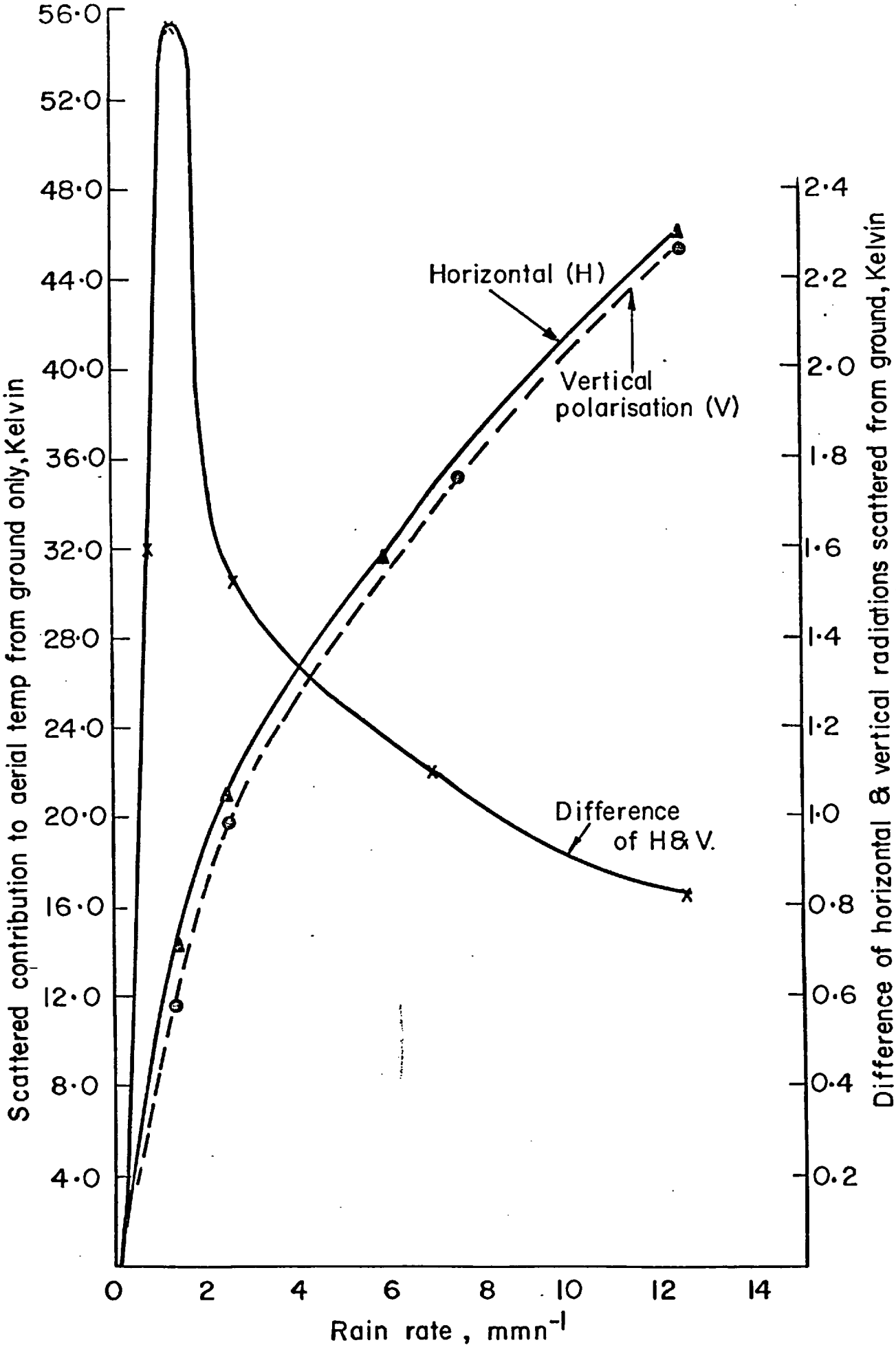


FIGURE 7

NEG NO. REF NO. 2249/21

AERIAL ELEVATION = 18.0°

Rain Rate mm h^{-1}	Contribution from Ground K		Contribution from Rain and Ground K		Effective Temperature of Rain and Ground 273.0 K						Effective Temperature of Rain and Ground 295.0 K							
					α_{R+G} dB		α_R dB		Difference dB ($\alpha_{R+G}-\alpha_R$)		Percentage Contribution from Ground		α_{R+G} dB		α_R dB		Difference dB ($\alpha_{R+G}-\alpha_R$)		Percentage Contribution from Ground	
	H	V	H	V	H	V	H	V	H	V	H	V	H	V	H	V	H	V	H	V
2.5	21.08	19.65	185.78	175.8	4.96	4.49	4.02	3.69	0.94	0.80	19.0	18.0	4.32	3.93	3.54	3.27	0.78	0.66	18.1	16.7
12.5	46.09	45.27	265.58	255.94	15.65	12.04	7.07	6.41	8.58	5.63	54.8	46.76	10.0	8.78	5.92	5.43	4.08	3.35	40.8	38.1

α_{R+G} = Attenuation from Rain and Ground

α_R = Attenuation from Rain

$\alpha_{R+G} - \alpha_R$ = Attenuation from Ground

TABLE 3

vertical and horizontal contributions from ground tend to decrease as the temperature of the rain and ground is increased i.e. ground contribution tends to become isotropic as the temperature of the rain and ground is increased.

From a practical point of view we must also consider how the apparent vertical and horizontal temperatures are affected if only the ground temperature varies whereas the temperature of the rain remains constant. At a rain rate of 2.5 mm h^{-1}, the horizontal and vertical aerial temperature of 185.9 K and 175.9 K has a ground contribution of 21.1 K and 19.7 K respectively at an elevation of 18.0 degrees, the temperature of rain and ground being 273.0 K. If the ground temperature is increased to 295.0 K, keeping the rain temperature at its original 273.0 K, the ground would contribute 22.8 K and 21.3 K to the horizontal aerial temperature of 187.6 K and vertical aerial temperature of 177.5 K respectively. This is equivalent to an apparent horizontal attenuation of 5.05 and vertical attenuation of 4.56 decibels, compared with 4.96 decibels and 4.49 decibels for 185.9 K and 175.9 K respectively. This means that true horizontal and true vertical attenuations will be overestimated by 0.09 decibels and 0.07 decibels respectively. The error will be larger for heavy rainfall rates but for higher elevations where the ground contribution is lower, the error will be smaller.

/Table 4

RAIN RATE = 2.5 mm h^{-1}

GROUND TEMPERATURE = 295.0 K RAIN TEMPERATURE = 273.0 K

ELEVATION = 18.0°			ELEVATION = 36.0°			ELEVATION = 54.0°			ELEVATION = 90.0°		
α_{AH} dB	α_{AV} dB	DIFF	α_{AH} dB	α_{AV} dB	DIFF	α_{AH} dB	α_{AV} dB	DIFF	α_{AH} dB	α_{AV} dB	DIFF
5.05	4.56	0.49	2.81	2.52	0.29	2.07	1.84	0.23	1.68	1.5	0.18

GROUND TEMPERATURE = 273.0 K RAIN TEMPERATURE = 273.0 K

ELEVATION = 18.0°			ELEVATION = 36.0°			ELEVATION = 54.0°			ELEVATION = 90.0°		
α_{AH} dB	α_{AV} dB	DIFF	α_{AM} dB	α_{AV} dB	DIFF	α_{AH} dB	α_{AV} dB	DIFF	α_{AH} dB	α_{AV} dB	DIFF
4.96	4.49	0.47	2.78	2.49	0.29	2.05	1.83	0.23	1.66	1.48	0.18

TABLE 4

2.5.5 Rain Temperature

Unfortunately no experiment has been performed to measure the effective temperature of the rainy medium as a function of height. Theoretical calculations by Jonas[12] suggest that the temperature of the raindrops is about 2 K below ambient, and decreases with height at a rate of about 5.1 K per km.

Temperature variations of rain cause changes in the complex dielectric constant of water thereby altering the values of attenuation coefficient. Values of attenuation coefficient normalised with respect to the value at 20°C have been calculated for the range 0-30°C at 36.0 GHz for Laws and Parson's drop size distribution and changes were found to be very small at this frequency. Therefore temperature variations is not a problem for an actual transmitting and receiving system.

But for radiometric measurements the variation of temperature of rain in deriving total attenuation is important. The correct choice of effective temperature of the medium is the most serious if the aerial temperature measured is high i.e. when the attenuation is large.

For a difference between atmospheric (say at 273.0 K) and aerial to be 20 K, a variation in 5 K around 273.0 K leads to a change of + 0.89 decibels or - 1.15 decibels in 11.4 decibels. Therefore it is unreasonable to evaluate attenuation by assuming that each point along the path of the beam is at a constant temperature, we must calculate the attenuation and scattering at a height h using attenuating medium temperature at that height and the overall results along the beam should be added. The results were evaluated and compared by assuming an exponential temperature-profile of rain with height and constant temperature of 273.0 K. The exponential temperature profile of rain with height is

given by

$$T(h) = T_g \exp(-Kh) \qquad (53)$$

where

T_g = temperature of rain at the surface of Earth i.e. at sea level

h = height in metres

K = constant = 0.0000182

T(h) = temperature of rain at height h

The true and apparent aerial temperatureswere calculated using exponential and constant temperature profiles and are plotted in Figure (8). Curve 'a' corresponds to true versus apparent aerial temperature for exponential temperature profile of rain and curve 'b' for constant temperature. The calculations correspond to spherical drops obeying Laws and Parson's drop size distribution, temperature of ground 288.4 K, rain depth 3 kms and aerial elevation 18.0 degrees. Curve 'b' estimates higher values than curve 'a' for the same apparent aerial temperature. For apparent attenuation of 9.18 decibels constant temperature profile gives an attenuation value of 14.8 decibels, whereas the exponential temperature profile gives a value of 13.2 decibels i.e. true attenuation is being over estimated by 1.6 dBs, if the constant-temperature profile is used.

2.5.6 Effect of Depth and Horizontal extent of Rain on Scattering and and Polarisation of Emitted Energy

It was assumed throughout the calculations that rain is formed at the height of 3 kms and is of horizontal extent 10 kms. The vertical and horizontal extent of rain varies significantly with the seasons and type of storms because of attenuation being dependent on path length and drop size distribution on rainfall rate. The variation of horizontal extent of rain is important if it is less than minimum extent and will have

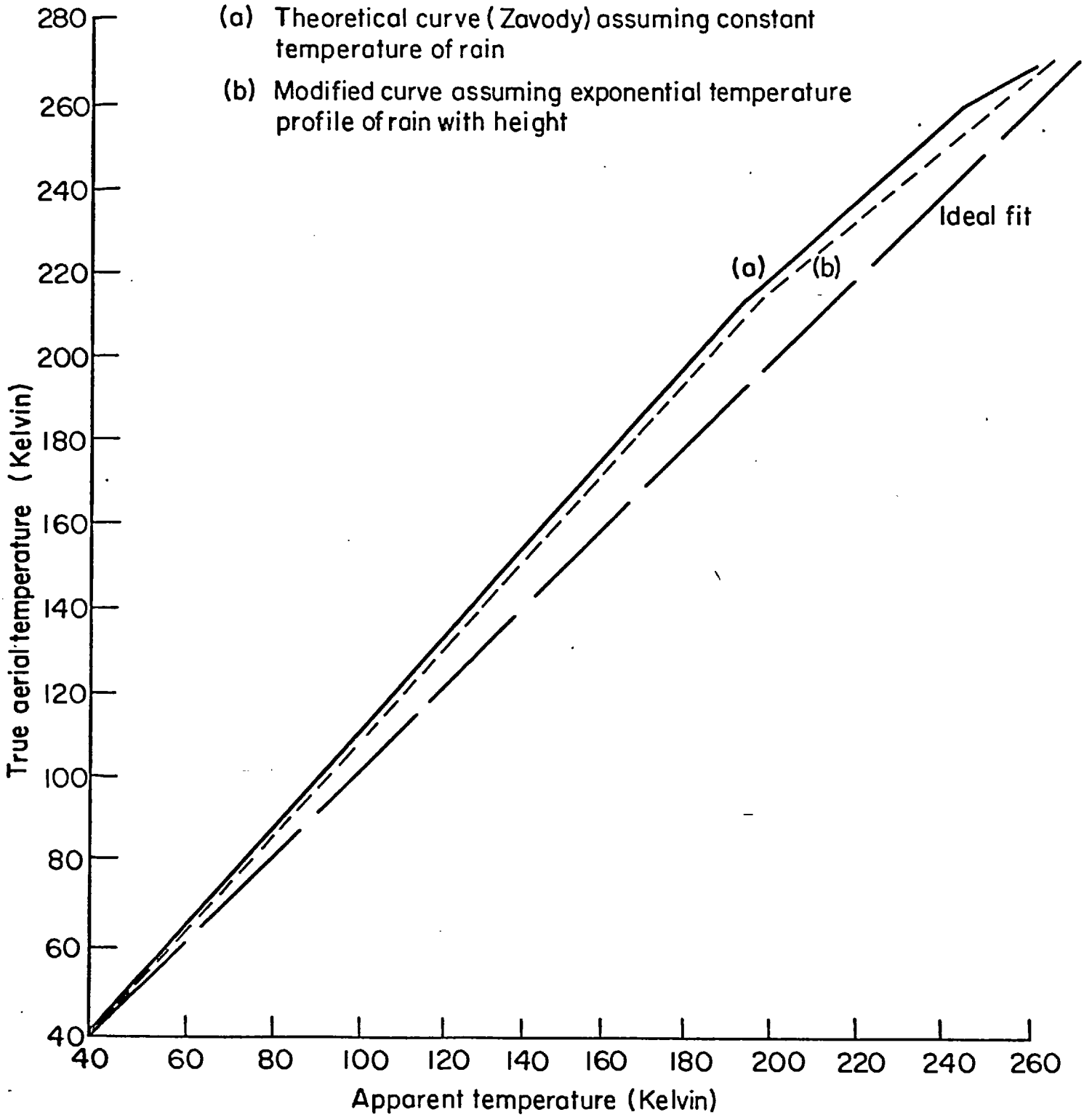


FIGURE 8

REF.NO.2249/22 Neg.NO.

low effect if the distance is greater than the minimum because emitted and scattered energy from a certain distance will have negligible effect on the aerial temperature due to the following reasons.

(a) The flux is inversely proportional to the square of distance therefore decreases with distance from the point of observation.

(b) The emitted energy within the solid angle experiences rain attenuation.

The minimum horizontal extent of rain is computed by Zavody[5] for a layer depth of 3 kms and aerial elevation 36° and found to be at least 4.1 kms. The largest diameter required is 10 kms. If rain depth is infinite then the aerial temperature giving 0.1 dB of attenuation would require a contribution from an infinitely large horizontal extent. If the horizontal extent is smaller than the minimum, the energy scattered can be substantially less for certain rainfall rates than for an infinite slab resulting in lower apparent attenuation and, therefore the true attenuation can be under-estimated. The plot of true attenuation versus apparent attenuation for either of polarisation is almost the same for rain depth of 3 kms, 5 kms and 6 kms, although with rain depth the true and apparent attenuations for certain rainfall rates changes considerably. For 6 kms layer depth the attenuation at 37 GHz is 4% lower than for 3 kms, but for vertical polarisation it is lower by 1.5% only, the aerial elevation being 18.0 degrees. The effect of changes of layer depth of rain on scattering error is comparatively low for vertical polarisation. The calculations were done for constant layer depth (3 kms) but variable horizontal extent. The variation of horizontal extent from 10 kms to 5 kms resulted in lower estimation of apparent attenuation by less than 1% for either of the polarisations at 2.5 mm h^{-1} but for higher rainfall rates the error is

considerable. At 12.5 mm h^{-1} the apparent attenuation will be underestimated by 10%. If we lower the horizontal extent to an extreme case of the rain filling the aerial beam only, then the aerial temperature will be just the sum of the contributions due to direct emission by the rain beam and first order scattered radiation from the ground. The results at 2.5 mm h^{-1} for apparent attenuation were lower by 21.1 and 19.1 for horizontal and vertical polarisations respectively. For higher rainfall rate one could have underestimated the apparent attenuation by as much as 50%. The discussion of above results is important so as to explain the possible discrepancies which may exist in estimating true attenuation by short duration intense rain due to patches of heavy cloud. The short duration rain storm by patches of clouds are frequent, especially in summer.

The results discussed above correspond to an aerial elevation of 18.0 degrees, and calculations show that at higher elevation angles the effect of variation of the vertical and horizontal extent of rain is less, compared to lower elevation angles.

2.5.7 Orders of Scattering

In general three orders of scattering were adequate for moderate rainfall rates. For extremely heavy rainfall higher orders cannot be neglected. The calculation showed that the number of orders required for vertical polarisation were less compared to horizontal polarisation. The various orders of scattering are related through a geometrical series. The geometrical ratio is 0.27 and 0.28 for vertical and horizontal polarisation.

Because the attenuation is lower at higher elevation angles, the number of orders required decreases with elevation angle (Figure 9).

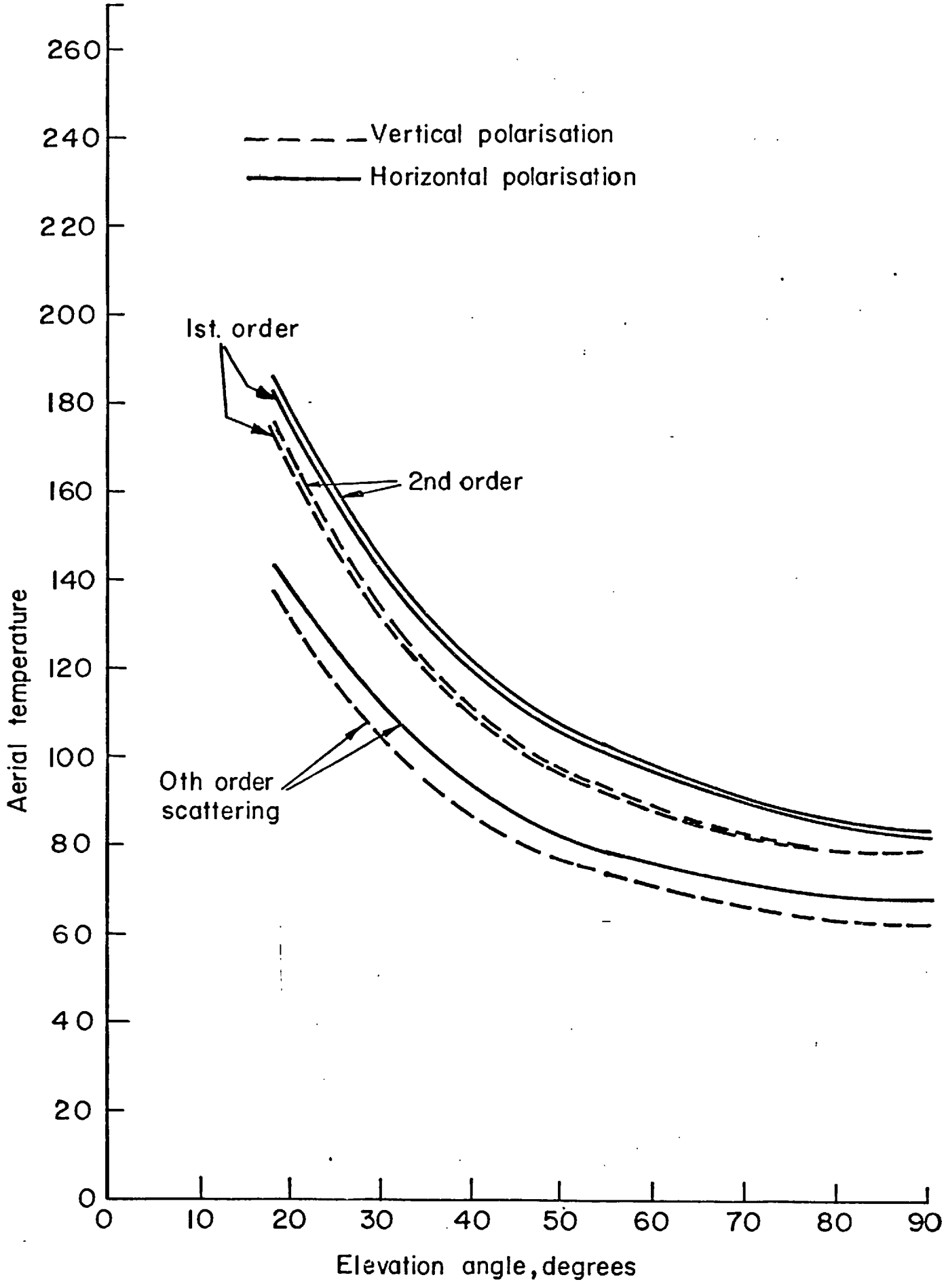


FIGURE 9 NEG.NO. REF.NO 2249/23

2.5.8 Aerial Efficiency

The aerial efficiency was assumed to be 100% i.e. no side lobes or ohmic losses and is perfectly matched since the solid angle subtended by the side lobes is large, therefore, although their gains may be many decibels down on the main lobe, the emitted and scattered radiation can enter the receiver through the side lobes. Because of this contribution background radiations are not constant and tend to vary, thereby posing a problem for an accurate estimation of attenuation.

If the beam solid angle efficiency for the present aerial is 94%, this means that minor lobes on the average are about 12 decibels below isotropic level. The contribution to the aerial will be 8.5 K. Wilson[1] has reported a contribution of 8.3 k at 30 GHz from side lobes. The corresponding error is 0.1 dB in the range up to 15 dB and will increase steeply for aerial temperatures very close to the temperature of the rain.

3. EXPERIMENTAL PROCEDURE FOR STUDYING SCATTERING EFFECTS BY RAIN

3.1 Equipment

3.1.1 Equatorial Mount

The antenna together with the R.F. head is carried by a weather-proof equatorial mount (Fig. 10). The equatorial mount is erected on a firm base of concrete measuring about 5 ft. square. It was levelled to eliminate any possible risk of the R.F. head over-balancing and to ensure proper tracking. The levelling was done using a spirit level and the levelling screws provided on the base of the mount. Detachable covers are provided over parts of the system which may require maintenance or adjustment to prolong the life of the equipment. It is capable of operating in wind speeds of up to 50 km per hour and is easily transportable because of its construction. It can be set on installation to any inclination between 0^{o} and 90^{o}.

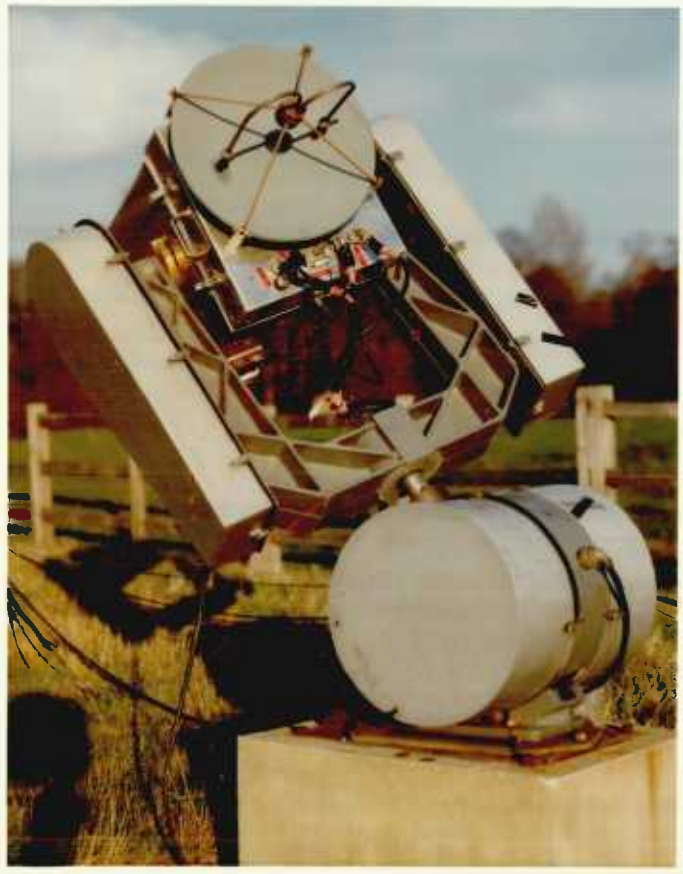


FIGURE 10

In order that the aerial could track the Sun during daylight, the axis of the mount was aligned accurately parallel to the axis of the Earth's rotation by aligning the mount base along (N-S) line using a magnetic compass and the axis of the mount at an angle of $57^{o}29'$ (latitude of Slough) using an inclinometer. The Right Ascension (RA) drive, which rotates the antenna about its axis is produced by a stepping motor. This receives 3000 pulses per minute from a pulse circuit in the control unit. The motor shaft is next coupled to a reduction gear box (reduction being 1:250), followed by a differential gear box, and finally to a worm which drives the hour angle wheel (shown in Fig. (11). The worm is being driven at 0.25 revolution per minute. The design of hour angle wheel and drive is discussed in Appendix A5.

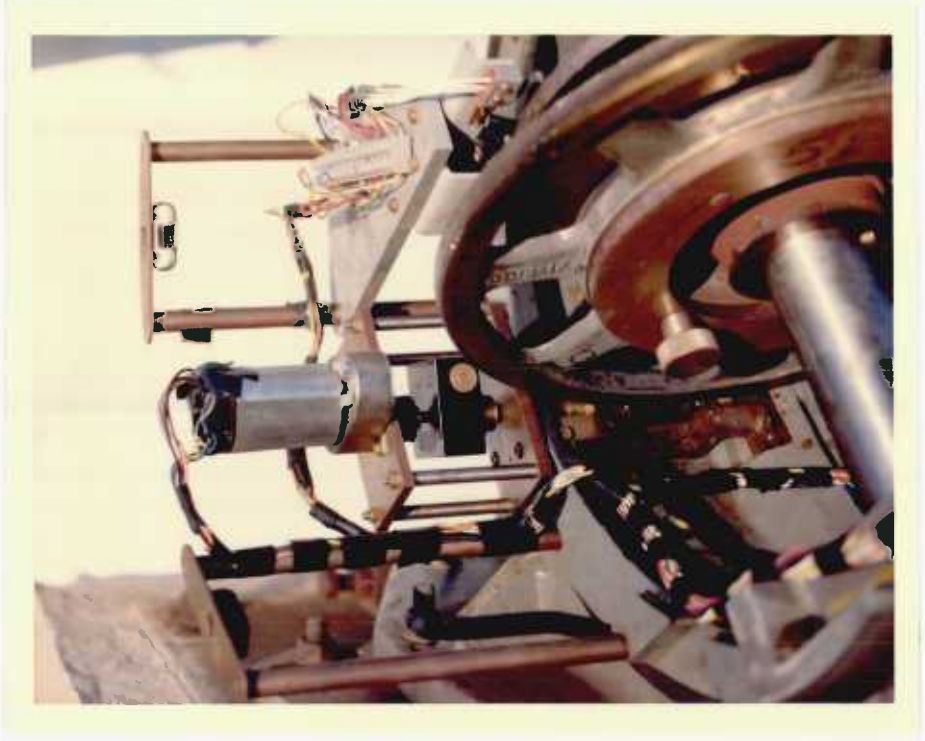


FIGURE 11

After a days tracking, when the aerial is in the sunset position, it is reversed to the sunrise position ready to track the Sun the next day; reversing procedure is achieved by simultaneously closing of the micro-switches. In the sunset position microswitches are closed by a bulge on the hour angle wheel and the cam on the end of the worm, a latching relay operates and the drive operates in the reverse mode. The mount is driven at twice the speed of the forward mode. The aerial is driven back to the sunrise position, the latching relays operate again and the motor now drives in the forward direction at the normal speed, to follow the Sun again. By adjustment of microswitches on the hour angle wheel and on the cams, the aerial was made to track the Sun from sunrise to sunset.



FIGURE 12

There are two more motors on the mount, both situated in one support arm of the mount. One motor is the declination off set, or "nodding", motor provides a 3^{o} offset to the declination axis in order to produce comparison between sky signal and the radiation from the Sun. The other is a declination motor which can alter the declination of the antenna by $\pm$ 0.5^{o} per 24 hours. The differential gear box between this motor and the drive worm also facilitates manual adjustment of the declination. The details of evaluating zenith angle from GMT are given in Appendix A5.

3.1.2 Control Unit

A remote control system is provided which, by driving the hour angle and declination motors, will allow the mount to perform the following operations :-

(a) Follow the Sun in hour angle to within 2 mins of arc throughout the day.

(b) Reverse at night.

(i) In winter at 1800 hours maintaining the original speed.

(ii) In summer at 2000 hours doubling the original speed.

(c) Reverse in the morning.

(i) In winter at 0600 hours maintaining the original speed.

(ii) In summer at 0400 hours returning to the original speed.

(d) Change between fast and slow hour angle drive on manual command.

(e) Change between forward and reverse hour angle drive on manual command.

(f) There are three switches, Spring, Off, Autumn to take into account the daily changes in declination of the Sun. Thus the declination axis is controllable in the forward and reverse direction.

In order that cables do not interfere with the movement of the mount cable interfaces are provided.

3.1.3 Aerial

The aerial system is designed to detect radio frequency radiations from the Sun in the microwave region. The aerial dish is an 18" diameter parabolic reflector made of aluminium, designed to receive radiations at 37.0 GHz. It has at the focus copper waveguide feeds; the mouth of the feeds has been sealed with insulating tape and the assembly is provided with mechanical stays to maintain its accurate location with respect to the reflector. The main characteristics of the aerial are

(1) Beam width 1.49^{o}.

(2) The gain relative to an isotropic aerial is 39.5 dB.

(3) Side lobes are below $\frac{-25.0\ db}{h}$* relative to the main beam and are not measurable with the system.

* Dynamic Range of Solar-Tracking Radiometer is 25.0 db.

The aerial dish is bolted to an aluminium plate and the feeder horn passes through its centre into the R.F. compartment. The aerial feed is connected to the input port of a remotely operated waveguide switch. The antenna feeds were covered with a small plastic cylinder so that layer of water is not formed over the feeds during intense periods of rain.

3.1.4 R.F. Head Structure

The R.F. head is fixed to the mount in such a way that the following conditions are met :-

(a) The whole system is weatherproof.

(b) The R.F. head can be easily dismounted and taken away for repairs or alterations.

(c) The antenna and microwave compartment was coated with a white surface to minimise solar heating effects.

(d) The temperature of the microwave compartment was kept constant to $\pm 1^{\circ}C$ at $22^{\circ}C$.

The individual component specifications are tabulated in Appendix A1.

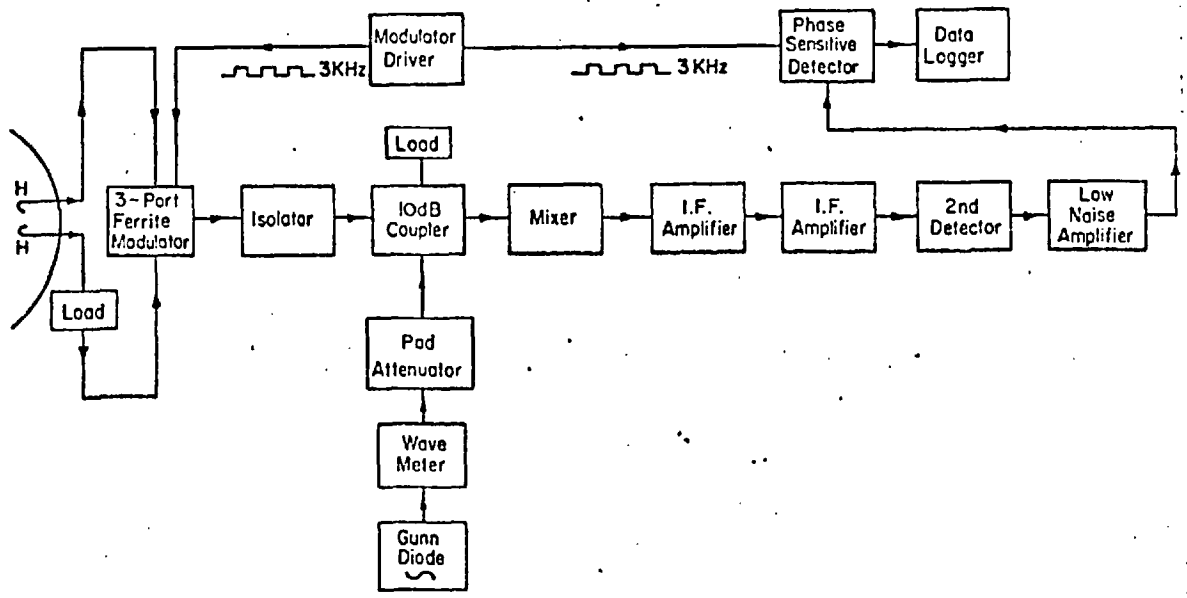


FIGURE 13

3.1.5 The Receiving System

The receiver is basically a Dicke-type radiometer. The incoming radiations are compared to the radiation from an internal load using a Ferrite switch. This switch utilises Faraday rotation to switch the microwave signals entering the two input ports to a common output port. The switch used is a T.R.G. type 140 having a centre frequency of 37.0 GHz and a bandwidth of $\pm$ 1 GHz. Switching is accomplished by energising the Ferrite magnetising coil which is wound around the rotator section. The isolation between ON and OFF states is greater than 30 decibels. The internal load is maintained at a constant temperature with a maximum deviation of 1.0°C. The comparison between load and incoming radiations is made at the rate of 3000 c.p.s. using a square wave.

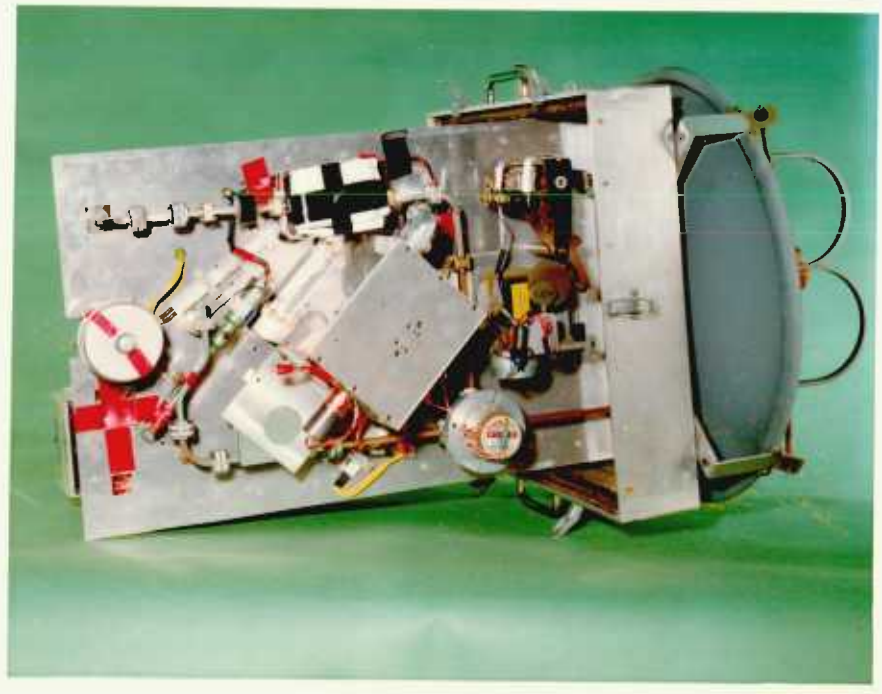


FIGURE 14

An isolator is provided between the Ferrite switch and the mixer so as to prevent any local oscillator signal from reaching the input to the radiometer. This is most important since any leakage of local oscillator power to the Ferrite stages would be reflected back and passed into the receiver, indistinguishable from the true signal. The isolator has an insertion loss in the forward direction of 0.5 dB and a reverse insertion loss of 31 decibels. The radiations coming out of the isolator after passing through a 10 dB coupler are mixed using a Hitachi mixer and local oscillator signal.

A varian VSA-9010 type, solid-state microwave oscillator using the Gunn-effect was used to provide a reliable local oscillator at low cost and without heating problems. The constant current power supply for this oscillator was mounted adjacent to the oscillator. In this manner the changes of fluctuations in the operating voltage are kept to an absolute minimum and since the oscillator is enclosed within the temperature controlled microwave compartment the drift due to temperature change will be very small. The oscillator is tunable over a frequency range of $\pm$ 500 MHz and the output power is approximately 30 mW. The power and frequency temperature coefficient being - 0.02 dB's/^{o}C and - 1.0 MHz/^{o}C respectively. A preset attenuator and a Decca wave meter with its tuning plunger, controlled via a micrometer is also introduced between the local oscillator and 10 dB coupler. The wave meter enables the local oscillator frequency to be set to 37.0 GHz $\pm$ IF. The Q-factor of the cavity in this wave meter is greater than 10,000 giving a frequency accuracy of less than 15 MHz per mm division. The pre-set attenuator is necessary because the mixer will only require a level of about 1 mW of local oscillator power to operate under optimum low noise conditions.

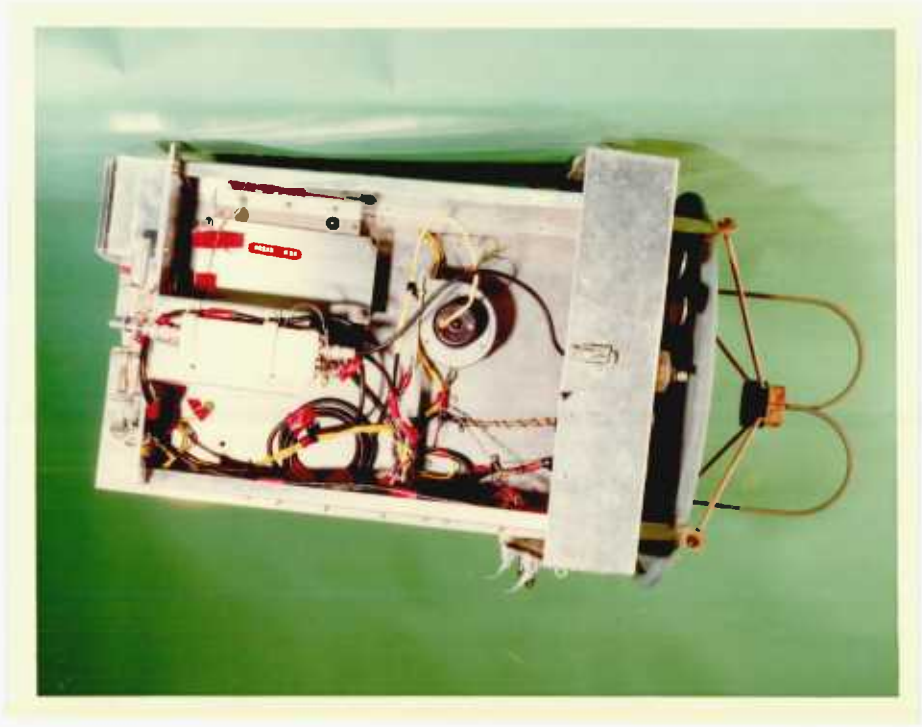


FIGURE 15

The Hitachi mixer has bandwidth compatible with the Ferrite switch and uses a high grade point contact microwave mixer diode (RF diode IN53D). The noise figure of the microwave mixer diode is 9.0 decibels for 1 mW local oscillator input power. A moving coil meter is also mounted adjacent to the mixer in the microwave compartment to monitor the DC crystal currents. The mixer is next mounted directly on to the IF pre-amplifier. The IF amplifier system is designed so that the minimum detectable temperature ΔT for a time constant of 1 second is such that the tangential sensitivity conditions can be achieved with a change in input temperature of less than $1^{o}K$. To meet the above requirement a low noise IF pre-amplifier is followed by a main IF amplifier. The complete system has the following parameters.

Bandwidth to 3 dB points	(80-400) MHz
Voltage gain	82.5 decibels
Noise figure	5.0 decibels
Input impedance	50 Ω
Output impedance	100 Ω

The pre-amplifier gain is 42.0 decibels. Particular attention was given to the gain stability of the IF amplifier against time and temperature by installing thermostatically controlled heaters close to the IF amplifier. The IF amplifier is followed by a detector stage of tangential sensitivity - 50 dB m (For 8 dB S/N at the output) (10-1000 MHz)bandwidth detector has a gain of 23 dB.

The output from the IF amplifier is amplified prior to phase sensitive detection by means of a low noise amplifier (Brookdeal type 450). It has a frequency range of 1 Hz to 300 kHz, a gain of 100 decibels and a typical noise factor of 2 decibels. The linearity is such that the total harmonic distortion will not exceed 0.05%. By use of a high degree of feedback the gain stability is kept to better than 100 parts in 10^6 at full output power.

The amplified composite low-frequency signal is compared with a reference signal from the Ferrite-switch driver unit. The recovery of very small signals (changes in Sun or sky noise temperature) is accomplished by means of "phase" sensitive detector technique followed by a long time constant. The output of the phase sensitive detector is a DC proportional to the difference between the aerial temperature and the temperature of the load. It was operated under 1 sec integration time and (1-10) kHz frequency range. The phase sensitive detector is of high stability i.e. zero drift with temperature is less than 0.005% per ^{o}C of full output. The frequency range is 1 Hz to 1 MHz and under normal operating conditions an output of 3V peak can be obtained.

3.2 Data Recording

The data was recorded using a Telsec Chart Recorder, having seven measuring ranges from 10 mV to 1 V, the recording width of 200 mm. The input impedance varies from 100 K ohms to 11 M ohms depending on the sensitivity range. The paper drive is via a 12 speed gear box and ranges from 1 cm/min down to 0.017 cm/min. The data is recorded on a heat treated chart moving at a speed of 10 cm/hr.

3.3 Calibration of the System

The system was calibrated using three different levels of temperature namely, (i) noise tube; (ii) constant temperature of load and (iii) liquid Nitrogen temperature.

Noise Tube Calibration

The receiver was connected to the noise tube via a calibrated stepped attenuator using a waveguide switch. The noise source is an argon discharge tube (CV1881) having v.s.w.r. 1.2:1 in the fired condition. The noise power output is 16 dB above 290^{o}K corresponding to an effective noise temperature at the output of 11,000^{o}K. Response of the radiometer was obtained by switching the waveguide switch to the noise tube and varying the calibrated attenuator, the insertion loss of the attenuator being less than 0.2 decibels. Six levels of attenuation i.e. 0, 5, 10, 15, 20 and 30 dB could be provided by means of a remote command by operating a cam mechanism. A series of remote operations suggested the levels obtained were approximate only, therefore the response of the radiometer was obtained using different levels of attenuation by setting the attenuator manually before operating it in the field. The frequent checks were made using one level of attenuation only i.e. 14.0 decibels which corresponds to 754.4^{o}K at 295.0 K of ambient obtained from the following relation

$$T_{14.0} = \frac{T_{NT} - T_o}{\alpha} + T_o \qquad (54)$$

where,

T_{NT} = Effective temperature of the discharge tube °K

T_o = Effective temperature of the attenuator °K

α = Coefficient of attenuation.

The 14.0 decibel level was not only used for checking the stability but also to obtain temperature of the Sun-signal using load calibration, the temperature of the attenuator was maintained at the load temperature. The equation used is as follows :-

$$\text{Sun-signal in Kelvins} = \frac{(CH_{SUN} - CH_{LOAD})}{(CHNT_{14.0} - CH_{LOAD})} \cdot (TNT_{14.0} - T_{LOAD}) + T_{LOAD} \qquad (55)$$

where

CH_{SUN} = Sun signal in Chart divisions

CH_{LOAD} = Load signal in Chart divisions

$CH\ NT_{14.0}$ = Noise tube signal at 14.0 decibels in Chart divisions

$TNT_{14.0}$ = Noise tube signal at 14.0 decibels in Kelvins

T_{LOAD} = Temperature of load in Kelvins

The level was introduced in the morning, afternoon and evening.

Load Calibration

The temperature inside the microwave compartment and the load is kept constant to within $\pm$ 1.0°C by installing thermostatically controlled heaters within the compartment. Sudden and rapid changes of outside ambient temperature were avoided by thermally-insulating the inner walls of the microwave compartment.

The load calibration was done by switching the wave guide towards the noise tube and switching off the noise tube. The corresponding reading on the chart was used in obtaining "SUN" and "SKY" temperatures in Kelvins. This calibration was done twice a day.

Liquid Nitrogen Calibration

Because of the non-linear response of the radiometer, the noise tube temperature cannot be used accurately to obtain low sky-noise temperature, therefore liquid nitrogen calibration is important to assess accurately sky noise temperature.

The technique used was to subject the aerial feeds to the emission from liquid nitrogen contained in the container of TOFLEN. An absorbing material called ecosorb, manufactured from carbon impregnated foam was fixed to the bottom of the container and had number of holes of about 2 cm depth so as to reduce the effect of liquid nitrogen reflection. The front-end of the container had just enough opening for the feed in order that the effect of changes in atmosphere are minimum. This simple calibrator is ideal for field calibration of the overall radiometer, because of its size (diameter of the container 12 cms and depth 10 cms). A comparison between this method of calibration and that obtained using waveguide termination immersed in liquid nitrogen were in agreement within the limits of experimental accuracy. This technique gives accurate calibration and was done once a day.

The sky-noise temperature was obtained using the following equation.

$$\text{Sky-signal in Kelvin} = T_{LOAD} - \frac{(CH_{LOAD} - CH_{SKY})(T_{LOAD} - 77.0)}{(CH_{LOAD} - CH_{LN})} \qquad (56)$$

where

T_{LOAD} = Temperature of load in Kelvins

CH_{LOAD} = Load signals in chart divisions

CH_{SKY} = Sky signals in chart divisions

3.4 Experimentation and Analysis

In this program of analysis 37.0 GHz radiometer was operated in a nodding mode i.e. the antenna was mechanically nodded off the Sun by 3^{o} in declination

with a cycle time of 1 minute. To ensure that the receiver has attained the peak value of Sun, the aerial was nodded through the centre of Sun's disc. The half minute of cycle time is equally divided in taking observations on Sun, sky and Sun, the rest of the cycle time is spent in attaining the levels from Sun to sky and sky to Sun.

The attenuation derived from thermal emission measurements (apparent attenuation) is compared to the excess of attenuation (true attenuation) derived from Sun-Sky signals. In an ideal case (no scattering) the attenuation derived from the two methods should be equal. The recorded data were digitised manually every minute on an 8-track paper tape and the records have been analysed on an individual basis. The unattenuated envelope of Sun and sky signal during periods of attenuation was extrapolated[7]. The processing of the edited tape is carried out using a computer. The compiled Fortran program used for the analysis produces a line printer output giving true attenuation, apparent attenuation and error due to scattering for each elevation angle for each data point fed in. The program takes care of the losses in the wave guide system and the background radiation. The Fortran program also gives cumulative results in 0.5 dB steps and in 10° ranges of zenith angle. The attenuation less than 0.5 dB has been ignored.

During periods of intense rain one expects a decrease in the Sun's signal. The reduced Sun signal includes the emission from the rain, and the scattered radiations from rain and ground. During times the antenna is 'off' the Sun, the contribution to the aerial comes not only from the thermal emission from the rain but also from the emitted radiation which have been scattered by raindrops or ground into the beam. In an ideal case (no scattering) the thermal emission term in the Sun signal will be completely balanced by the self emission of the rain. Practically, this is not true and a large proportion of the

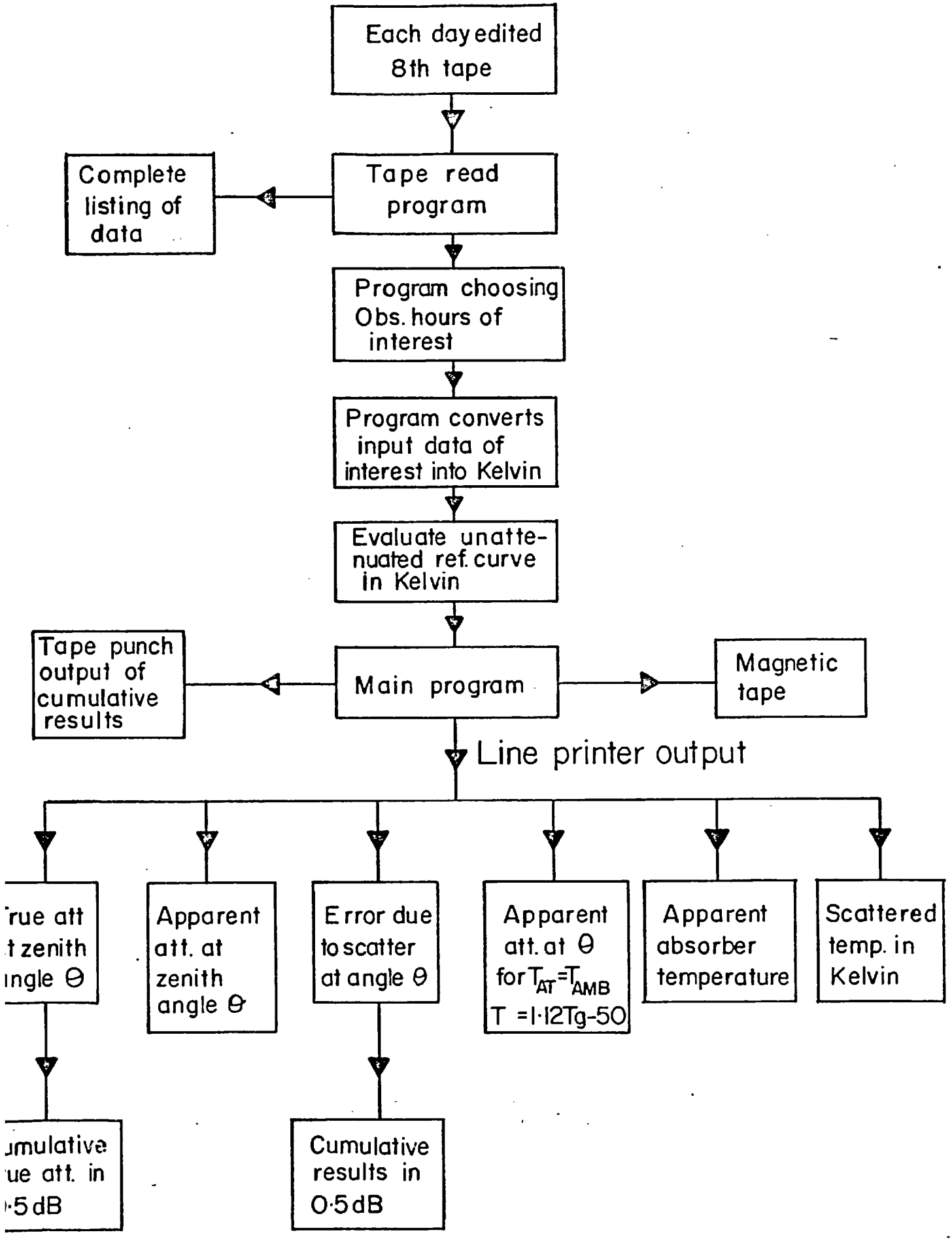


FIGURE 16

NEG. NO. REF NO. 2249/30

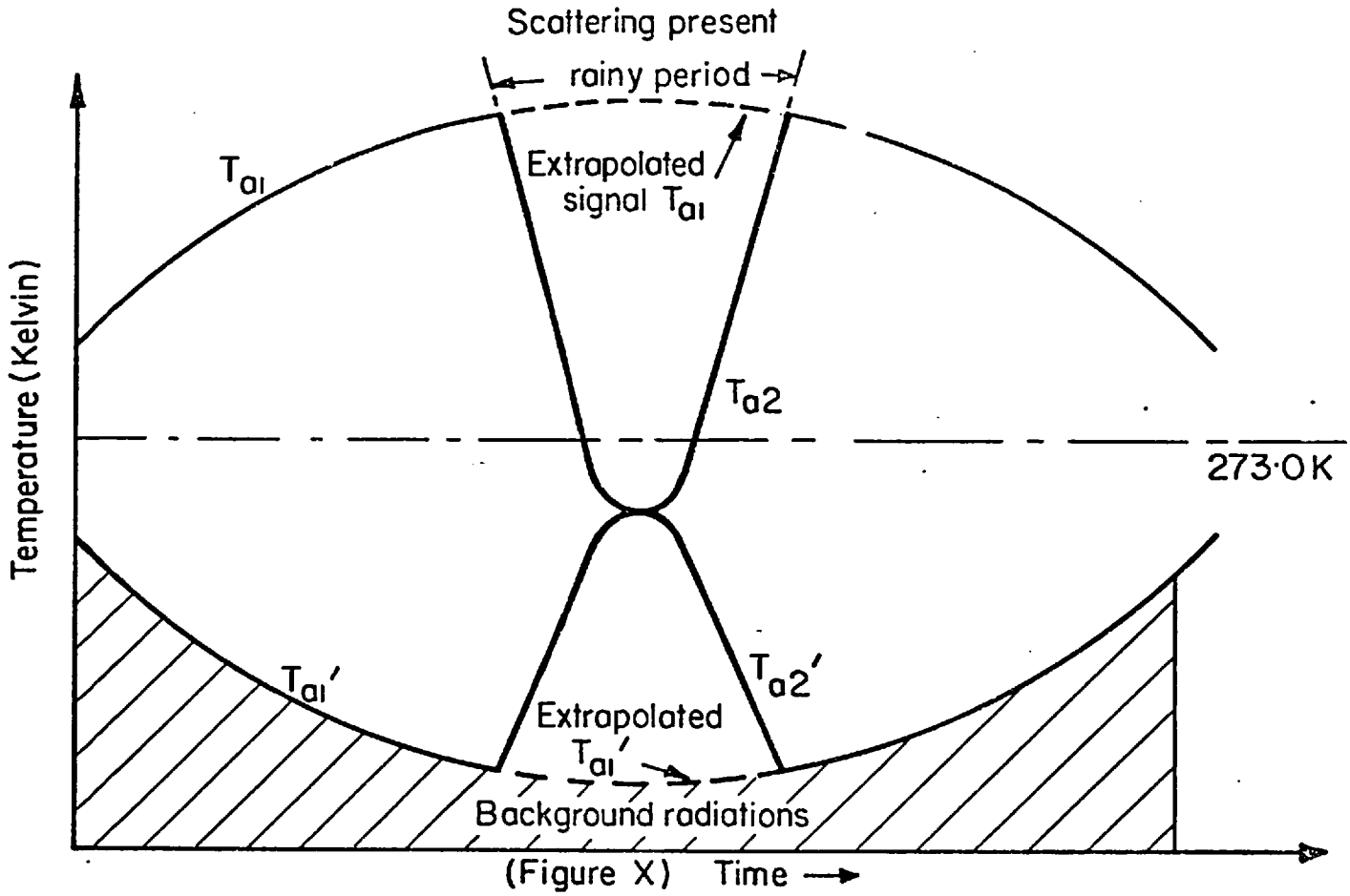
radiation will be scattered out of the Sun-beam and only a small amount of energy will be scattered back into the beam. Radiation will be scattered out of the Sun beam, because of the beam being surrounded by relatively low emission regions. This implies that the excess of attenuation obtained using Sun-Sky signal will not be equal to the attenuation derived from sky only.

This is best explained by referring to figure (17)[13]. Let $T_{a1}(\chi_o)$ and $T_{a1}'(\chi_o)$ represent unpolarised signals due to Sun and atmosphere respectively on a clear day at the zenith angle χ_o. $T_{a2}(\chi_o)$ and $T_{a2}'(\chi_o)$ represent attenuated signals of Sun and Sky respectively on a rainy day. $T_{a2}(\chi_o)$ and $T_{a2}'(\chi_o)$ should in the absence of scattering approach each other and obtain the thermodynamic temperature of rain, i.e. below ambient by 2 K[12]. But because of radiation being scattered, the $T_{a2}(\chi_o)$ and $T_{a2}'(\chi_o)$ tend to meet at a temperature which is much lower than the freezing point of water. Also, the Sun signal dips more in the presence of scattering compared to non-scattering case. The meeting of T_{a2} and T_{a2}' at a much lower temperature than rain temperature in presence of scattering should not be interpreted as though the temperature of rainy medium has changed thereby violating thermodynamic principle. This is the apparent temperature of the medium, and not the actual thermodynamic temperature of rain. The reason for such a difference is scattering.

We treat the above problem mathematically. The basic technique is to point the antenna on the Sun and then in a direction about 3^o away in elevation.

The radiative transfer equation developed by Chandrasekhar[4], governs the energy balance at a position Z along the direction $\bar{K}$ of a ray pencil due to absorption and emission along the path and due to scattering into and out of the path, given by

/Equation (57)



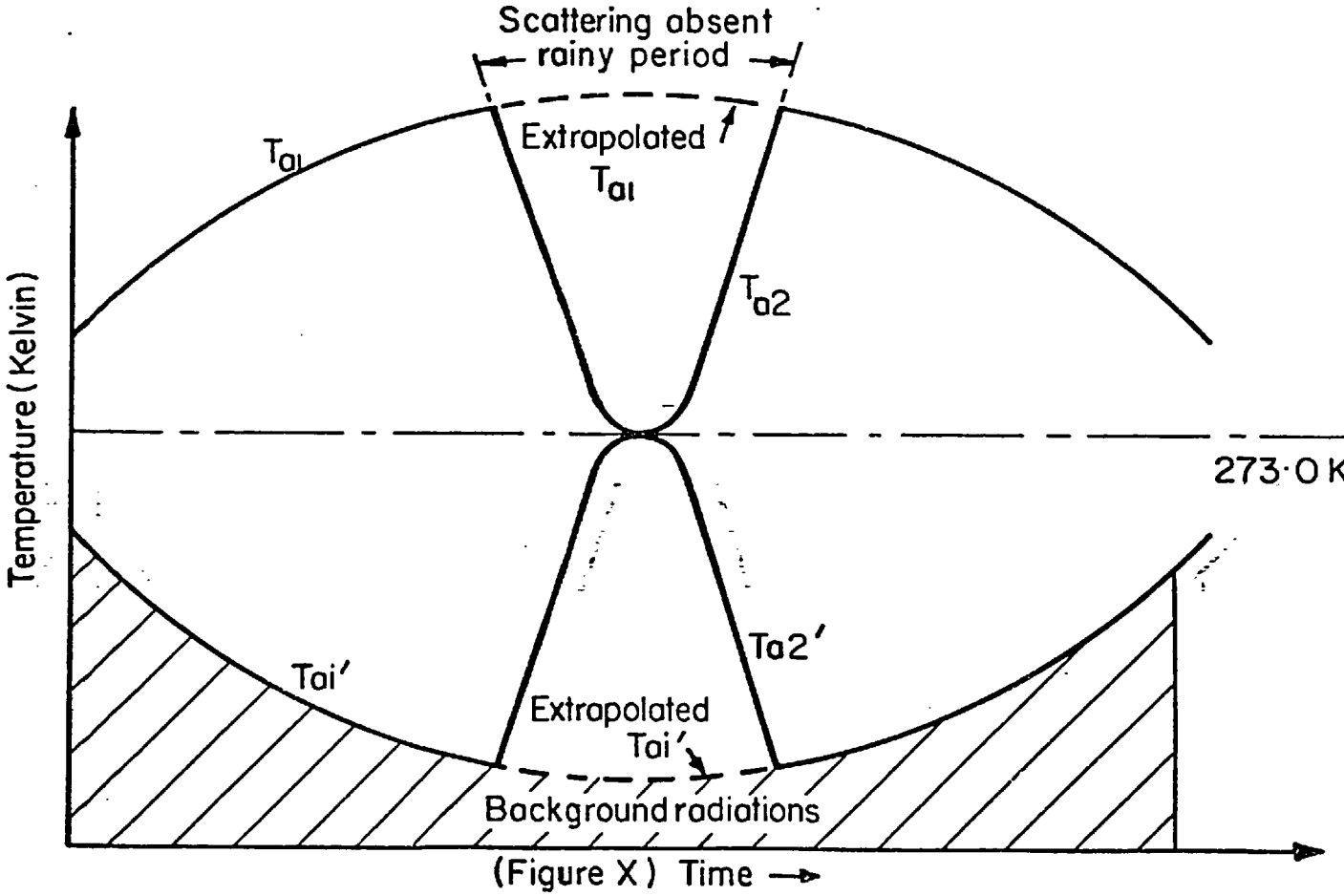


FIGURE 17

REF.NO 2249/2 NEG. NO.

$$-\frac{1}{\alpha(Z)}\frac{d}{dZ}[I(\bar{K},Z)] = [I(\bar{K},Z)] - [E(\bar{K},Z)] \qquad (57)$$

where

$[I]$ = Intensity matrix defining the state of polarisation by four Stokes parameters in Wm^{-2} Hz^{-1} $steradian^{-1}$.

$[E]$ = Source function matrix in Wm^{-2} Hz^{-1}

$\bar{K}$ = unit vector defining the ray pencil

$\alpha(Z)$ = attenuation constant in m^{-1}.

For unpolarised radiation, the solution of (57) in terms of antenna temperature (T_a) can be written as

$$T_a = T_s \exp(-t) + T_b[1 - \exp(-t)] \qquad (58)$$

where

T_b = temperature of some component of atmosphere (e.g. rain) °K

T_s = brightness temperature of the Sun °K

$\exp(-t)$ = transmissivity of the medium

Equation (58) can be modified to take into account the losses in the wave guide, contribution from back and side lobes.

$$T_a = (1 - a_g)\left[\int_{\Omega 1} \frac{G(\theta,\varphi)}{4\pi}\left\{T_s(1 - \gamma_3(\chi)\right\} + \gamma_3(\chi)\, T_b\, d\Omega_1 + \int_{4\pi-\Omega_1} \frac{G(\theta,\varphi)}{4\pi}\left\{\gamma_3(\chi)\, T_g + \rho\, T_b\right\} d\Omega_1\right] + a_g\, Twg$$

where

$G(\theta,\varphi)$ = gain-pattern of the antenna

Ω_1 = solid angle directed towards the sky

T_b = kinetic temperature of atmosphere (in particular, rain) °K

a_g = fractional absorption in wave guide

T_{wg} = temperature of wave guide °K

T_g = temperature of ground °K.

$\gamma_3(\chi)$ = fractional absorption at zenith angle χ during rain

ρ = ground power reflection coefficient

We are assuming that cosmic radiations, and the radiations from radio stars, are extremely small. The terms T_{a1}, T_{a1}', T_{a2}, T_{a2}, are function of zenith angle only.

Clear day ON-SUN Aerial temperature.

$$T_{a1}(\chi) = (1 - a_g) \int_{\Omega_1} \frac{T_s\, G(\theta,\varphi)}{4\pi}\, d\Omega_1 [1 - \gamma_2(\chi)] + (1 - a_g) \int_{\Omega_1} \frac{T_a G(\theta,\varphi)}{4\pi} \gamma_2(\chi)$$

$$\cdot d\Omega_1 + (1 - a_g) \int_{4\pi - \Omega_1} (\gamma_2\, T_g + \rho\, T_a) \frac{G(\theta,\varphi)}{4\pi}\, d\Omega_1 + a_g\, T_{wg} \qquad (59)$$

where

T_a = kinetic temperature of atmosphere on a clear day

γ_2 = fractional absorption on a clear day

Clear day OFF-SUN aerial temperature

$$T_{a1}' = (1 - a_g) \int \frac{T_a\, G(\theta,\varphi)}{4\pi}\, \gamma_2(\chi)\, d\Omega_1$$

$$+ (1 - a_g) \int_{4\pi - \Omega_1} [T_g\, \gamma_2(\chi) + \rho\, T_a]\, d\Omega_1 + a_g\, T_{wg} \qquad (60)$$

/Intense Rainy Day

Intense Rainy Day ON-SUN Aerial temperature

$$T_{a2} = (1 - a_g) \int_{\Omega} \frac{G(\theta,\varphi)}{4\pi} \Big[\Big\{ T_s [1 - \gamma_3(\chi) - s_3(\chi)^* \Big\} + \gamma_3(\chi) T_b \Big] d\Omega_1 + (1 - a_g) \int_{4\pi - \Omega_1} \Big\{ \gamma_3(\chi)\, T_g + \rho\, T_b \Big\} \frac{G(\theta,\varphi)}{4\pi}\, d\Omega_1 + a_g\, T_{wg} \tag{61}$$

where

$s_3(\chi)$ = scattered contribution during rain at zenith angle χ

$^*[\gamma_3(\chi) + s_3(\chi)]$ = fractional extinction at zenith angle χ during rain

Rainy Day OFF-SUN Aerial temperature

$$T_{a2}'(\chi) = (1 - a_g) \int_{\Omega_1} \frac{G(\theta,\varphi)}{4\pi}\, T_b\, \gamma_3(\chi)\, d\Omega_1 + (1 - a_g) \int_{4\pi - \Omega_1} \frac{G(\theta,\varphi)}{4\pi} \Big\{ \gamma_3(\chi)\, T_g + \rho\, T_b \Big\} d\Omega_1 + a_g\, T_{wg} \tag{62}$$

We further assume that the thermal emission is isotropic in nature on a rainy day and scattering on a clear day is too small to be taken into account. γ_2, γ_3, T_a and T_b are constant over the solid angle subtended by the main lobe in receiving the radiations.

Under the above assumptions equations (59) to (62) can be simplified, we can write

$$T_{a1}(\chi) = (1 - a_g) \Big[h \Big\{ T_s\, (1 - \gamma_2(\chi)) + \gamma_2(\chi)\, T_a \Big\} + (1 - h) \Big\{ \gamma_2(\chi)\, T_g + \rho\, T_a \Big\} \Big] + a_g\, T_{wg} \tag{63}$$

$$T_{a1}'(\chi) = (1 - a_g)\left[h\, T_a\, \gamma_2(\chi) + (1 - h)\left\{T_g\, \gamma_2(\chi) + \rho\, T_a\right\}\right] + a_g\, T_{wg} \quad (64)$$

$$T_{a2}(\chi) = (1 - a_g)\left[h\, T_s\left\{1 - \gamma_3(\chi) - s_3(\chi)\right\} + h\, \gamma_3(\chi)\, T_b + (1 - h)\left\{\gamma_3(\chi)\, T_g + \rho\, T_b\right\}\right] + a_g\, T_{wg} \quad (65)$$

$$T_{a2}'(\chi) = (1 - a_g)\left[h\, T_b\, \gamma_3(\chi) + (1 - h)\left\{T_g\, \gamma_3(\chi) + \rho\, T_b\right\}\right] + a_g\, T_{wg} \quad (66)$$

Rearranging the above equations

$$T_{a2} - T_{a2}' = [1 - \gamma_3(\chi) - s_3(\chi)].h.T_s\,(1 - a_g)$$
$$T_{a1} - T_{a1}' = [1 - \gamma_2(\chi)].h.T_s\,(1 - a_g) \quad (67)$$

True attenuation in decibels $= \alpha_{True} = 10\ \mathrm{Log}_{10}\left\{\dfrac{1 - \gamma_2(\chi)}{1 - \gamma_3(\chi) - s_3(\chi)}\right\}$

Now during periods of rain whatever is absorbed will be radiated

$$\gamma_3(\chi)\, T_b = \alpha_a\, \gamma_2(\chi)\, T_a + (1 - \alpha_a)\, T_m$$

T_m = mean atmospheric absorption temperature

$\alpha_a(\chi)$ = apparent fractional transmission at zenith χ

$$T_{a2}'(\chi) = (1 - a_g)\left[h\left\{(\alpha_a(\chi)\, \gamma_2(\chi)\, T_a + (1 - \alpha_a(\chi))\, T_m\right\} + (1 - h)\,(T_g\, \gamma_3(\chi) + \rho\, T_b)\right] + a_g\, T_{wg}$$

or $$T_{a2}'(\chi) = (1 - a_g)(1 - \alpha_a(\chi))\, T_m + \alpha_a(\chi)\,[T_{a1}'(\chi) - a_g\, T_{wg} - X_2] \quad (68)$$

$+ X_1 + T_{wg}.a_g.$

where

$$X_1 = [T_g \gamma_3 (\chi) + \rho T_b] (1 - h)(1 - a_g)$$

$$X_2 = [T_g \gamma_2 (\chi) + \rho T_a] (1 - h)(1 - a_g)$$

Rearranging equation (68), we get

$$\alpha_a(\chi) = \frac{T_{a2}'(\chi) - a_g T_{wg} - h(1 - a_g)T_m - X_1}{T_{a1}'(\chi) - a_g T_{wg} - h(1 - a_g)T_m - X_2} \tag{69}$$

Apparent attenuation in decibels = $\alpha_{Apparent} (\chi) = 10 \text{ Log}_{10} \left[\frac{1}{\alpha_a(\chi)}\right]$

Error due to scattering = $[\alpha_{True} (\chi) - \alpha_{Apparent} (\chi)]$ (70)

It is expected that first order scattering will only be detected because of uncertainty in T_m.

4. EXPERIMENTAL-TECHNIQUE FOR STUDYING POLARISATION PROPERTIES

As is clear from section (2), to study the polarisation properties of the emitted and scattered radiations and their effects on passive millimetre radiometer measurements on an Earth space path, the experiment must be capable of measuring four parameters simultaneously or in short duration during which storm conditions do not change. These parameters are True horizontal attenuation, apparent horizontal attenuation, True vertical attenuation and apparent vertical attenuation. The polarisation properties of the emitted energy by rain was studied by building a cross-polarised radiometer and operating it in a 'Fixed Elevation Thermal-Emission Mode', and that of scattered energy and its effect on passive radiometry during intense rain using a 'Nodding Cross-Polarised Radiometer'. The cross-polarised radiometer as such is basically a Dicke-receiver receiving two linear perpendicular polarisations in a short span of time. The associated equipment is discussed in the following section.

4.1 Experimentation for Studying Polarisation Properties of Emitted Energy (including scattering) by Rain

4.1.1 Equipment Mounting

The cross-polarised receiver is placed immediately behind the antenna and could be carried by a weather-proof equatorial mount discussed in section (3.1.1). The hour angle drive and declination drive were switched off so that the radiometer could be operated in a fixed elevation mode. The equatorial mount was adjusted so that the aerial was looking towards the south-west at an elevation of 35.8 degrees; exact elevation was obtained from the Sun's co-ordinates as the axis of the mount is aligned accurately parallel to the axis of the Earth's rotation.

4.1.2 Aerial and Aerial Feeds

General design requirements for the polarised aerial feeds in association with the parabolic reflector are

(i) It should respond equally and independently to two perpendicular linearly polarised radiations.

(ii) Any variation in response should be identical in magnitude and phase for both polarisations.

(iii) The aerial should be well matched to the receiver for either of the polarisations.

It is difficult to achieve the above requirements, but they can be approached by careful design. The requirements (i) and (ii) both depend on the physical and electronic symmetry of the aerial system, and on the perfection of the Ferrite switch. Requirement (ii) is difficult to achieve but if the gain function is equally smooth, without large superimposed variations, it will be satisfactory. The last requirement is mainly a matter of feed design and implies that VSWR must be less than 1.02:1.

The aerial is an 18" diameter parabolic reflector having horizontal and vertical copper wave guide feeds at its focus. The aerial is basically the same used earlier in the experiment (section 3.1.3). The polarised aerial feeds are connected to the programmed ON/OFF electronic attenuator inside the microwave cabin.

Because of the non-availability of a proper anechoic chamber, the present aerial response was obtained using the Sun as a point source and the beam widths for horizontal and vertical polarisations were found to be 1.3^{o} and 1.2^{o} respectively (Appendix A2), allowing for the finite source width. The peaks of the curves are separated by approximately 3.0 degrees in declination. This figure was confirmed not only by a drift curve in the Right Ascension plane but also by moving the aerial in declination. As such no overlapping of the horizontal and vertical pattern was observed, when the present aerial is nodded on and off the Sun, if at all it is imbedded in the noise of the receiver.

Both the feeds were covered with a small plastic cylinder.

4.1.3 The Receiving System and Calibration

The layout of the cross-polarised radiometer is shown in Figure (18). The microwave components used in the receiving system are the same as those discussed earlier in section (3.1.5) except for the electronic ON/OFF attenuator in the vertical feed. The TRG Ferrite switch was programmed to act as an ON/OFF attenuator with a time period of 1 minute, the maximum attenuation introduced during 'ON' period being 30.0 decibels. A square wave of time period 1 minute i.e. 0.0167 cycles per second was used to energise the Ferrite magnetising coil wound around the rotator section. The associated electronics for driving the switch is discussed in Appendix (A4).

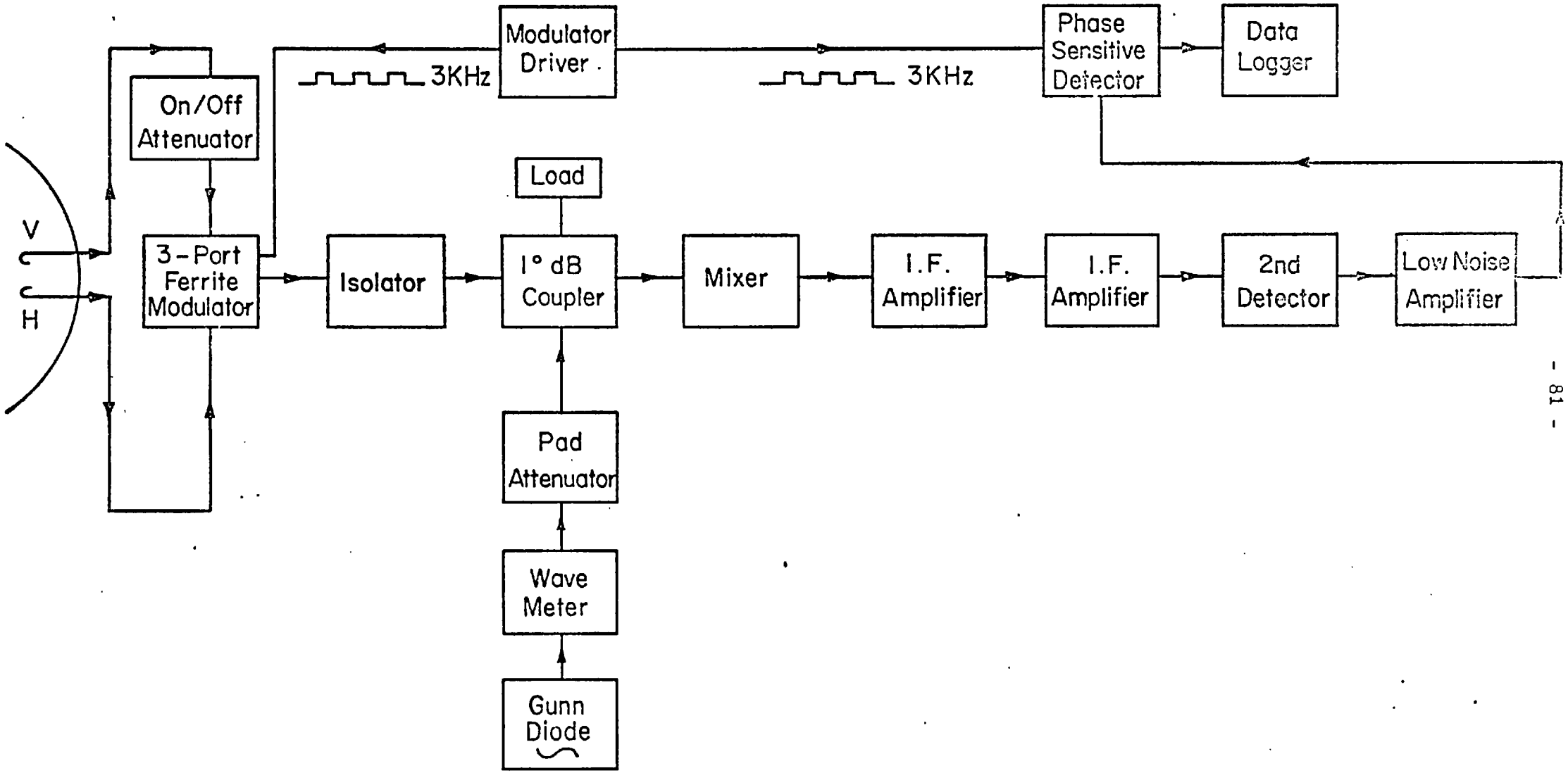

Modulator Driver
3KHz
3KHz
Phase Sensitive Detector
Data Logger
On/Off Attenuator
Load
V
H
3-Port Ferrite Modulator
Isolator
10 dB Coupler
Mixer
I.F. Amplifier
I.F. Amplifier
2nd Detector
Low Noise Amplifier
Pad Attenuator
Wave Meter
Gunn Diode

FIGURE 18

By introducing the ON/OFF attenuator we could compare not only the incoming horizontal radiation with the vertical radiation but also the horizontal radiation with the radiation from an internal load for simultaneous measurement of absolute horizontal attenuation. Using the TRG Ferrite switch the receiver could be switched continuously between vertical and horizontal feeds. This mode of operation corresponds to the attenuator in the 'OFF' position. The latter parts of the receiver i.e. isolator, mixer, IF amplifier, low noise amplifier, source and phase sensitive detector are the same for both the polarisations. Therefore internal phase changes of the system and fluctuations in source output will be common to both. The reference for the phase sensitive detector was obtained from the Ferrite switch itself i.e. a square wave. The output of the phase sensitive detector is proportional to the difference of vertical and horizontal aerial temperatures. Basically the operation performed by the phase sensitive detector corresponds to multiplying the signal by a square wave and performing Fourier analysis of the input signal.

During periods when the attenuator is in 'ON' position due to 30.0 decibels of attenuation in the vertical beam, it effectively acts as a load. In this mode, therefore, the receiver is being switched between incoming horizontal radiations and the radiations from the load. The output from the phase sensitive detector is proportional to the difference of horizontal aerial temperature and the load, thus enabling us to measure simultaneously horizontal attenuation. The operation of the system has already been discussed in section (3.1.5).

In order to provide information about short-lived events, the number of noise pulses per second defined by the IF bandwidth, are averaged after detection over a short time. Since this post-detection integration

time is also inversely proportional to the sensitivity of the receiving system, the phase sensitive detector was adjusted to a compromise 1.0 sec time constant. Although the very wide IF bandwidth (80-400) MHz used does degrade the performance of the cross-polarised radiometer through dissimilarities in phase characteristics of cross-polarised channels, the advantage of sensitivity outweighs the above disadvantage.

The output was recorded on heat-treated charts using a Telsec Chart recorder moving at a speed of 10 cm/hr. The overall system response was obtained using two different levels of calibration

(i) Ambient temperature

(ii) Liquid Nitrogen temperature

The above calibrations were done only when the ON/OFF attenuator is in the 'ON' position.

4.2 Experimentation and Analysis

The cross-polarised radiometer was operated at a fixed elevation of 35.0^{o}, receiving radiation emitted by rain. The difference between vertical and horizontal, and absolute value of horizontal aerial temperature are recorded simultaneously. In order to interpret the results accurately, the attenuation encountered by incoming radiation in the two polarised feeds should be equal up to the Ferrite switch. Another important condition is that the gain response of the high frequency section should remain the same from one polarisation state to another. The attenuation in the two different polarised paths differed because of the extra length of wave guide used in the horizontal path. Therefore some extra attenuation was introduced in the vertical beam, and the attenuation in each beam is 1.2 dBs.

A simple experiment was conducted to verify the above. The receiver was switched between two loads maintained at constant temperature, connected at

the ends of the Ferrite switch. The output was recorded on the chart recorder. Then one of the loads was removed and the receiver was switched between load and horizontal feed (end of feed at the temperature of load) and the output level recorded. The difference of the two levels represents the insertion loss of the horizontal feed. The above experiment was repeated by connecting vertical feeds with the ON/OFF attenuator in place of horizontal feed, and the insertion loss was obtained. Extra attenuation in the vertical feed was introduced; until the two insertion losses become equal. The experiment could have been better performed by maintaining the load temperature much higher than ambient i.e. $22.0^{\circ}C \pm 1.0^{\circ}C$. Unfortunately, this could not be done due to lack of a proper constant heating furnace. A further check on the accuracy of the above experiment was conducted using the Sun as the intense source during field operation. During 'OFF' position of the ON/OFF attenuator, the vertical and horizontal feeds were focussed in turn on the Sun on a clear day. The output was found to be the same, within experimental limits.

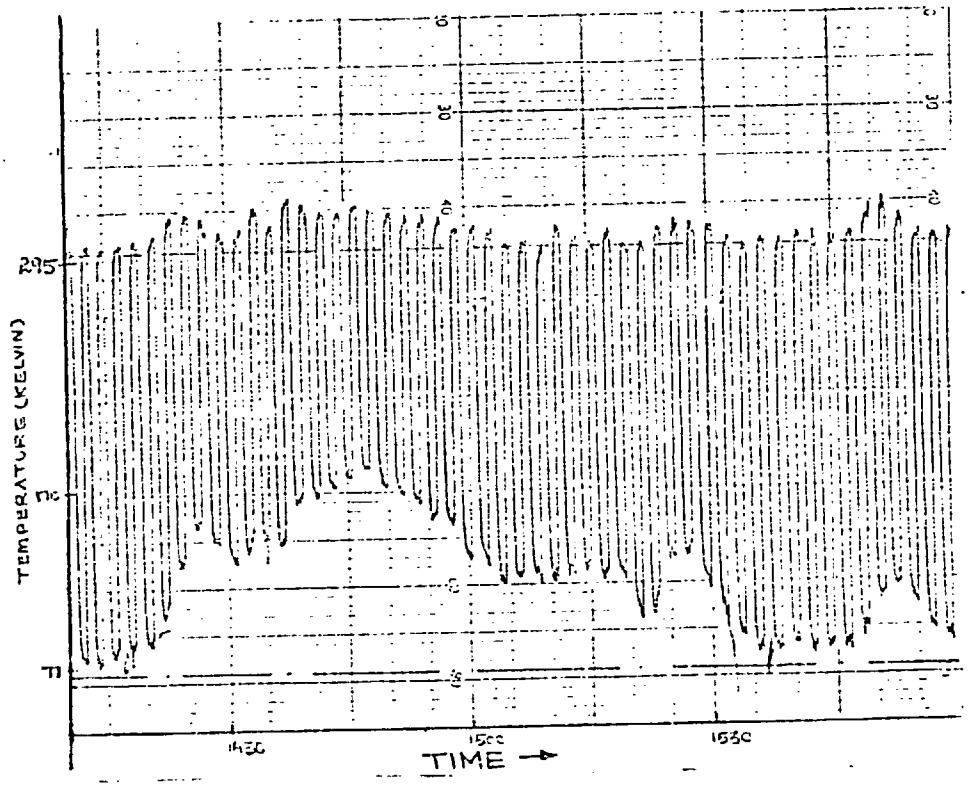
The recorded results were analysed using calibrated levels and the references obtained from clear day record. Figure (19) shows one of the recorded outputs during an intense period of rain on 30th April 1976. Any positive increase above zero corresponds to a positive difference of $T_{AH} - T_{AV}$ i.e. the horizontal aerial temperature greater than the vertical aerial temperature, and any reading below zero correspond to $T_{AV} > T_{AH}$.

Vertical aerial temperature was obtained by subtracting the difference from the horizontal aerial temperature and the corresponding attenuation evaluated using equation (58) derived in section (3.4) and is as follows

$$\underset{\text{dB's}}{\alpha_{AV}}(\chi) = 10\ \text{Log}_{10}\left[\frac{T_{a1}{}'_{V}(\chi) - ag\,T_{wg} - h_{v}(1 - ag)\,T_{m} - X_{2v}}{T_{a2}{}'_{V}(\chi) - ag\,T_{wg} - h_{v}(1 - ag)\,T_{m} - X_{1v}}\right] \qquad (71)$$

Clear Day Polarisation Difference – – – – –

Clear Day Reference for Horizontal Polarisation ——— · ——— · ———



Recording of cross-polarised Radiometer on 30th April, 76

FIGURE 19

Similarly, for the horizontally polarised radiometer, we can write

$$\alpha_{AH}(\chi) = 10 \text{ Log}_{10}\left[\frac{T_{a1}'_H(\chi) - ag\, T_{wg} - h_H(1 - ag)T_m - X_{2H}}{T_{a2}'_H(\chi) - ag\, T_{wg} - h_H(1 - ag)T_m - X_{1H}}\right] \qquad (72)$$

where

$T_{a1}'_V(\chi) = T_{a1}'_H(\chi)$ = Antenna temperature due to atmosphere on a clear day at zenithal χ. °K

T_{a2V} = Antenna temperature of vertically polarised radiometer due to Sun on a rainy day at zenithal χ. °K

$T_{a2}'_V$ = Vertically polarised antenna temperature due to atmosphere on a rainy day at zenithal χ. °K

T_{a2H} = Horizontally polarised antenna temperature due to Sun on a rainy day at zenithal χ. °K.

$T_{a2}'_H$ = Horizontally polarised antenna temperature due to atmosphere on a rainy day at zenithal χ. °K

$\alpha_{AH}(\chi)$ = Apparent horizontal attenuation (dB's) at χ

$\alpha_{AV}(\chi)$ = Apparent vertical attenuation (dB's) at χ

$X_{1H} = [T_g\, \gamma_{3H}(\chi) + \rho_H\, T_b]\, [1 - h_H]\, [1 - ag]$

$X_{1V} = [T_g\, \gamma_{3V}(\chi) + \rho_V\, T_b]\, [1 - h_V]\, [1 - ag]$

$X_{2H} = [T_g\, \gamma_{2H}(\chi) + \rho_H\, T_a]\, [1 - h_H]\, [1 - ag]$

$X_{2V} = [T_g\, \gamma_{2V}(\chi) + \rho_V\, T_a]\, [1 - h_V]\, [1 - ag]$

ρ_H, ρ_V = Horizontal ground power reflection coefficient, vertical ground power reflection coefficient.

T_g = Temperature of ground °K.

ag = Fractional absorption in wave guide

T_{wg} = Temperature of wave guide °K.

T_m = Mean absorption temperature of the atmosphere. °K.

T_a, T_b = Effective kinetic temperature on a clear and rainy day °K.

γ_{3H}, γ_{3V} = Horizontal and vertical fractional absorption on a rainy day.

γ_{2H}, γ_{2V} = Horizontal and vertical fractional absorption on a clear day.

h_H, h_V = Horizontal and vertical radiation pattern of antenna.

5. EXPERIMENTAL TECHNIQUE FOR STUDYING THE EFFECT OF POLARISED SCATTERED RADIATION ON PASSIVE RADIOMETER MEASUREMENTS

5.1 Equipment

5.1.1 Mounting and Aerial

The mounting and tracking for this experiment is basically the same as that discussed in section (3.1). The movement of the mount was controlled in such a way that if the horizontal beam is ON-Sun then the vertical beam is OFF-Sun or vice versa, with a cycle time of 1 minute. This nodding technique for the cross-polarised radiometer demands extra-design requirements for the aerial used, beside those discussed in section (4.1.2), which are as follows

(i) There should not be any overlapping of radiation-patterns while the beams are 3^o apart.

(ii) The aerial should receive adequate power from the quiet Sun and the response should be equal.

(iii) The beam width should not be so narrow that excessive steering accuracy is required.

All the above requirements are achieved (section (4.1.2)) by careful approach and design. The beam width of horizontal and vertical polarised

aerials at half power point is 1.3^{o} and 1.2^{o} respectively.

5.1.2 Receiving System

The layout of the cross-polarised receiving system is shown in Figure (20). It is essentially two perpendicularly polarised Dicke radiometers for the measurement of incoming radiations with respect to the load. Two Ferrite switches in the path of the polarised radiation compare either of the polarisations to the r.f. radiation from the load maintained at constant temperature. Either of the receivers separately uses point contact microwave mixers (RF Diode 1N53D), and IF amplifiers with a pass band of (80-400) MHz. The source is a solid state microwave oscillator at 37.0 GHz manufactured by EMI-Varian of VSA-9010 type and is common to both the receivers. Therefore noise from the source and its output changes will contribute to the receivers to the same extent. For the measurement to be meaningful it is important that the gains of the high frequency sectionsare equal. The output of either receivers after audio detection and amplification is fed to separate phase sensitive detectors set to 1 sec integration time constant. The references for the phase sensitive detectors are derived from the Ferrite switches themselves.

Both the receiver's microwave sections are enclosed in a weather-proof and temperature controlled cabin and are placed immediately behind the aerial. The temperature of the cabin was maintained at $22.0^{o}C$ using thermostatically controlled heaters. The constant current power supply for the Gunn-diode was mounted adjacent to the oscillator so as to keep fluctuations in the operating voltage to the minimum. Basically the set-up and the function of the components for individual polarisations is the same as discussed in section (3.1.5). The receivers before operating in the field were tested under normal conditions of operation and showed that either of the receivers was able to detect change in input temperature of

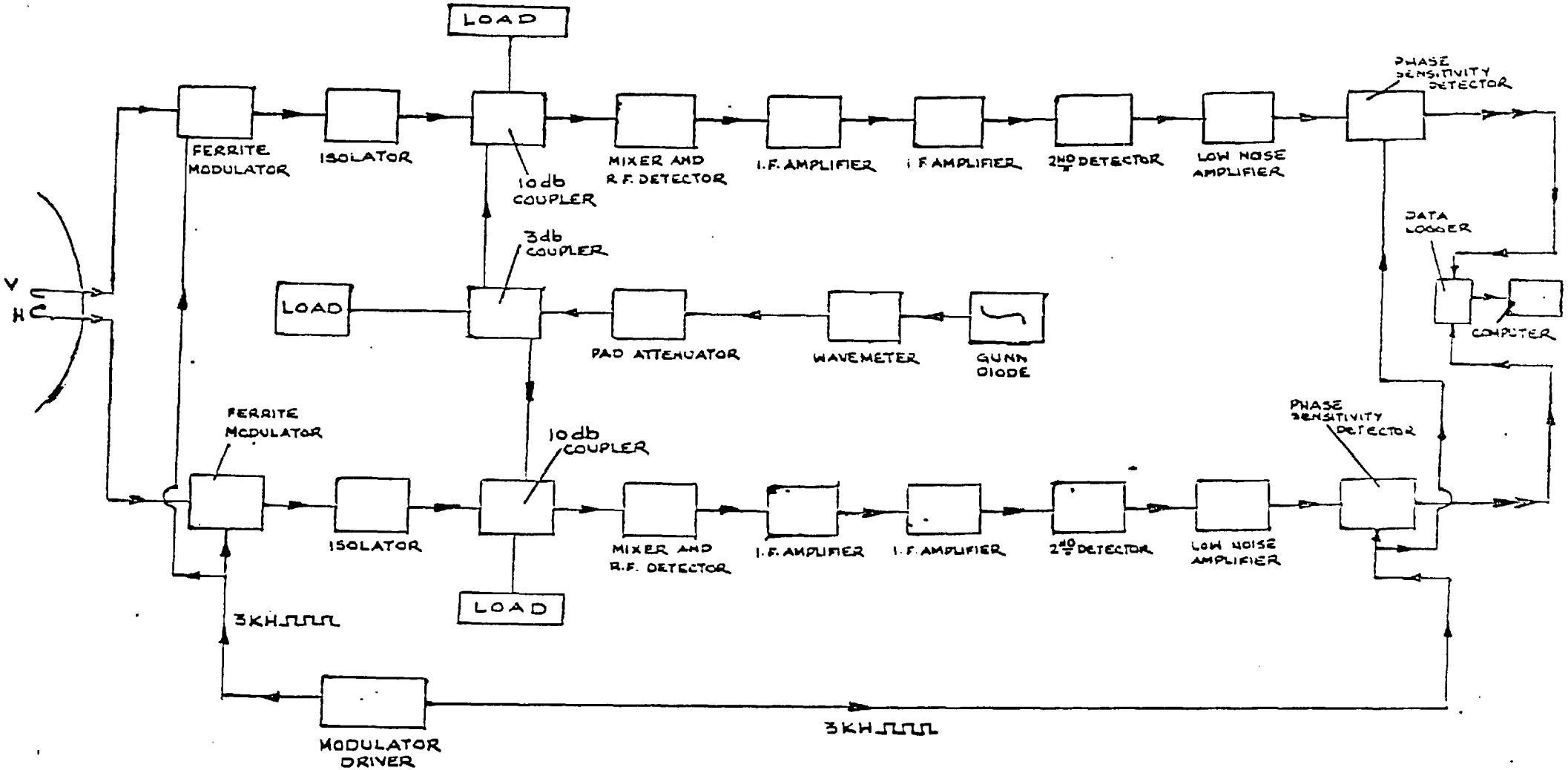

LOAD
FERRITE MODULATOR
ISOLATOR
10db COUPLER
MIXER AND R.F. DETECTOR
I.F. AMPLIFIER
I.F. AMPLIFIER
2ND DETECTOR
LOW NOISE AMPLIFIER
PHASE SENSITIVITY DETECTOR
DATA LOGGER
COMPUTER
3db COUPLER
LOAD
PAD ATTENUATOR
WAVEMETER
GUNN DIODE
V
H
FERRITE MODULATOR
10db COUPLER
ISOLATOR
MIXER AND R.F. DETECTOR
I.F. AMPLIFIER
I.F. AMPLIFIER
2ND DETECTOR
LOW NOISE AMPLIFIER
PHASE SENSITIVITY DETECTOR
LOAD
3KH
MODULATOR DRIVER
3KH

FIGURE 20

$1.0^{o}K$. The check on gain stability showed that after a few hours of operation the receivers were stable in gain to within 2%.

5.2 Recording and Calibration

The outputs from the two cross channels were recorded separately on heat treated charts using the Telsec-Chart recorder. The speedsof both charts were synchronized to 1/6 cm/min and zero level reading was the same on both the charts.

The system was calibrated in Kelvins using a noise tube*, liquid nitrogen and ambient temperature as discussed in section (3.3). The liquid nitrogen container had just enough of an opening for both the feeds, so as to calibrate both the systems simultaneously.

5.3 Experimentation and Analysis

The analysis program used is essentially the same as that discussed in Section (3.4) and was applied separately to the two polarised radiometers. The cross-polarised radiometer was nodded on and off the Sun by 3^{o} in declination beside following it, so that if the horizontal beam is ON-Sun then the vertical beam is OFF-Sun or vice versa with a cycle time of 1 minute. Within 1 minute we were able to record four sets of readings needed for analysis during rainy periods, namely horizontal sky signal ($T_{a2'H}$), horizontal Sun signal (T_{a2H}), vertical sky signal ($T_{a2'V}$) and vertical Sun signal (T_{a2V}). Out of one minute cycle time, ½ minute is spent taking observations and the remaining time is spent in attaining Sun to sky and sky to Sun level by the nodder. The scattering error is obtained by comparing the attenuation derived from the thermal emission method with time attenuation derived from Sun-sky signals for either of the polarisations.

---

* Due to lack of space in the microwave cabin the noise tube reduced by 14.0 dBs could only be introduced in the vertically polarised radiometer and in the final analysis it was assumed that the same level of noise tube is applicable for horizontally polarised radiometer.

The recorded data were digitised every minute on an 8-track paper tape. The unattenuated envelope of Sun and sky signal during periods of rain was extrapolated[7] and the analysis was carried out using a compiled Fortran Program. The program takes care of the waveguide losses and changes in background radiations. The horizontal and vertical attenuation from the thermal emission measurements was calculated using equations(71) and (72) respectively. The true horizontal and vertical attenuation, and the corresponding scattering error was calculated using the following equations derived in Section (3.4).

$$\alpha_{TV}(\chi) = 10 \text{ Log}_{10}\left[\frac{T_{a1V}(\chi) - T_{a1}{}'_{V}(\chi)}{T_{a2V}(\chi) - T_{a2}{}'_{V}(\chi)}\right] \tag{73}$$

$$\alpha_{TH}(\chi) = 10 \text{ Log}_{10}\left[\frac{T_{a1H}(\chi) - T_{a1}{}'_{H}(\chi)}{T_{a2H}(\chi) - T_{a2}{}'_{H}(\chi)}\right] \tag{74}$$

From equation (60) and (61)

$S_H(\chi)$ = Horizontal scattering error at $\chi = \alpha_{TH}(\chi) - \alpha_{AH}(\chi)$ (75)

$S_V(\chi)$ = Vertical scattering error at $\chi = \alpha_{TV}(\chi) - \alpha_{AV}(\chi)$ (76)

where

$\alpha_{TV}(\chi)$, $\alpha_{TH}(\chi)$ = True vertical and horizontal attenuation respectively in decibels at zenithal χ.

$T_{a1V}(\chi)$, $T_{a1H}(\chi)$ = Vertical and horizontal aerial temperature respectively due to Sun on a clear day at χ.

$T_{a1}{}'_{V}(\chi)$, $T_{a1}{}'_{H}(\chi)$ = Vertical and horizontal antenna temperature respectively due to atmosphere on a clear day at χ.

$T_{a2V}(\chi)$, $T_{a2H}(\chi)$ = Vertical and horizontal antenna temperature respectively due to Sun on a rainy day.

$T_{a2'V}(\chi)$, $T_{a2'H}(\chi)$ = Vertical and horizontal aerial temperature respectively due to atmosphere on a rainy day.

In order that the above analysis could usefully be interpreted it is important that the gain of the high frequency section of the two receivers is the same. A noise tube reduced by 14.0 decibels was alternately connected to the two receivers and the IF output was measured using a Hewlett-Packard power meter. The IF output was equalized by introducing extra insertion loss in the horizontal channel using a TRG Ferrite seitch. This was done by slightly off-setting the current applied to the Ferrite magnetizing coil.

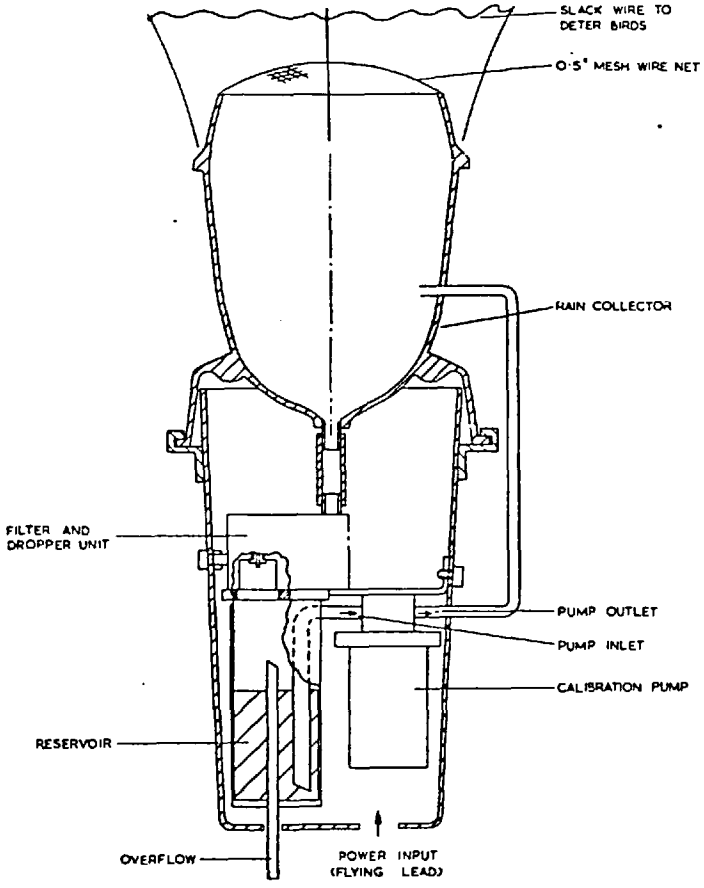
This particular experimentation is ideally suited for short duration rain during the day. Any observation far removed from mid-day i.e. early morning or late afternoon needs polarisation correction because the electric vector which is perpendicular at zenith is inclined to the vertical at different zenith angles. Therefore the feed assembly will rotate at angles w.r.t. to zenith position as the radiometer traverses through the sky, which is discussed in detail in Section (8.0).

6. Rainfall Measurements

Rainfall data was obtained from rapid response rain gauge (Figure (21)) and was operational at about 120 metres from the radiometer. The rainfall data was kindly provided by Dr. Norbury.

The response time of the rain gauge is in the region of 10-20 sec and is mainly determined by the time delay between the catcher and dropper unit. The collected water after channelling through the filter is converted into drops of constant volume by dropper unit. These drops are detected when they intersect the light beam between a light bulb and a photo-transistor. The rainfall rate is determined by the collector area and the number of drops per second.

Time and rainfall rate records were produced in paper tape form by a Data



RAIN GAUGE

FIGURE 21

logging system using the output pulses produced by the photo-transistor. The final analysis was done to yield results only for the days and time the radiometer was operational using computer.

7. Long-Term Performance

Since installing the equipment at Appleton Laboratory, Slough, it has been run continuously from December 1974-December 1975 as a 37.0 GHz Nodding Radiometer. The aerial system, the mounting and the driving mechanism have been trouble free except on occasions when the driving motor was switched off due to jamming of a 1:250 reduction gear box. After proper alignment of the mount, the Sun could be tracked accurately during the day and was within the beam next morning. However, the hour angle drive was checked every morning and the radiometer calibrated using the noise tube, load and liquid nitrogen. There were occasions when the radiometer could not be calibrated using liquid nitrogen because of its non-availability.

The receiving system during the term of operation suffered only one component failure i.e. jamming of the waveguide switch, and has also been incapacitated on a small number of occasions by power supply and local oscillator failures. Due to inadequate cooling of the microwave receiving system, the overall performance of the receiver deteriorated on hot days and therefore was switched off.

Later, the above system was converted to a cross-polarised radiometer for fixed angle operation and in Nodding mode. The operation of fixed angle cross-polarised radiometer during period February 1976-April 1976 has been absolutely trouble free as the system did not have any mechanical movable part and was completely electronic. The Nodding cross-polarised radiometer could only be operated for three months and some difficulties with the nodder was observed and corrected. The output of a horizontally polarised radiometer showed a shift in its zero level on occasions and the fault was due to malfunctioning of the phase sensitive detector. It was rectified and otherwise the overall performance of the radiometers has been satisfactory.

8. A COMPLETE SURVEY OF POSSIBLE ERRORS IN THE MEASUREMENT

The present system can be used to measure attenuation up to 18 dB with an accuracy of 1 dB, when used in the Sun-tracking mode. The maximum measurable attenuation in thermal emission mode is 13.0 dB with an accuracy of 1·0 dB. However, we consider all possible errors in our measurement:

(a) Calibration accuracy

(b) Error due to changes in radiation pattern

(c) Contribution from background radiation

(d) Error in calculating attenuation from absorption

(e) Error in the measurement of extinction.

(a) Calibration Accuracy

The system was calibrated using three different sources (i) noise tube, (ii) liquid nitrogen and (iii) load at 295 K. The three equations for the calibration can be written using equivalent circuits shown in Figure (22).

$$T_1 = \text{Noise tube calibration} = \left\{ \frac{T_g}{La'd} + \left(1 - \frac{1}{La'd}\right) T_o \right\} + \frac{T_a}{a'.b.d} + \left(1 - \frac{1}{a'b.d}\right) T_o \quad (77)$$

$$T_2 = \text{Liquid Nitrogen calibration} = \left\{ \frac{T_g'}{a'd} + \left(1 - \frac{1}{a'd}\right) T_o + \frac{T_g''}{b} \right\} \quad (78)$$

$$T_3 = \text{Load calibration} = \frac{T_g''}{a'd} + \left(1 - \frac{1}{a'd}\right) T_o \quad (79)$$

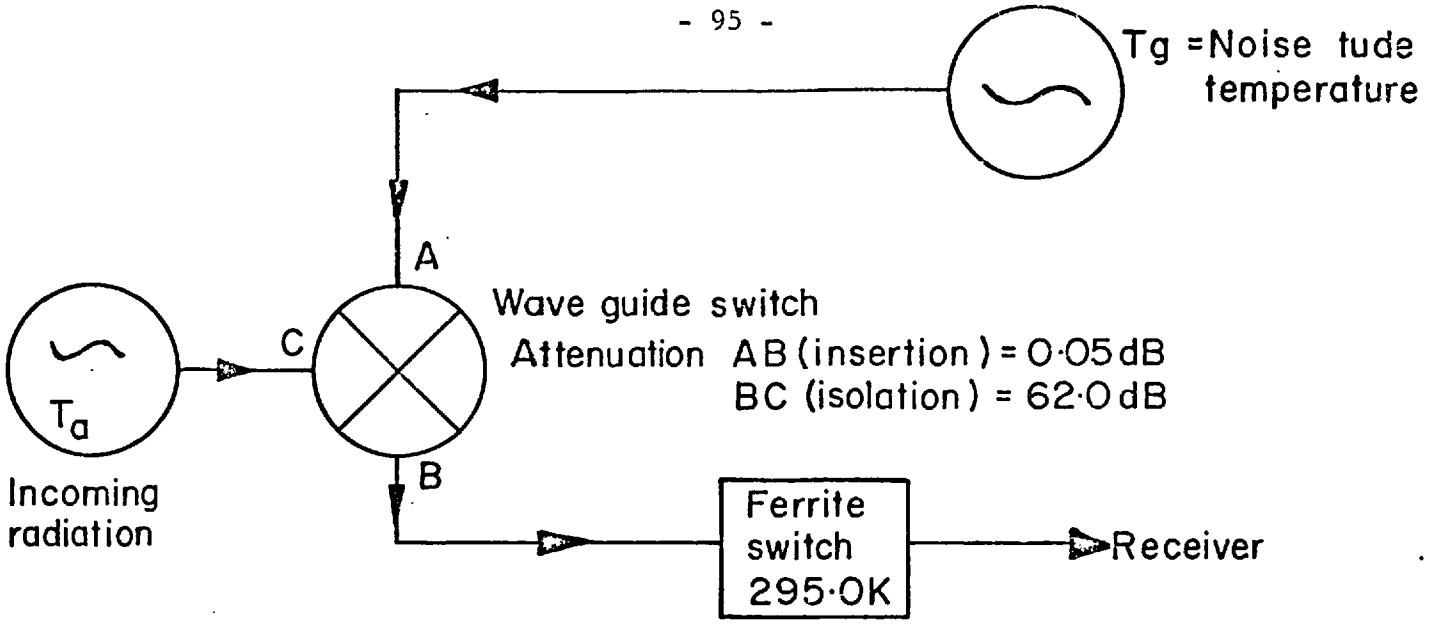
where

a' = Insertion loss of wave guide switch

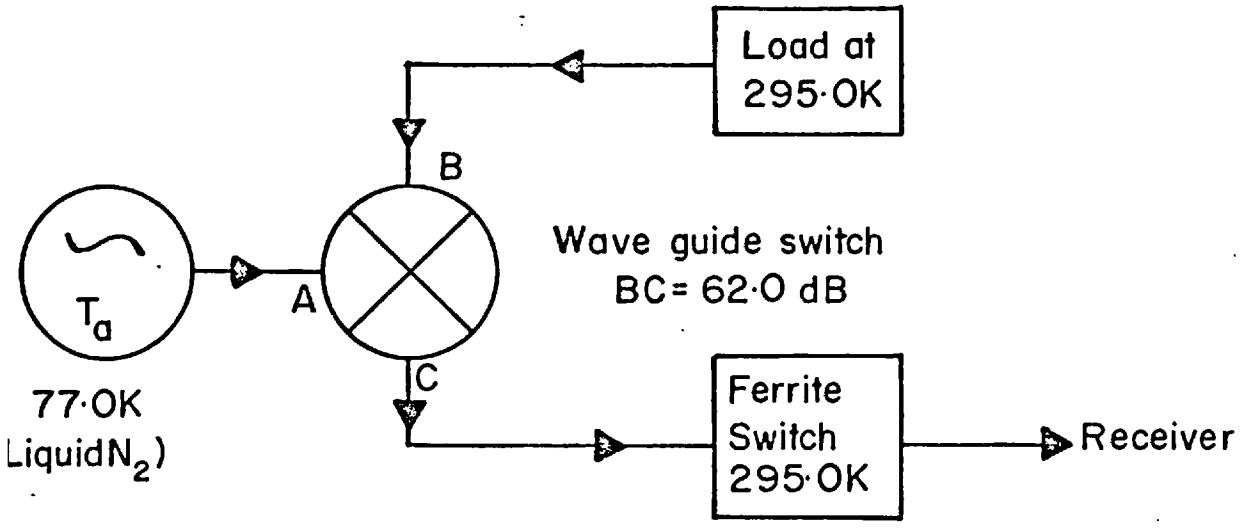
b = Isolation of wave guide switch

L = 14.0 dB + Insertion loss

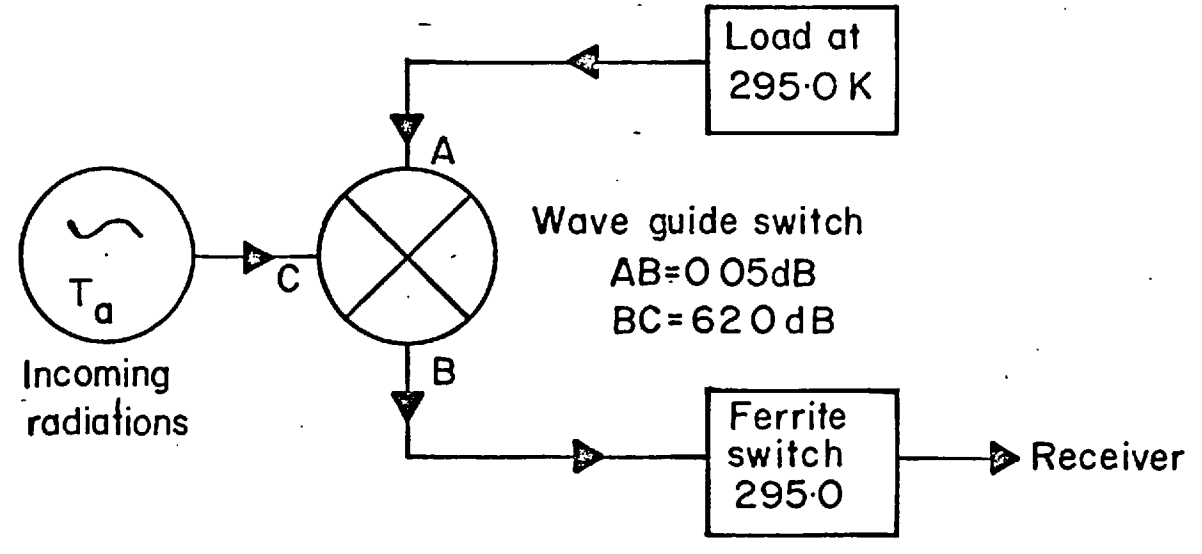
d = Wave guide loss



Equivalent circuit for noise tube calibration



Equivalent circuit for liquid nitrogen calibration



Equivalent circuit for load calibration

FIGURE 22

NEG.NO REF.NO 2249/

T_g = Noise tube temperature

T_g' = Liquid nitrogen temperature

T_g'' = Load temperature

T_a = Incoming radiation temperature

$$\Delta(T_3 - T_2) = \Delta T_g'' \left(\frac{1}{a'.d} - \frac{1}{b}\right) - \frac{\Delta T_g'}{a'.d} + \frac{T_g'' \Delta b}{b} - \frac{(T_g'' - T_g')\Delta a'}{d.a'^2}$$

$$- \frac{(T_g'' - T_g')\Delta d}{a' d^2}$$

$$\Delta(T_1 - T_3) = \frac{\Delta T_g}{La'd} + \left(1 - \frac{1}{La'd} + \frac{1}{a'd} - \frac{1}{a'bd}\right) \Delta T_o$$

$$+ \frac{\Delta T_a}{a'b.d} - \frac{\Delta T_g''}{a'.d} - \frac{(T_g - T_o)\Delta L}{a'.d.L^2}$$

$$- \frac{\left\{\frac{T_g - T_o}{L'.d} + (T_g'' - T_o - \frac{T_o}{b})\frac{1}{d} + \frac{T_a}{bd}\right\} \Delta a'}{a'^2}$$

$$- \frac{\Delta d'}{d^2}\left[\frac{1}{d'}\left\{\frac{(T_g - T_o)}{L} - T_g' + \frac{1}{b}(T_a - T_o)\right\}\right]$$

$$- \frac{\Delta b}{b^2 a'd}(T_a - T_o)$$

Assuming $T_g' = (77.0 \pm 1.0)$ K, $T_g'' = (295.0 \pm 1.0)$ K

$T_g = (11.700 \pm 30)$ K, $T_o = (290 \pm 1.0)$ K

$a' = (0.05 \pm 0.001)$ dBs, $b = (62.0 \pm 0.1)$ dB

$L = (14.0 \pm 0.01)$ dBs, $d = (0.1 \pm 0.01)$ dB

Using above values one estimates an error of 1.25% in liquid calibration w.r.t. load and 1.5% error in noise tube calibration w.r.t. load.

(b) Error due to Changes in Radiation Pattern

Attenuation on an Earth-satellite path derived from a radiometer operating in the solar tracking mode is subjected to continuous changes in the polarisation of the system. The electric vector which is perpendicular at zenith is inclined to the vertical at different zenithal angle, the basic principle involved is outlined in Figure (23a). The aim is to find the inclination (χ_o) in the tracking mode. It is evident from Figure (23b) that the angle χ_o is a function of declination (S), hour angle (H) and latitude (φ). The magnitude of χ_o can easily be obtained in terms of above known parameters by solving the spherical triangle ZBA.

By referring to standard results in spherical astronomy[13], we can show that

$$\frac{\sin a}{\sin H} = \frac{\sin (90 - \varphi)}{\sin \chi_o} \tag{80}$$

Also

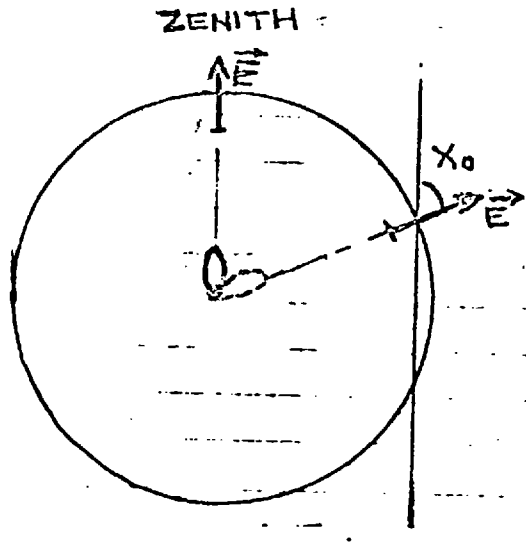
$$\cos a = \cos (90 - \varphi) \cos (90 - \delta) + \sin (90 - \varphi) \sin (90 - \delta) \cos H \tag{81}$$

$$\therefore \sin \chi_o = \frac{\cos \varphi}{\sin a} \cdot \sin H$$

or

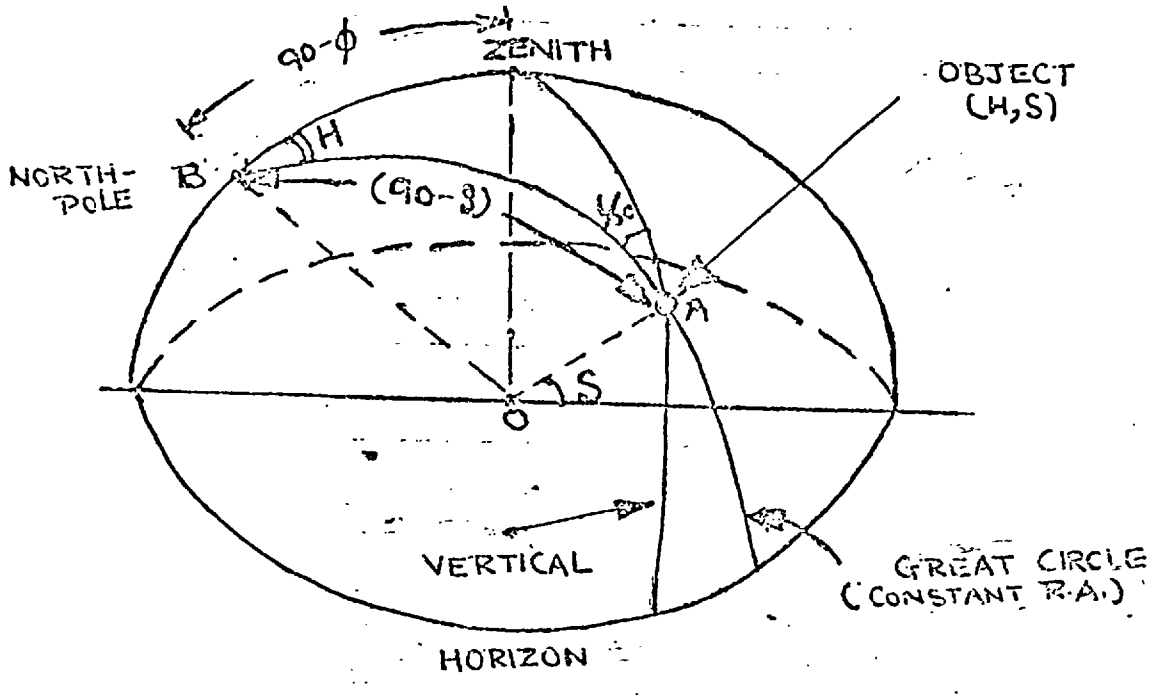
$$\chi_o = \sin^{-1}\left[\frac{\cos \varphi \sin H}{\sin\left[\cos^{-1}\left\{\sin \varphi \sin \delta + \cos \varphi \cos \delta \cos H\right\}\right]}\right] \tag{82}$$

The above equation shows that any vertically polarised aerial at zenith will behave as horizontally polarised aerial at 90^o from zenith. The cross-polarised feed assembly will also tilt with respect to its zenith position and therefore H, δ, φ parameters must be indicated in polarisation experiments for results to be meaningful. This does not have a marked effect on the final statistics of the present study because the rain attenuation could vary almost



Principle of Change of Polarisation During Tracking

FIGURE 23(a)



Geometry for Change of Polarisation Measurements

FIGURE 23(b)

by a factor of two but is definitely of immense importance in the recovery of polarised apparent temperature distributions from antenna temperature measurements.

(c) Contribution from Background Radiations

The contribution from background was as high as 35.0 K although the side lobes were not detectable by the present system. An estimate could be made from the measured zenith temperature and extrapolated attenuation using the method discussed in Section (9.1.1). The zenith temperature measured on 11th September, 1975 was 54.0 K, and the extrapolated attenuation at zenith was 0.31 decibels. The attenuation at 0.31 decibels corresponds to 18.9 K at 275.0 K (mean atmospheric temperature). The difference 25.0 K can be attributed to background radiation.

(d) Error in Calculating Attenuation from Absorption

Equation (58) can be rewritten under the assumption that wave guide losses are small and its variation with temperature is negligible.

$$\alpha_{\text{Apparent}} = \text{Loss due to absorption} = \frac{h\,T_m - T_{a'1} + (T_g\gamma_2 + \rho T_a)(1-h)}{h\,T_m - T_{a'2} + [T_g\gamma_3 + \rho T_b)(1-h)} \qquad (83)$$

We differentiate the above equation partially w.r.t. various parameters.

$$\Delta\left(\frac{1}{\alpha_{\text{Apparent}}}\right) = \frac{K_1}{K_2}\Delta\,T_{a1}' - \frac{\Delta T_{a2}'}{K} + \Delta T_m\left(\frac{h}{K} - \frac{K_1}{K_2}h\right)$$

$$+ \Delta h\left[T_m - \left(\frac{T_g\gamma_3 + \rho T_b}{K}\right) - \frac{K_1}{K_2}\left(T_m - \left\{T_g\gamma_2 + \rho T_a\right\}\right)\right]$$

$$+ \Delta T_g\left[\frac{(1-h)\gamma_3}{K} - \frac{K_1}{K_2}(1-h)\,\gamma_2\right] + \Delta\rho\left[\frac{(1-h)T_b}{K} - \frac{K_1}{K_2}(1-h)T_a\right]$$

$$+ \frac{\Delta\gamma_3\,T_g(1-h)}{K} + \frac{\Delta T_b(1-h)\rho}{K} - \frac{K_1}{K_2}\Delta T_a(1-h)\rho - \frac{K_1}{K_2}(1-h)\,T_g\Delta\gamma_2$$

(84)

where

$$K = hT_m - T_{a1}' + (T_g\gamma_2 + \rho T_a)(1 - h)$$

$$K_1 = hT_m - T_{a2}' + (T_g\gamma_3 + \rho T_b)(1 - h)$$

$$\Delta(\alpha_{Apparent})^{dB} = 4.35\ [\Delta(1/\alpha_{Apparent})/1/\alpha_{Apparent}]$$

The above equation was solved for

$$T_g = (280 \pm 20.0)\ K \quad , \quad \rho = 0.5 \pm 0.01$$

$$h = 0.87 \pm 0.013 \quad , \quad T_a = T_b = (273 \pm 5.0)\ K$$

$$\gamma_2 = 0.9311 \pm 0.005$$

The values of $T_m = (273.0 \pm 10)$ K and $T_m = (273.0 \pm 5)$ K.

The results are tabulated in Table 5.

The analysis shows that

(1) Maximum error in low attenuation comes from variation in antenna temperature, variation in ground temperature and the radiation pattern.

(2) Maximum error in high values of attenuation comes from T_g and variation in T_m.

(3) The error due to h, T_{a1}', T_{a2}' decreases with increasing attenuation.

(4) The error due to variation in T_m, T_g and ρ increases with increasing attenuation.

(e) Error in the Measurement of Extinction

$$\alpha_{True} = \text{Loss due to extinction} = \frac{T_{a1} - T_{a1}'}{T_{a2} - T_{a2}'} \tag{85}$$

Differentiating partially w.r.t. various parameters

$$\Delta\left(\frac{1}{\alpha_{True}}\right) = \frac{1}{(T_{a1} - T_{a1}')}\left[\Delta T_{a2} - \Delta T_{a2}' - \alpha_{True}\,(\Delta T_{a1} - \Delta T_{a1}')\right] \tag{86}$$

The maximum error comes from the third term, and tends to increase sharply with increasing attenuation. The error in the measurement of true attenuation is tabulated in Table 6.

ERROR IN ABSORPTION MEASUREMENTS

No.	$T_M = 273 \pm 10^oK$		$T_M = 273 \pm 5^oK$	
	A dB'	ΔA dB	A dB	ΔA dB
1	3.0	0.10	3.0	0.023
2	6.0	0.56	6.0	0.133
3	10.0	1.40	10.0	0.500
4	14.0	3.40	14.0	1.400

Table 5

ERROR IN EXTINCTION

No.	A dB	ΔA dB's
1	3.0	0.04
2	6.0	0.065
3	10.0	0.20
4	14.0	0.40

Table 6

9. EXPERIMENTAL RESULTS

9.1 Experimental Results on Scattering by Rain

The single beam nodding radiometer discussed in Section (3) was used to take observations over past twelve months (2nd December 1974 - 1st December 1975). The data recorded included a number of intense rain storms, medium rain, drizzle, wet snow and heavy clouds. The whole range of recorded data has been divided into six causes of attenuations in increasing order of importance.

(1) Clear weather

(2) Cloudy weather

(3) Drizzle (< 1 mm h^{-1})

(4) Light rain (< 5 mm h^{-1})

(5) Heavy rain (> 5 mm h^{-1})

(6) Wet snow.

9.1.1 Clear Weather Attenuation

Clear weather attenuation changes from day to day depending upon the water content in the beam and thickness of the atmosphere i.e. the elevation of observation. At low elevation beam traverses a thicker atmosphere, therefore higher attenuation is expected. The Sun as a source at various elevation angles is used to extrapolate the zenith attenuation. Throughout the observation period it was assumed that the atmosphere is horizontally stratified with a non-varying solar brightness. It could be shown[6] that clear weather zenith attenuation could be obtained from the slope of the plot of

$$\text{Log } [T_{a1}(\chi) - T_{a1}'(\chi)] \; V_s \text{ secant } \chi.$$

Mathematically, we can show this by subtracting equation (59) from (60), we get

$$T_{a1}(\chi) - T_{a1}'(\chi) = (1 - ag)h\, T_s\, (1 - \gamma_2(\chi)]$$

or

$$\text{Log}\, [T_{a1}(\chi) - T_{a1}'(\chi)] = \text{Log}\, [(1 - ag)h\, T_s] + \text{Log}\, [1 - \gamma_2(\chi)] \qquad (87)$$

Fractional absorption $\gamma_2(\chi) = [1 - \exp\, [-\alpha(\chi)]\,]$

Transmissivity of the medium at zenithal χ can be related to zenith transmissivity by the relation

$$\text{Exp}\, [-\alpha(\chi)] = \exp\, [-\alpha_o \sec \chi] = (1 - \gamma_o)^{\sec \chi}. \qquad (88)$$

where

γ_o = Fractional absorption at zenith

α_o = Total absorption due to medium at zenith

From equation (87) and (88), we get

$$\text{Log}\, [T_{a1}(\chi) - T_{a1}'(\chi)] = \log\, [(1 - ag)h\, T_s] + \log\, [\exp\, (1 - \alpha_o \sec \chi)] \qquad (89)$$

or

$$\text{Log}\, [T_{a1}(\chi) - T_{a1}'(\chi)] = \log\, [(1 - ag)h\, T_s] - \alpha_o \sec \chi \qquad (89)$$

Comparison of the above equation with the equation of straight line shows that plot of $\text{Log}[T_{a1}(\chi) - T_{a1}'(\chi)]$ against sec χ should be a straight line of slope α_o. Such a plot for 28th August 1975 (air temperature 31.0°C and relative humidity = 60%) is shown in Figure (24). The extrapolated attenuation on such a hot day was found to be 0.29 decibels per atmosphere. Attenuation on a partially clear day was found to be 0.33 dB per atmosphere. The maximum variation recorded about 0.29 dB was 0.04 decibels. The results were consistent at low elevation angles where the thickness of the atmosphere changes rapidly with hour angle.

9.1.2 Attenuation on a Cloudy Day

Attenuation as low as 0.42 decibels and as high as 6.0 decibels,

$$T_{a1}(\chi) - T_{a1}'(\chi) = (1 - ag)h\, T_s\, (1 - \gamma_2(\chi)]$$

or

$$\text{Log}\, [T_{a1}(\chi) - T_{a1}'(\chi)] = \text{Log}\, [(1 - ag)h\, T_s] + \text{Log}\, [1 - \gamma_2(\chi)] \qquad (87)$$

Fractional absorption $\gamma_2(\chi) = [1 - \exp\, [- \alpha(\chi)]]$

Transmitivity of the medium at zenithal χ can be related to zenith transmitivity by the relation

$$\text{Exp}\, [- \alpha(\chi)] = \exp\, [- \alpha_o \sec \chi] = (1 - \gamma_o) \sec \chi. \qquad (88)$$

where

γ_o = Fractional absorption at zenith

α_o = Total absorption due to medium at zenith

From equation (87) and (88), we get

$$\text{Log}\, [T_{a1}(\chi) - T_{a1}'(\chi)] = \log\, [(1 - ag)h\, T_s] + \log\, [\exp\, (1 - \alpha_o \sec \chi)] \qquad (89)$$

or

$$\text{Log}\, [T_{a1}(\chi) - T_{a1}'(\chi)] = \log\, [(1 - ag)h\, T_s] - \alpha_o \sec \chi \qquad (89)$$

Comparison of the above equation with the equation of straight line shows that plot of $\text{Log}[T_{a1}(\chi) - T_{a1}'(\chi)]$ against sec χ should be a straight line of slope α_o. Such a plot for 28th August 1975 (air temperature 31.0°C and relative humidity = 60%) is shown in Figure (24). The extrapolated attenuation on such a hot day was found to be 0.29 decibels per atmosphere. Attenuation on a partially clear day was found to be 0.33 dB per atmosphere. The maximum variation recorded about 0.29 dB was 0.04 decibels. The results were consistent at low elevation angles where the thickness of the atmosphere changes rapidly with hour angle.

9.1.2 Attenuation on a Cloudy Day

Attenuation as low as 0.42 decibels and as high as 6.0 decibels,

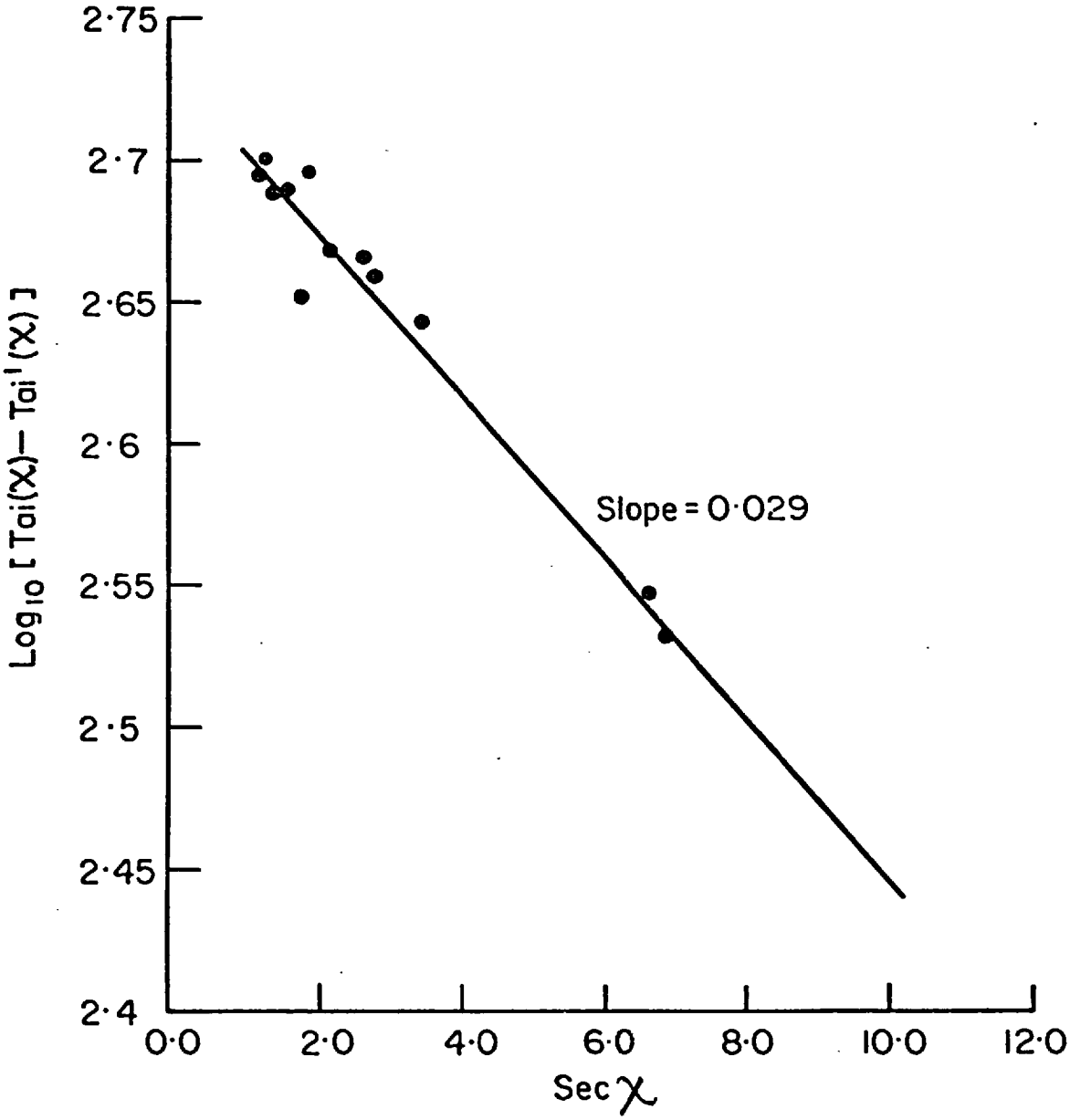

2·75
2·7
2·65
2·6
2·55
2·5
2·45
2·4
Log10 [Tai(χ)— Tai'(χ)]
Slope = 0·029
0·0
2·0
4·0
6·0
8·0
10·0
12·0
Sec χ

FIGURE 24

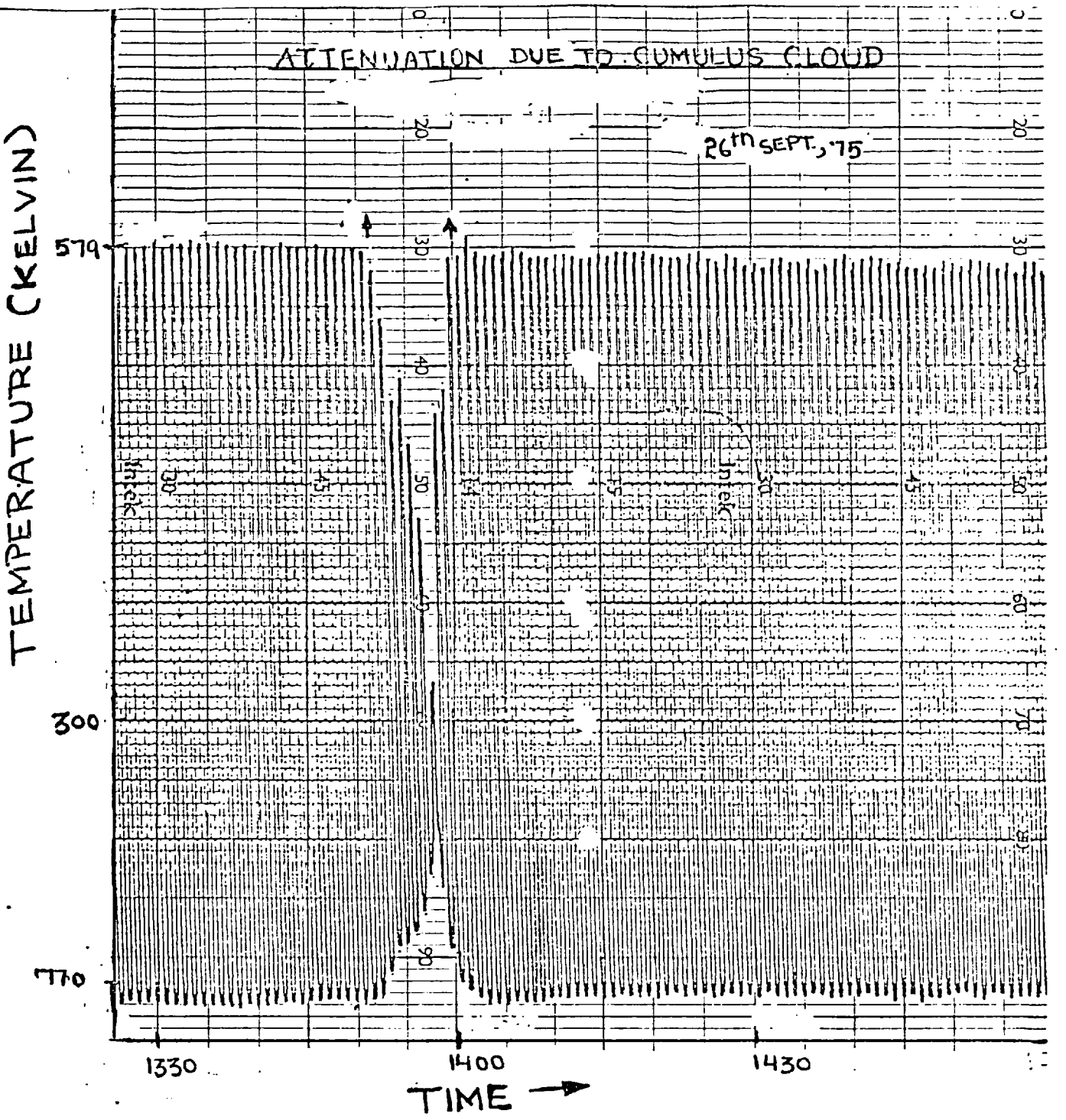

ATTENUATION DUE TO CUMULUS CLOUD
26th SEPT., '75
TEMPERATURE (KELVIN)
579
300
770
1330
1400
1430
TIME
Inlet
Outlet

FIGURE 25

although that rarely, were recorded on cloudy days. Such cases of high attenuations due to cloud were not included in the final statistics discussed in Section (10).

The visual identification of the cloud showed that in most cases a high value of attenuation was due to cumulus clouds, and no rainfall within 10 mile radii was recorded during periods of high attenuation. It seems likely that the cloud consisted of large drops and the powerful up-currents of several metres/sec are not letting the drops fall as rain. Figure (25) shows such a record due to a moving patch of cloud on 26th September, 1975 on otherwise a clear day. Analysis showed that for such cases the calculated apparent attenuation, assuming a mean atmospheric temperature of 273.0, equals excess of attenuation within experimental limits.

Effect of Solar Burst

It has already been indicated in Section (2.25) that the correct value of excess attenuation cannot be measured if rain and a solar-burst within the beam occur simultaneously but at the same time attenuation derived from thermal emission measurement is not affected. Simultaneous recording of a 130%* solar-burst and its effect on sky temperature on a cloudy day (21st August 1975) is shown in Figure (26). No measurable increase in the apparent brightness temperature due to the burst was noticed due to averaging of radiations over the large solid angle subtended by the upper hemisphere.

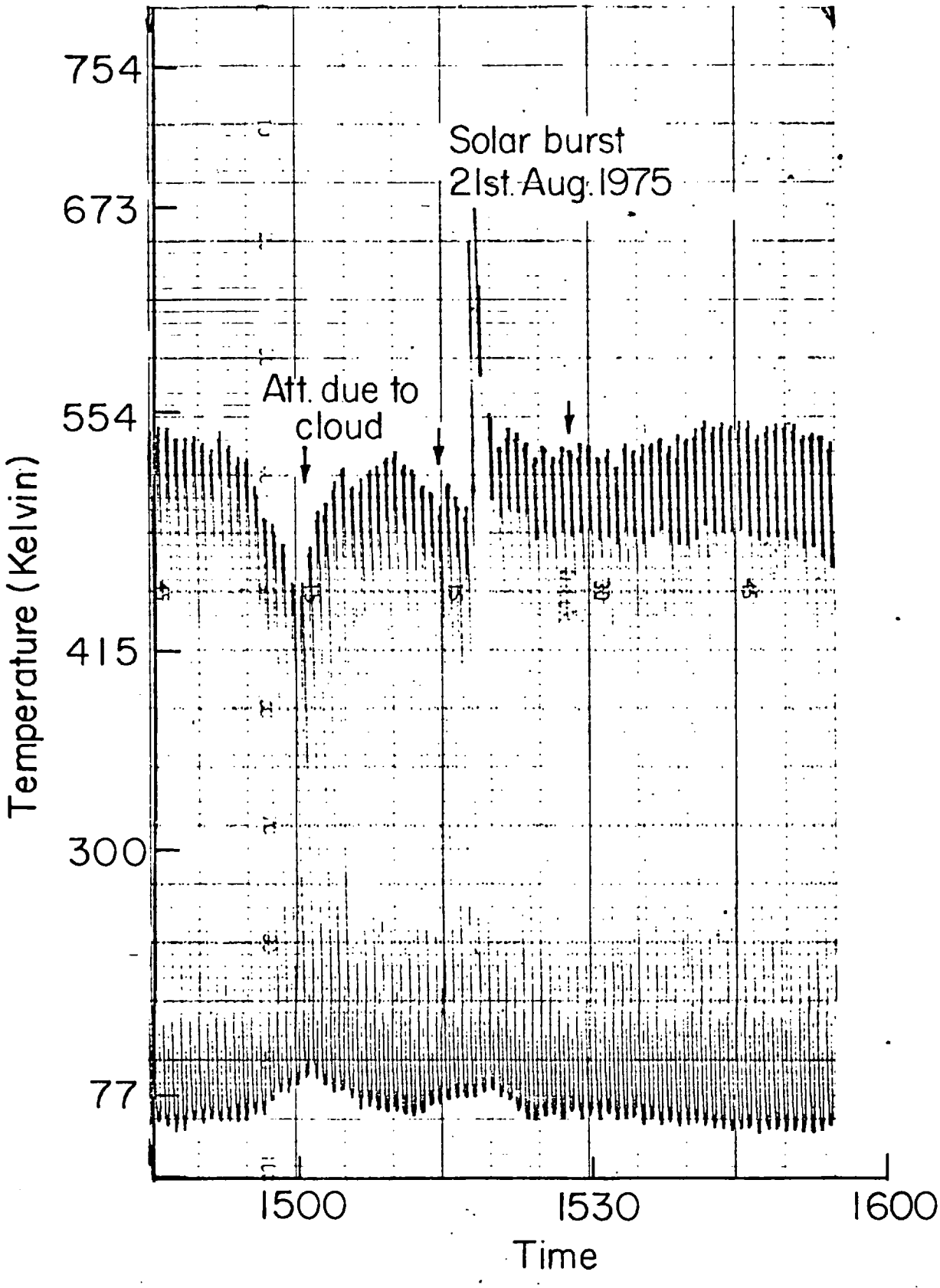
---

* Percentage solar burst = $\frac{T_{Burst} - T_{a1}}{T_{a1} - T_{a1}'} \times 100$

where T_{Burst} = Aerial temperature in Kelvin of the peak value of burst

T_{a1} = Aerial temperature of quiet Sun in Kelvin

T_{a1}' = Aerial temperature of sky in Kelvin



Recording of a Nodding Radiometer

FIGURE 26

9.1.3 Drizzle

The overall results suggest that rain rate less than 1 mm h^{-1} can give rise to the maximum of 3.0 decibels of attenuation and the ratio of scattering to absorption is estimated to be 0.20. Therefore, because of scattering even at low rainfall rates, the attenuation obtained using a passive radiometric technique could be underestimated by 20%.

True attenuation has been plotted against calculated apparent attenuation in Figure (27) and compared to Zavody's theory. The dots correspond to experimental data points and the solid curve is the theoretical curve for an aerial elevation of 18.0^{o}. The plot shows that there is an equal probability of finding experimental points on either side of the ideal fit. This is because drizzle consist of raindrops much smaller than the wavelength. The forward scattering lobe is weak and large in angular diameter. Therefore the ratio of energy scattered out of the beam to the energy scattered into the beam is approximately unity and the net result is that true attenuation should equal apparent attenuation.

For apparent attenuations greater than 1.5 decibels the plotted results show that the probability of finding a point above the ideal fit increases. It is possible that these attenuations may be due to larger drops of heavy rainfall within the beam but only recorded as drizzle at the ground. Also most of the hemisphere beyond the rain has a very low emission temperature and therefore a scattered portion of energy lost due to presence of cold sky remains unaccounted in the total attenuation. Since the magnitude of this scattered energy will be higher for Sun beam, therefore the true attenuation should be greater than the apparent attenuation although by a small amount.

9.1.4 Medium Rain

The effect of meteorological conditions is the most complex on

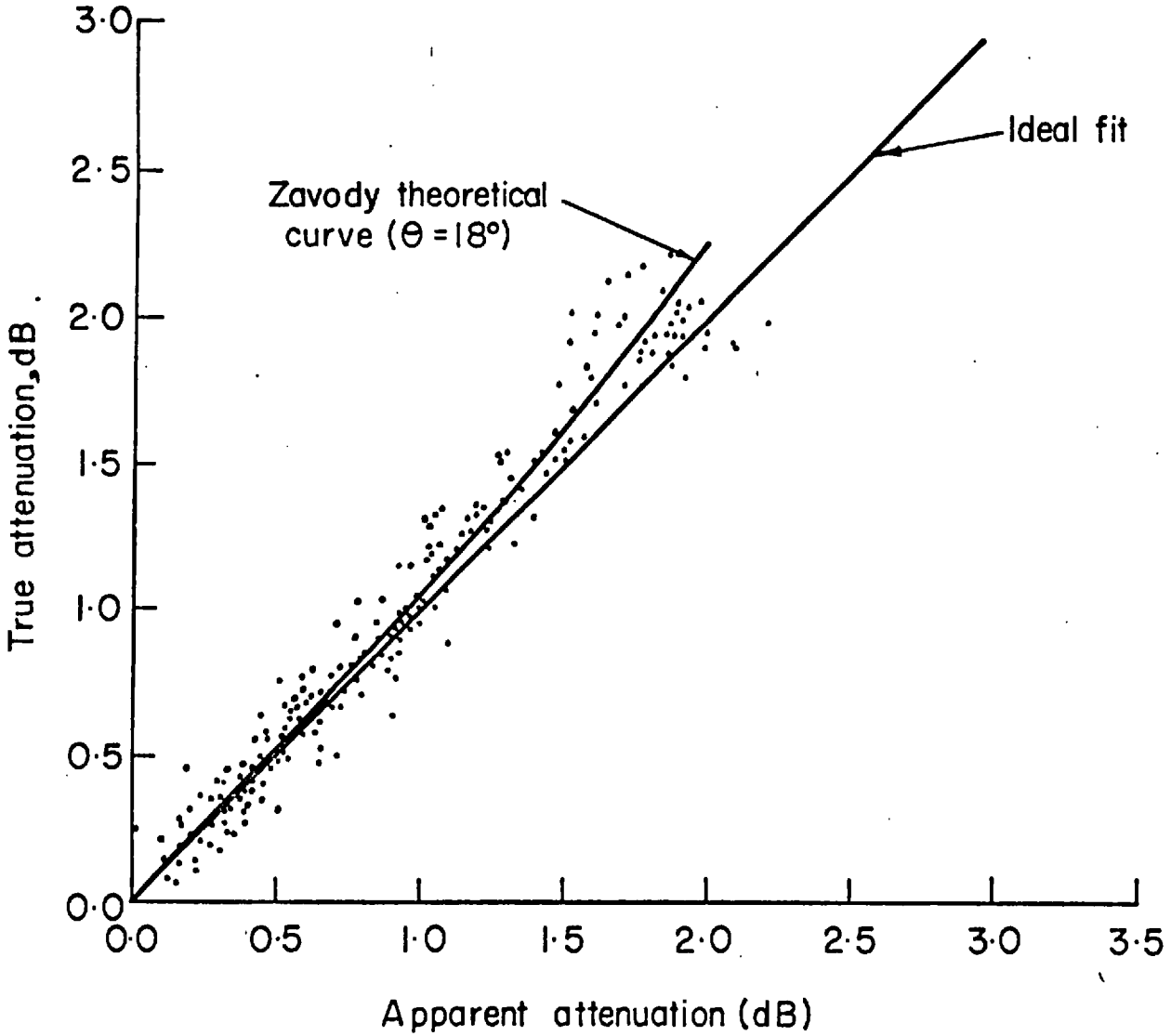

3·0
2·5
2·0
1·5
1·0
0·5
0·0
True attenuation, dB
Zavody theoretical curve (Θ = 18°)
Ideal fit
0·0
0·5
1·0
1·5
2·0
2·5
3·0
3·5
Apparent attenuation (dB)

FIGURE 27

the medium intensity rain and therefore on attenuation and scattering. True attenuation is plotted against apparent attenuation in Figure (28) for rainfall rate less than 5 mm h^{-1}, measured at the ground. The plot shows that an instantaneous rain of 5 mm h^{-1} can give rise to 3.75 dB's of scattering error. The theoretical error for the same rainfall rate and for an aerial at elevation 18^{o} is 3.8 dB's. Majority of points for apparent attenuation greater than 3.0 dB tend to lie above the ideal fit Figure (28). This is due to "apparent medium temperature" being less than 273.0 K (Figure 34), although ambient temperature may be much higher than 273.0 K. The points lying below the ideal fit are not only due to "apparent medium temperature" being higher than the effective medium temperature used in obtaining attenuation from emission measurements but can also be attributed to sudden changes in water content within the beam, kinetic temperature, drop size distribution. It is evident that attenuations derived using the thermal emission technique could be in error by as much as 3.75 dB's at medium rainfall rate.

9.1.5 Heavy Rain

Figure (29) shows the recorded output of the 37.0 GHz nodding radiometer on 1st October 1975. During a thunderstorm period, the measured results show that the noise temperature can correspond to temperatures well below freezing point. The low "apparent absorbing temperature" during period of high attenuation, as discussed in Section (2), can only be attributed to a large scattering component.

Another intense rainshower was recorded on 20th January 1975 and during periods of heavy rain, the sky and solar signal merged into a straight line and therefore can be assumed to correspond with the temperature of rain.

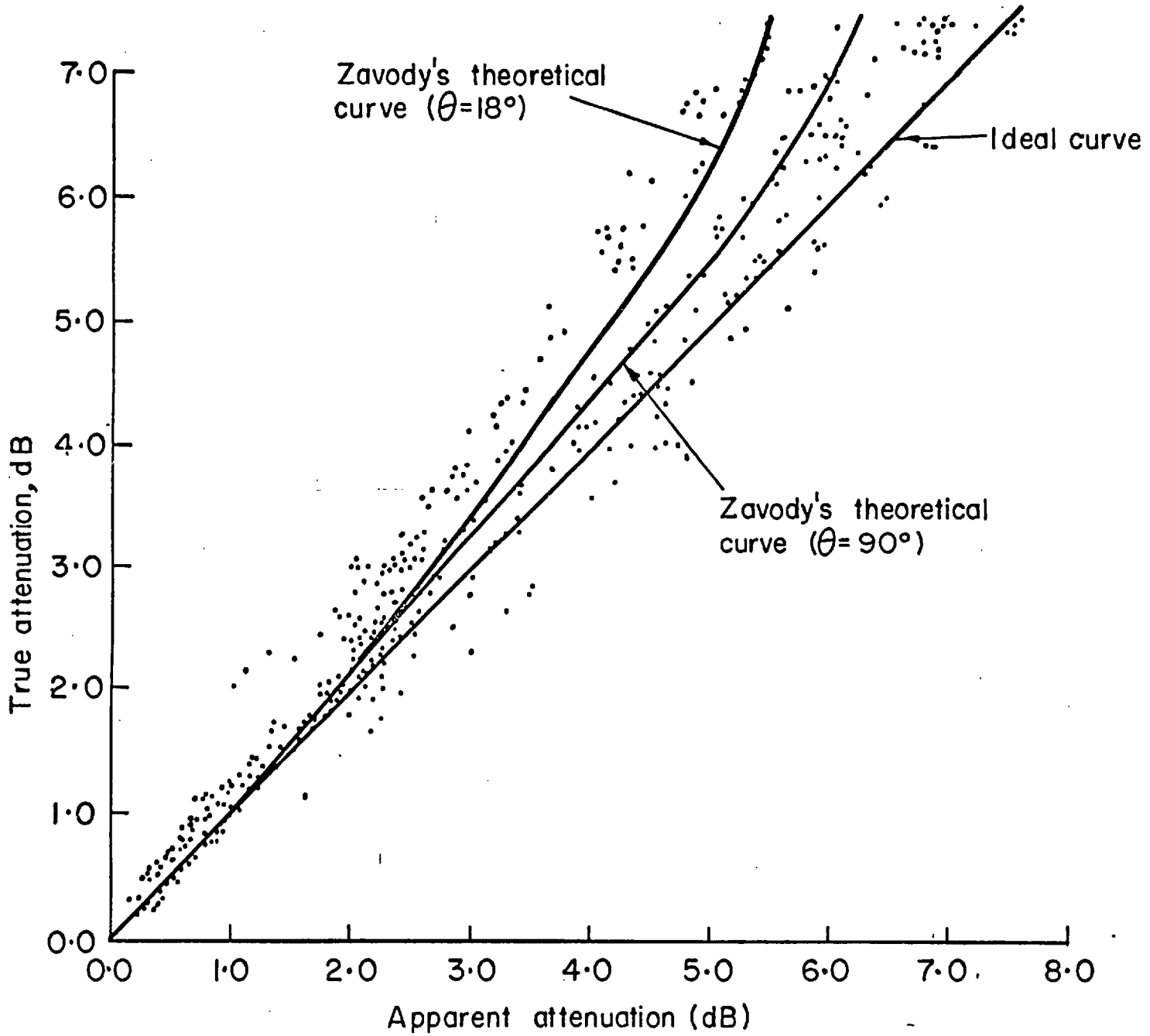

Zavody's theoretical curve (θ=18°)
Ideal curve
Zavody's theoretical curve (θ=90°)
True attenuation, dB
Apparent attenuation (dB)
0·0
1·0
2·0
3·0
4·0
5·0
6·0
7·0
8·0

FIGURE 28

The minimum noise temperature attained during the period is actually 21 K below the freezing point of water. The maximum rainfall recorded during the period is 18.5 mm h^{-1}. The ratio of the scattering coefficient to the absorption coefficient is approximately (0.72 $\pm$ 0.08) for rain rate 12.5 mm h^{-1}. For such heavy rainfall one can expect the majority of rain drops to be of large sizes (> 2 mm) having a strong forward scattering lobe of limited angular diameter, therefore a large amount of energy is scattered out of the Sun beam relative to the sky beam.

The simultaneous plot of attenuation, error due to scattering and instantaneous ground rainfall rate is shown in Figure (30). The rain rate as high as 18.5 mm h^{-1} was recorded around 11.20 a.m. on 20th January 1975. The excess of attenuation was 18.6 dB and the error due to scattering 6.45 dB. The plotted results show that there is a high cross-correlation between true attenuation and error due to scattering. The peak of true attenuation and error due to scattering occurred approximately 40 mins earlier than the peak of the rainfall measured at ground (1 m and 120 m distant from antenna). This time lag between true attenuation and instantaneous rainfall rate at ground could vary depending on the direction and velocity of the wind.

It is well known that the attenuation on an Earth-space path does not correlate with the instantaneous rain rate measured at the ground. This can be due to sudden changes of water content within the beam, horizontal and vertical extent of rain layer, drop size distribution within the beam and direction and velocity of wind. Therefore, one expects a large variation of attenuation and scattering for the same instantaneous rainfall rate measured at the ground. This may not be true for heavy intense showers as the scatter of points tends to decrease for the maximum value of attenuation and rainfall rate. To show the effect of meteorological conditions on attenuation,

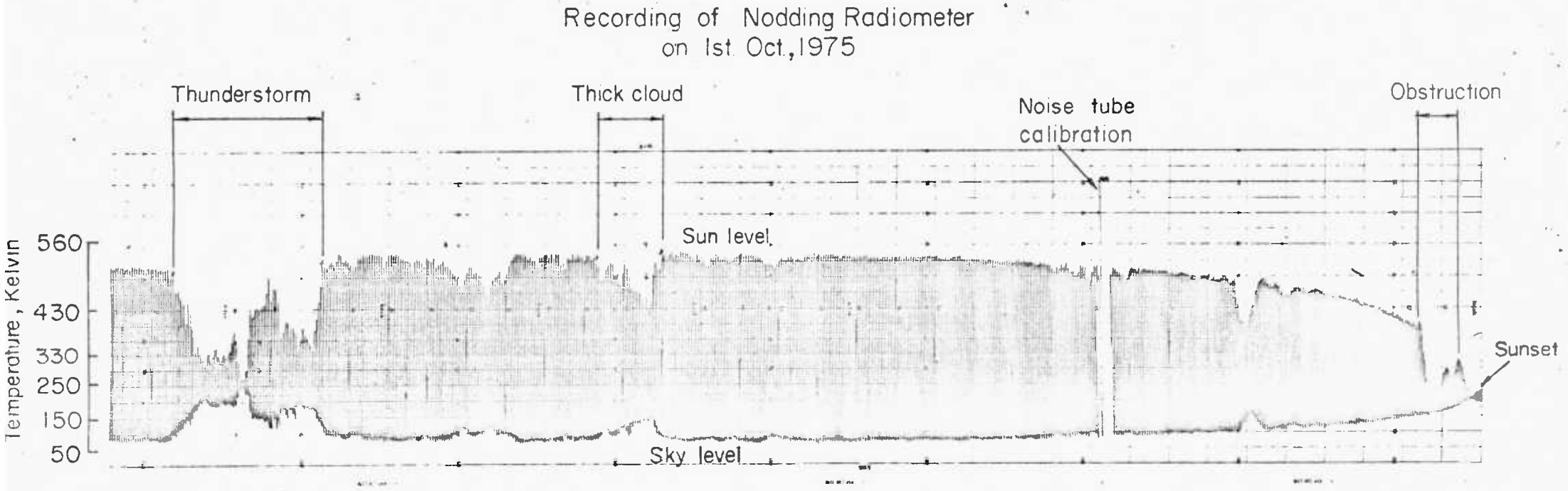

Recording of Nodding Radiometer
on 1st Oct., 1975
Thunderstorm
Thick cloud
Noise tube
calibration
Obstruction
Sun level
Sunset
Sky level
Temperature, Kelvin
560
430
330
250
150
50

FIGURE 29

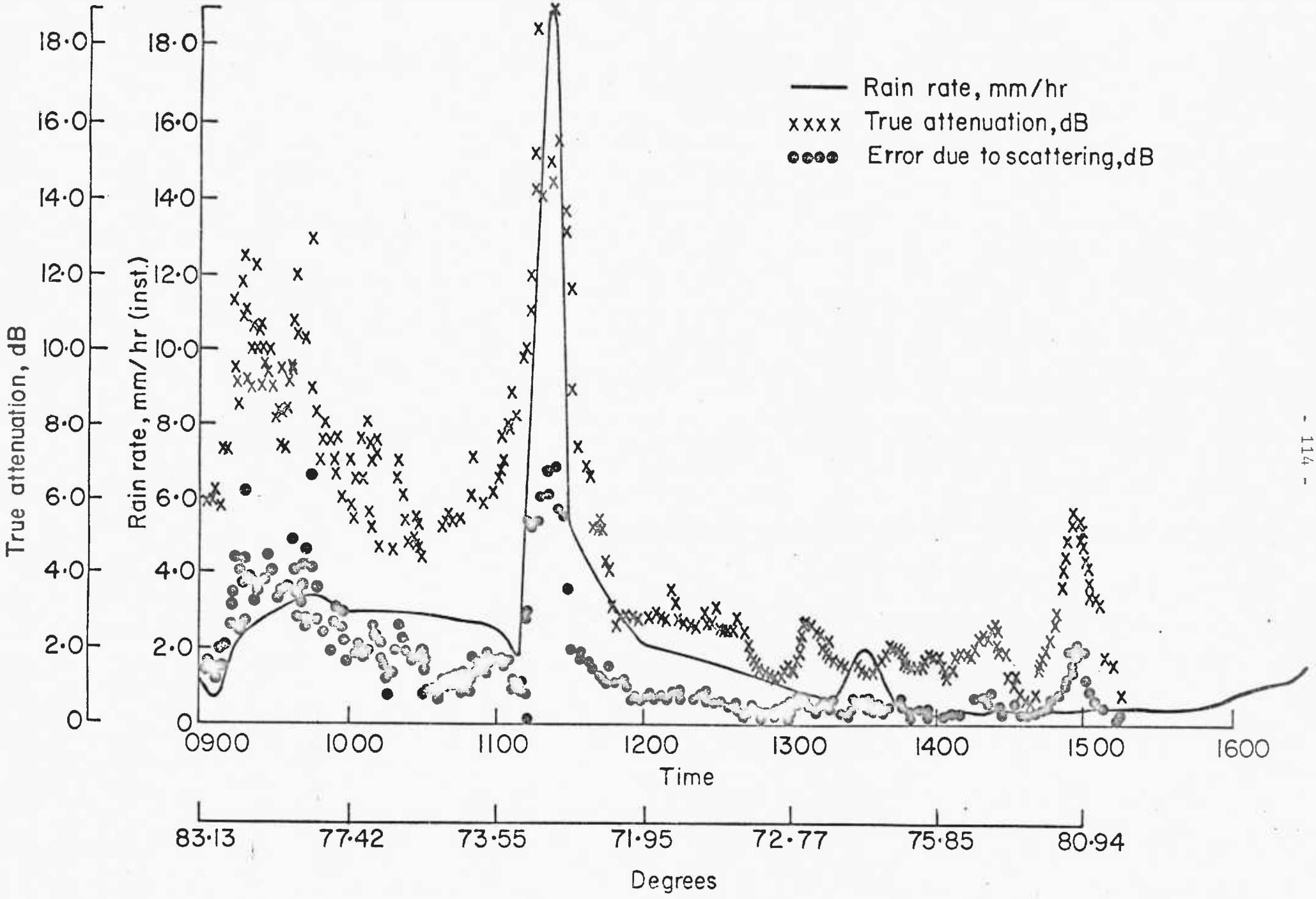

Rain rate, mm/hr
xxxx True attenuation, dB
●●●● Error due to scattering, dB
True attenuation, dB
Rain rate, mm/hr (inst.)
18·0
16·0
14·0
12·0
10·0
8·0
6·0
4·0
2·0
0
0900
1000
1100
1200
1300
1400
1500
1600
Time
83·13
77·42
73·55
71·95
72·77
75·85
80·94
Degrees

FIGURE 30

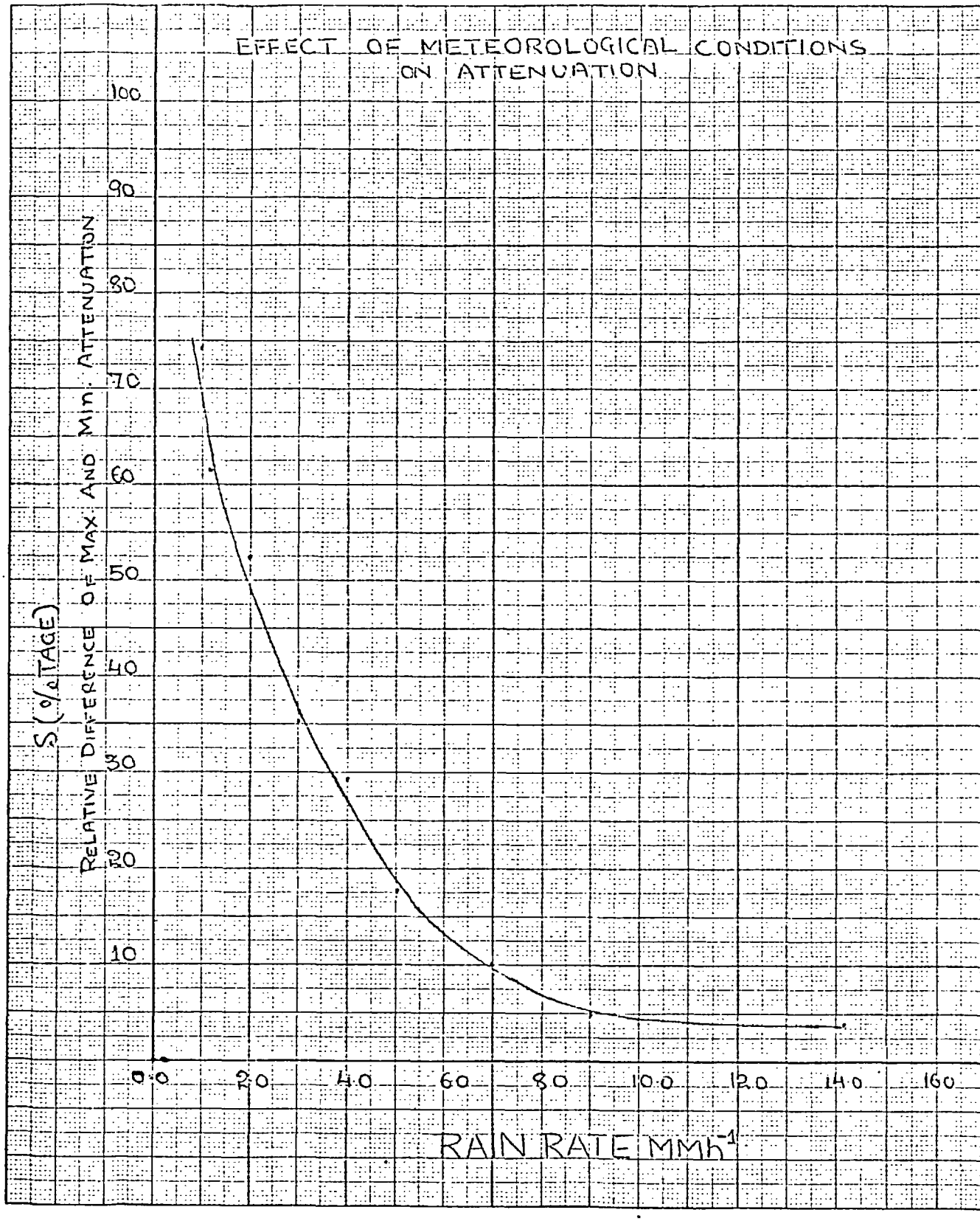

EFFECT OF METEOROLOGICAL CONDITIONS ON ATTENUATION
S (% AGE) RELATIVE DIFFERENCE OF MAX AND MIN ATTENUATION
100
90
80
70
60
50
40
30
20
10
0·0
2·0
4·0
6·0
8·0
10·0
12·0
14·0
16·0
RAIN RATE MMh⁻¹

FIGURE 31

relative difference of maximum and minimum attenuation was plotted against the rainfall rate and is shown in Figure (31). The percentage relative difference is less than 5.1% for rainfall rates greater than 14.0 mm h^{-1}, and for rainfall rates less than 1 mm h^{-1} the relative difference is as high as 75%. The maximum scatter of brightness temperature for the same rain intensity did not exceed 150 K. There were occasions when the attenuation due to small drops in rain was considerably higher than that for clouds producing steady rain. This difference in attenuation is explained mainly by the greater integrated water content within the beam.

It is obvious that scattering will increase with increasing rainfall rate or with excess of attenuation. The following relation holds between excess of attenuation (true attenuation) and scattering error for the measured results

$$\alpha_{True} = 4.4 \ [(S)]^{0.66} \tag{90}$$

Most of the intense showers during the period of observation were recorded during winter months and showers recorded during summer were far less. To give a feel of the seasonal effect we have separately plotted measurements for summer and winter shown in Figure (32) and (33) respectively. The experimental points are compared with theoretical calculations and aerial elevation is 18.0^{o}. Most of the summer and winter experimental points correspond to elevation range (18-36) degrees and (5-25) degrees respectively. The theoretical calculations are broadly in agreement but discrepancies do exist for apparent attenuation greater than 7.0 decibels* for both the seasons. There are experimentally measured data

* The points greater than 12.0 dB of apparent attenuation in Figure (32) and (33) can be in error by almost 100%. This is due to saturation of receiver or in other words is the limit of measurement.

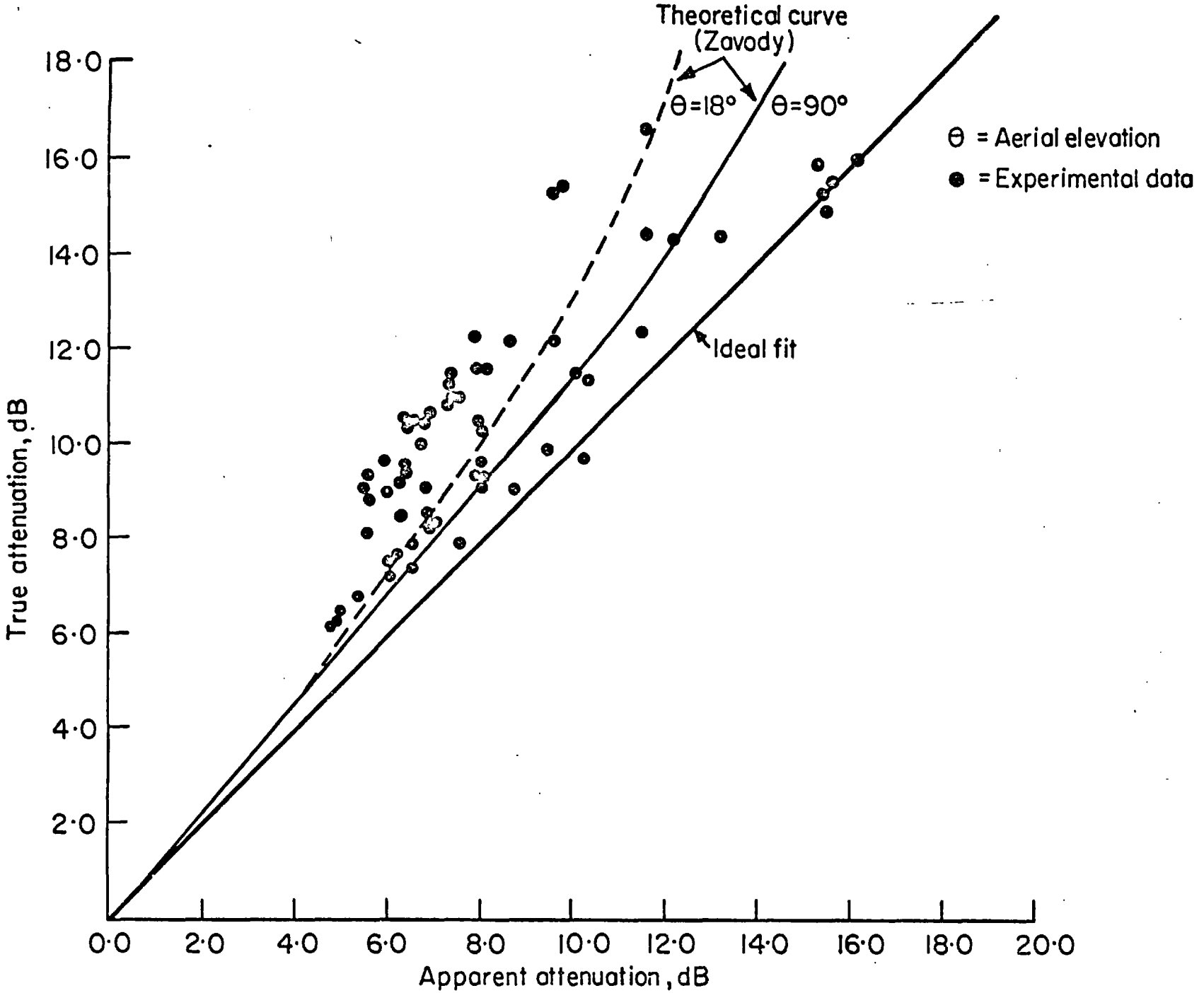

Theoretical curve
(Zavody)
θ=18°
θ=90°
θ = Aerial elevation
● = Experimental data
Ideal fit
True attenuation, dB
Apparent attenuation, dB
18·0
16·0
14·0
12·0
10·0
8·0
6·0
4·0
2·0
0·0
2·0
4·0
6·0
8·0
10·0
12·0
14·0
16·0
18·0
20·0

FIGURE 32

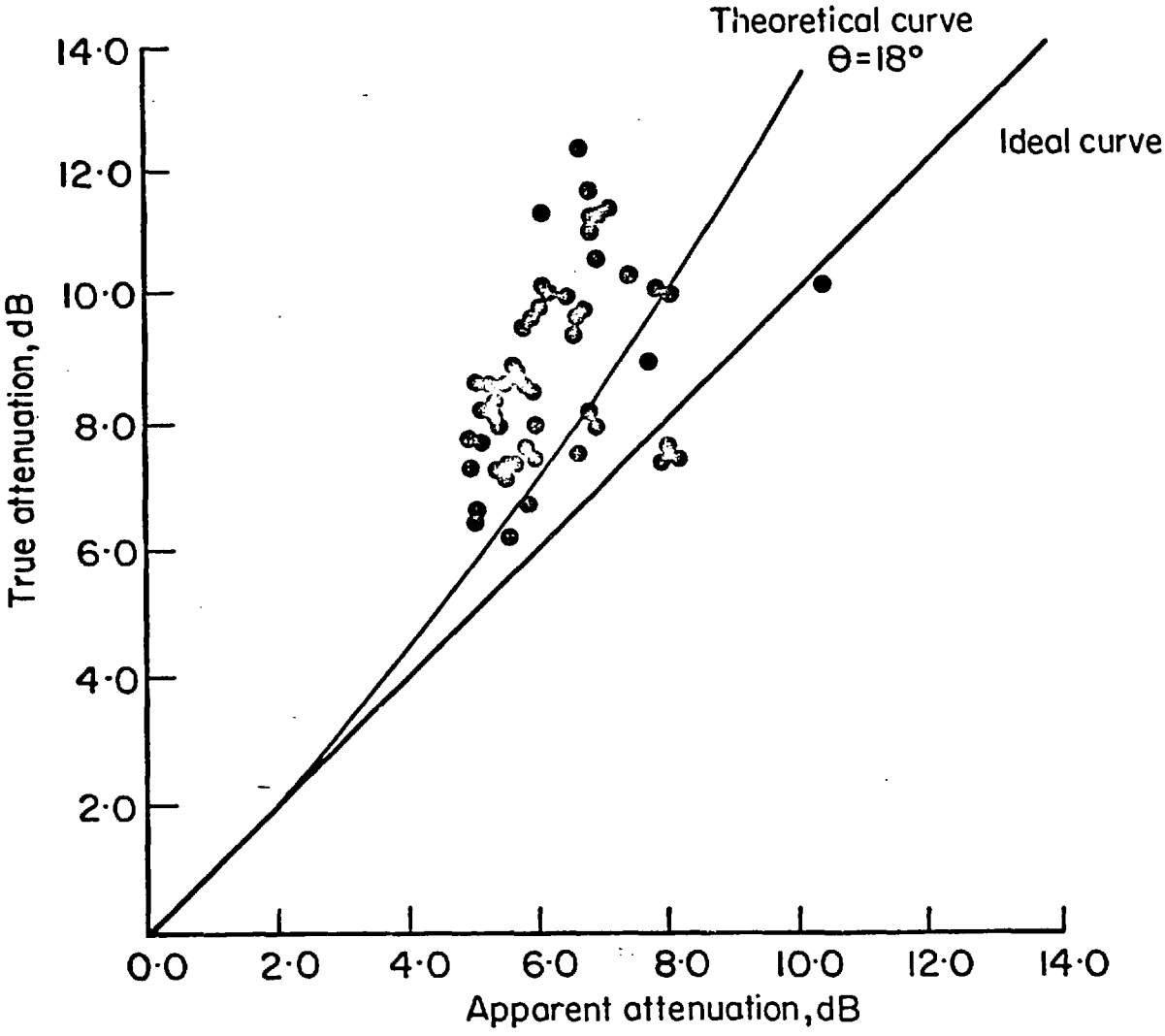


FIGURE 33

REF NO 2249/7 NEG NO

points which show as much as twice the scattering error compared to theoretical calculations. The error is larger for winter showers compared to summer and it does not necessarily imply that winter shower consist of larger drop sizes since the mean atmospheric temperatures for the two seasons are different.

The short duration intense showers due to patches of cloud were also recorded during the summer period. The maximum duration of the shower was 15 mins. For such cases the error due to scattering was much lower and as indicated earlier this is due to much smaller area occupied by the rain and therefore smaller solid angle in which scattered emission from rain would contribute.

It is interesting to invert the equations of Section (3.4) and compute the "apparent medium temperature" using measured data. We apply this to the measured data of 20th January 1975. The 12.0 dB of absorption at 273.0 corresponds to an emission temperature of 255.77 K without any addition of scattered radiation. The true attenuation corresponding to the above absorption is 18.5 dB. According to Crane[20] estimate, for this order of rainfall, about 50% of the total attenuation at 35 GHz will be due to scattering. Now 18.5 dB of true attenuation at 273.0 K corresponds to an aerial temperature of 269.14 K, a difference of 13.37 K. The "apparent absorber" temperature of the media corresponding to 255.77 K and 18.5 dB will be 259.37 K. This difference is at the expense of scattering error, not due to the absorption of the condensed water droplets.

The overall measured data were used to derive the apparent medium temperature and has been plotted against measured excess of attenuation, in Figure (34) at low values of attenuation the average value of the apparent medium temperature (T_m) is just above freezing point. Although

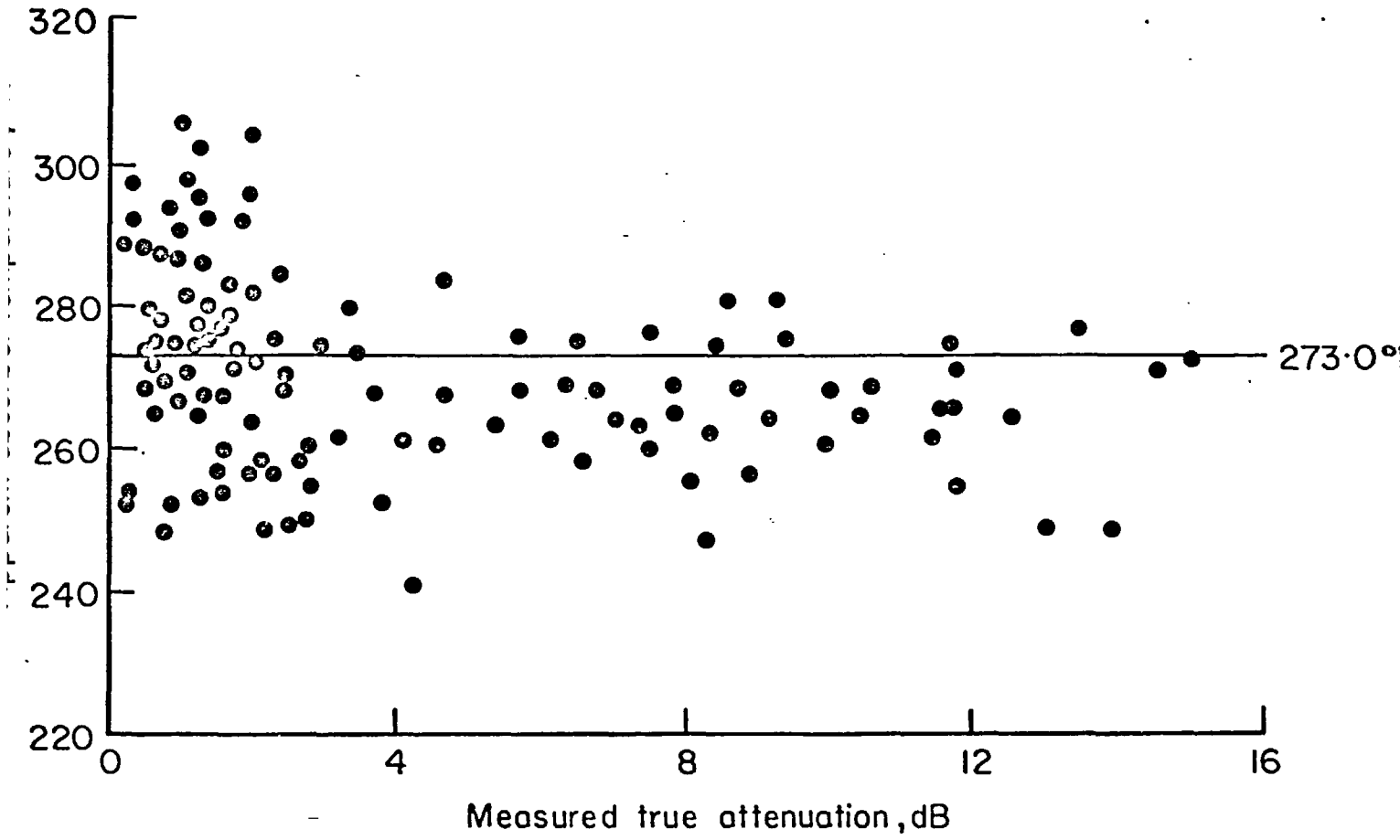

320
300
280
260
240
220
0
4
8
12
16
273·0°K
Measured true attenuation, dB

FIGURE 34

the air temperature near the Earth surface is much higher. At high values of attenuation the mean calculated value of T_m is much lower than freezing point. This situation is explainable only in terms of scattering and is discussed in detail in Section (2).

Thus the present observations show that not only the smaller attenuation but the larger and more important attenuations can also be in error.

9.1.6 Sleet

Attenuation as high as 5.0 dB due to wet snow was recorded during months of March, April 1975 (Figure 35). Because of lack of information on the shape and distribution of wet snow, it is difficult to talk about the nature of scattering i.e. radiation pattern etc. The contribution to the absorption seems to come from the lower uncondensed portion of the falling sleet. Difference of temperature between lower and upper portion of the sleet is created in the process of falling under gravity. The contribution to the scattering is from the overall shape of the falling sleet but larger contributions seem to come from the upper portion, because of its very low emission temperature.

The error due to scattering is as high as 1.6 dB's in 5.1 dB's of True Attenuation (theoretical ratio of scattering to absorption is ≈ 0.46) for elevation ranges (40-50) degrees. The theoretical ratio of scattering to absorption for rain producing 3.5 dB of apparent attenuation is only 0.15. Thus the theory underestimates the scattering error due to falling wet snow by a factor of three.

10. STATISTICAL ANALYSIS

The error due to scattering and attenuation statistics referring to one year of observations and the variability of these parameters for various elevation angles is shown in Figures (36 to 39). Because of the scattering error being a function

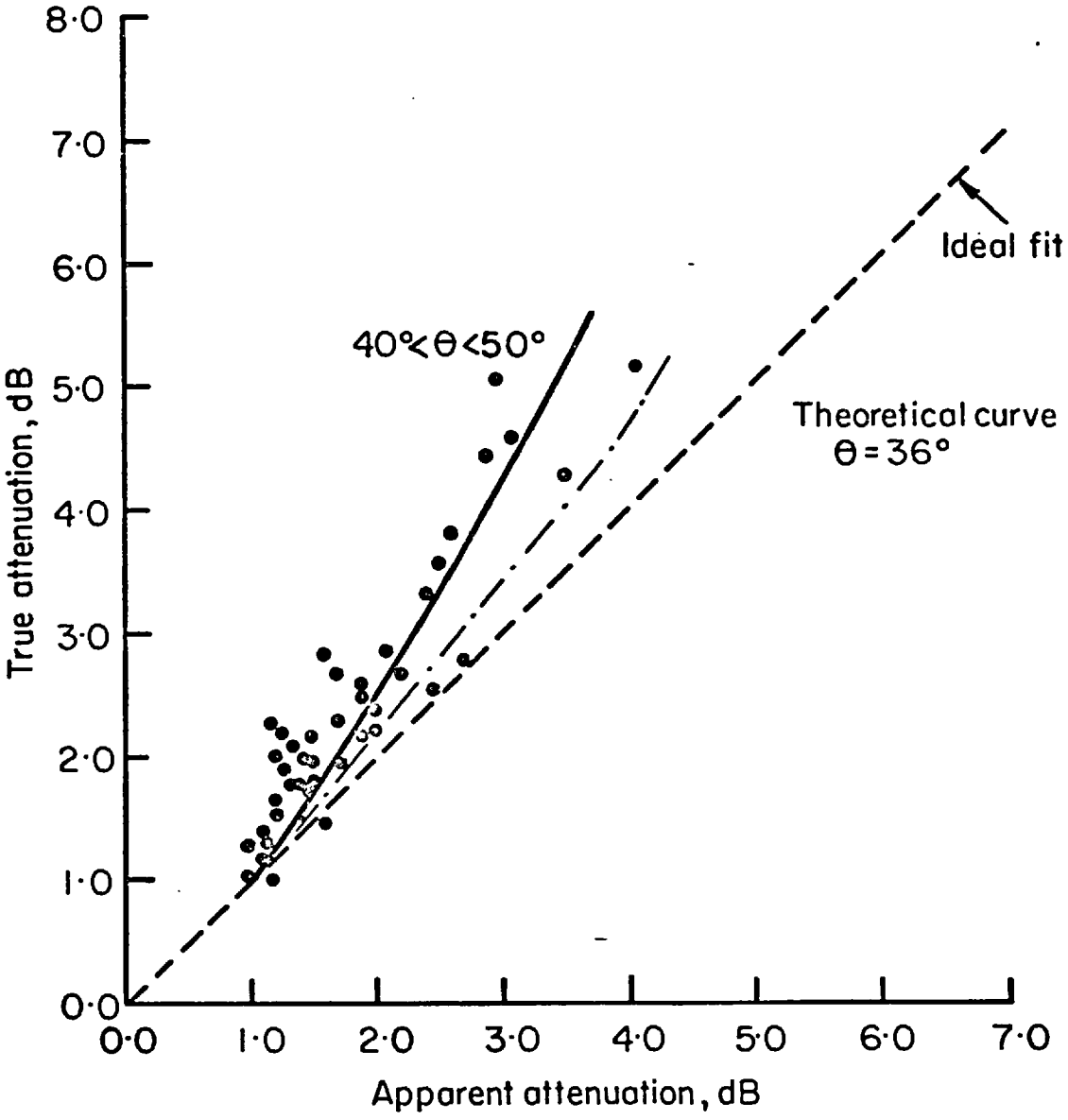


FIGURE 35

REF. NO. 2249/9 NEG. NO.

of true attenuation it is therefore expected that cumulative results of true attenuation and scattering error if used together will not differ much from year to year. This is dealt with under the section on 'seasonal variability'. We add a point of extra caution in using attenuation statistics alone for the planning of satellite communication system. The problem arises because of the variable attenuation characteristic from elevation to elevation and from year to year. Past results show that the attenuation could differ by a factor of two[3]. The object of the cumulative plot is not only to show True attenuation as a function of rainfall rate but also to emphasise how the true attenuation behaves with error due to scattering or vice versa at 37.0 GHz. This is the first time distribution curves for attenuation, error due to scattering and rain rate are plotted together. The report presents

(1) Cumulative distribution of attenuation, error due to scattering at all possible angles of elevation in conjunction with cumulative distribution of rain rate measured at the ground - Figure (36).

(2) Cumulative distribution of attenuation and error due to scattering for various ranges of elevation angle - Figure (37 and 38).

(3) Seasonal variation (Figure 39).

10.1 Cumulative Distribution of Attenuation and Scattering at all Possible Angles of Elevation

The percentage of time attenuation and error due to scattering exceed the value on the ordinate scale for the data obtained during the period (December 1974 - November 1975) is shown in Figure (36). On the same plot the cumulative distribution of instantaneous rainfall rate measured at ground is also shown. These distributions were obtained by adding individual measurements made at all possible angles of Sun-elevation in 0.5 dB step.

The cumulative results for the rainfall were obtained for the days that

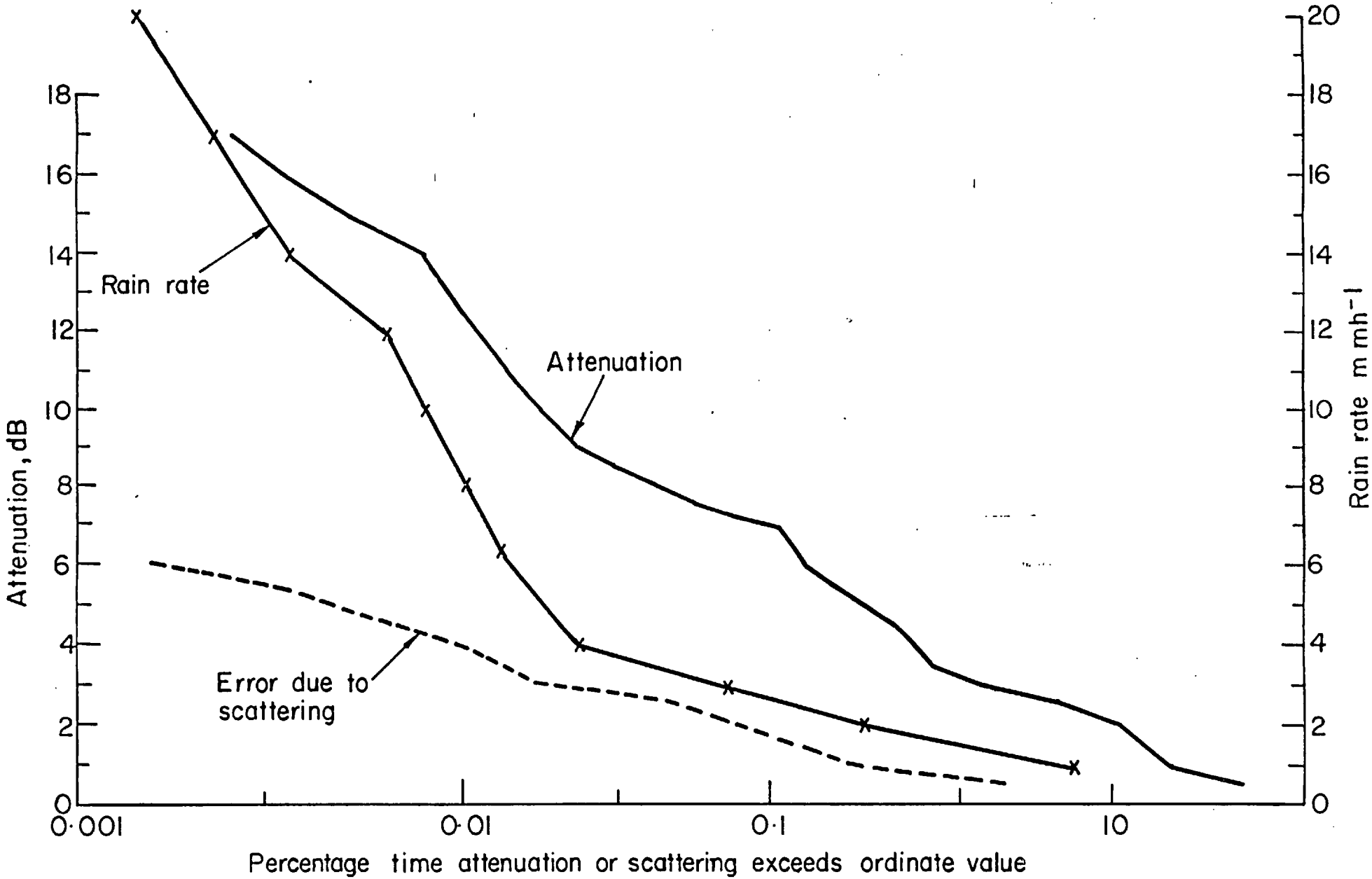


FIGURE 36

NEG NO REF NO 2249/13

Elevation Angle Degrees	Total Hours	Month	Total Hours
5-15	611.7	December	81.74
		January	103.1
15-25	649.0	February	145.8
		March	164.9
25-35	457.45	April	243.03
		May	212.5
35-45	279.5	June	287.3
		July	293.0
45-55	257.7	August	239.6
		September	223.8
55-62	159.8	October	229.7
		November	190.6

TOTAL OBSERVATION HOURS = 2415.1

Table 7

MONTH (1974-1975)	Range of Elevation Angle (Degrees)					
	Degrees 5-15	Degrees 15-25	Degrees 25-35	Degrees 35-45	Degrees 45-55	Degrees 55-62
	h	h	h	h	h	h
December	65.9	15.84				
January	59.5	43.7				
February	46.2	74.7	24.9			
March	30.6	44.2	60.6	29.5		
April	41.3	42.6	45.73	76.6	36.8	
May	33.5	32.0	35.0	34.9	49.8	27.3
June	45.2	42.1	41.1	42.3	48.9	67.7
July	46.31	43.5	43.1	45.2	55.3	59.6
August	39.6	38.9	40.65	48.33	66.9	52.0
September	58.5	81.7	82.1	1.5		
October	60.0	84.27	84.27	1.2		
November	85.1	105.5				

TOTAL MONTHLY TIME SUN IS WITHIN PARTICULAR RANGE OF ELEVATION ANGLE

Table 8

the radiometer was operational, part of the rainfall data was obtained from the G.P.O. and digitised by hand for obtaining the distribution. The total observational hours possible during the year were 2415.1 hours. The total observational hours within each month of the year and the total time the Sun is in that particular range of elevation angle is given in the accompanying tables (7 and 8).

The plot shows that for 0.01 percentage of time (corresponds to 14 mins per year), 14.0 dB of attenuation is exceeded, the corresponding error due to scattering and ground rainfall rate being 1.3 dB's and 10 mm h^{-1} respectively. Because of the limited measuring range of the radiometer in the emission mode, the values of error due to scattering above 0.01% are less reliable. As a matter of interest, we compare our results with reference (7) obtained over three years period applicable to the same observation site. According to ref. (3), 10 dB's of excess attenuation corresponds to 0.15% of time for data obtained over a range of elevation angles determined by the Sun. The present statistics show that the same percentage corresponds to 6.5 dB's of excess attenuation, 1.5 dB's of scattering error and 2.5 mm h^{-1} of ground rainfall rate. The difference can only be attributed to the fact that our statistics over one year do not include many intense storms which are included in 3 years of observation.

10.2 Cumulative Distribution of Various Elevation Angles

The data presented in Figures (37 and 38) represent the cumulative behaviour of attenuation and scattering for various ranges of elevation angle. The percentage time a particular level of attenuation or scattering is exceeded, in 0.5 dB step and 10^{o} of elevation step above 5^{o} elevation, was obtained using the computer. The maximum hours of observation were obtained in the elevation range $(15\text{-}25)^{o}$ and the minimum in the range (55-62) degrees. The maximum contribution to the attenuation and error due to scattering come from the low elevation range. As the elevation angle is increased, the α_{True} and 'S' decreases.

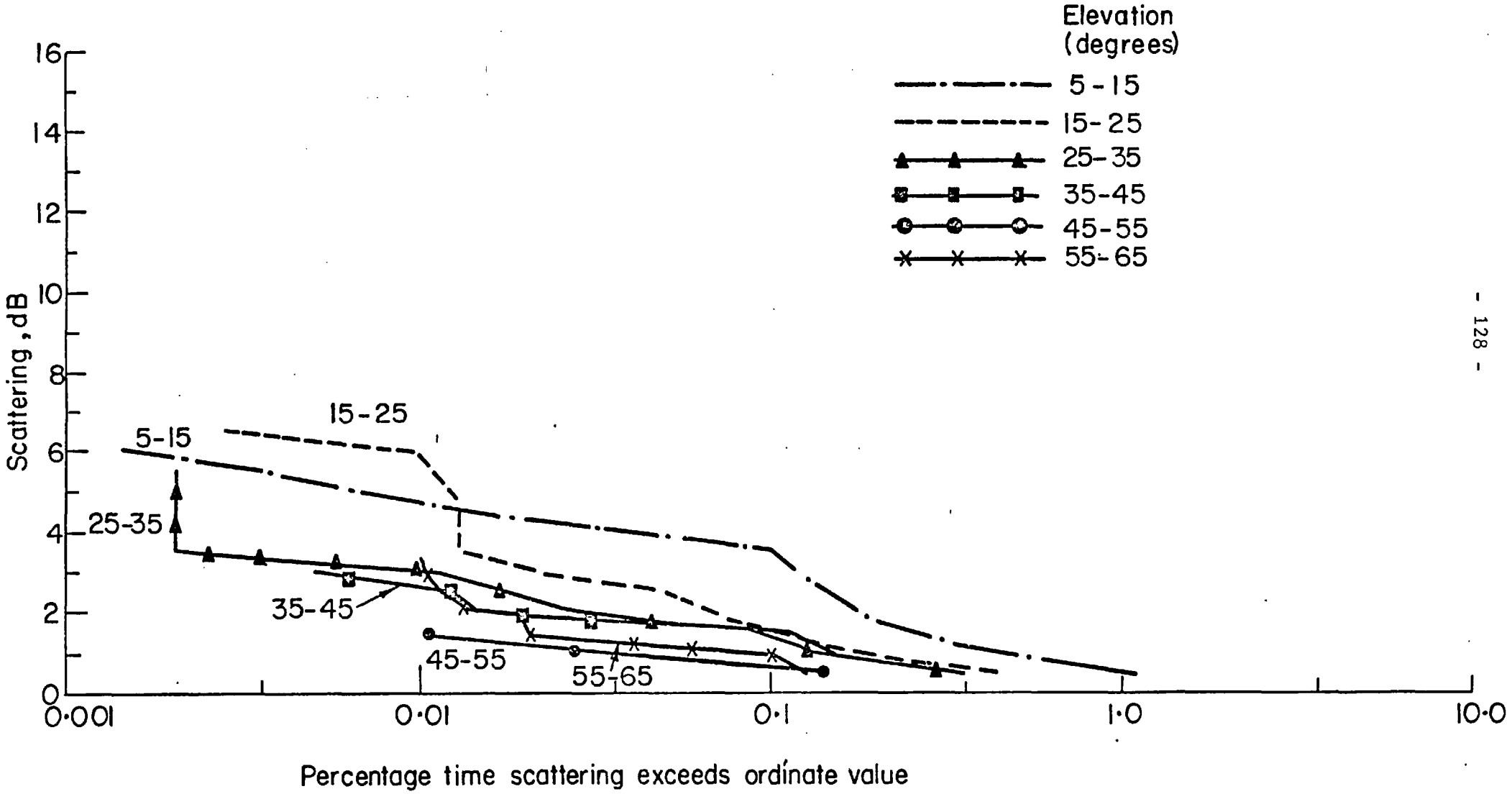

Elevation
(degrees)
5 - 15
15 - 25
25 - 35
35 - 45
45 - 55
55 - 65
Scattering , dB
16
14
12
10
8
6
4
2
0
0·001
0·01
0·1
1·0
10·0
5-15
15-25
25-35
35-45
45-55
55-65
Percentage time scattering exceeds ordinate value

FIGURE 37

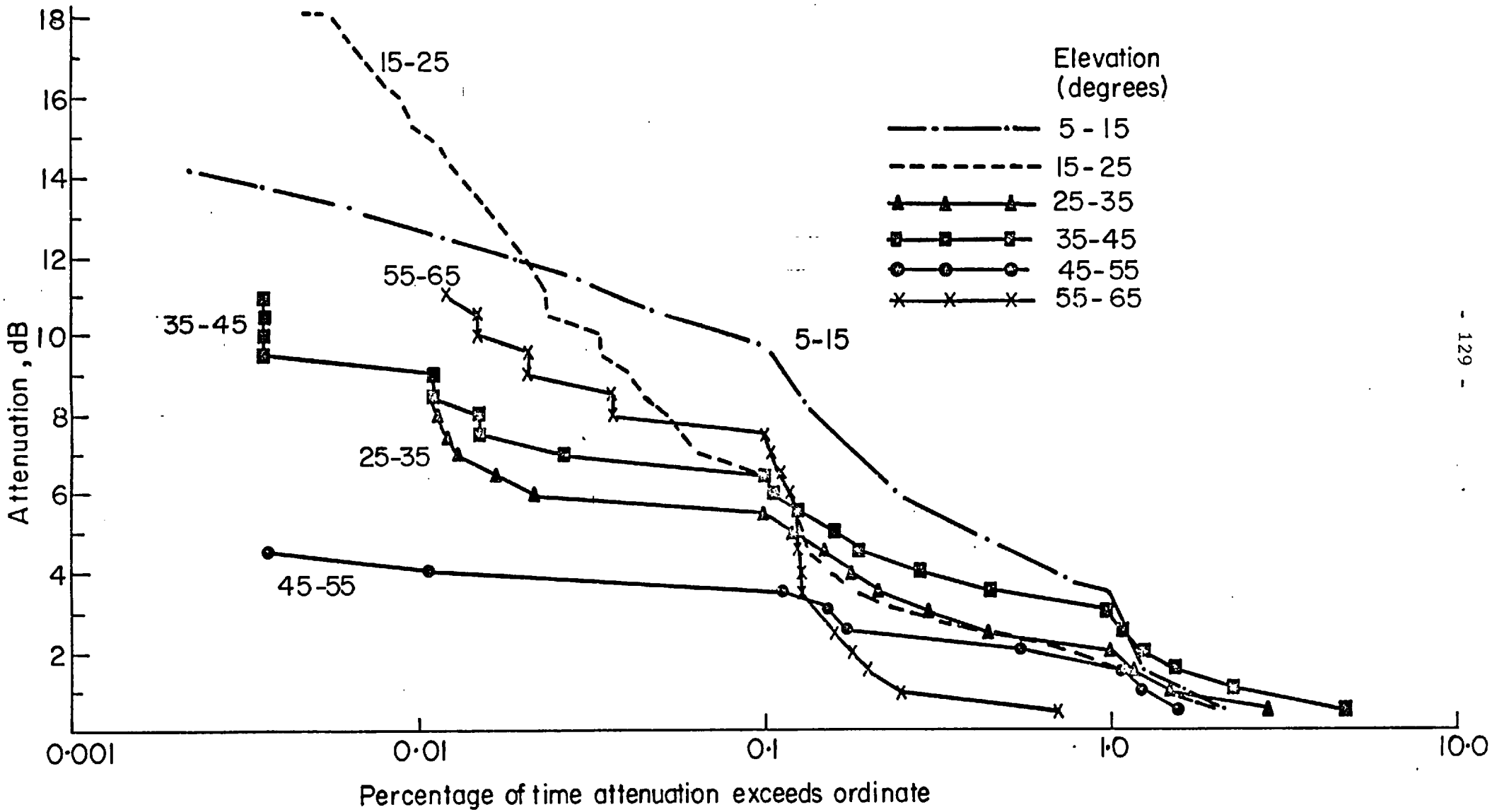

Elevation
(degrees)
5 - 15
15-25
25-35
35-45
45-55
55-65
15-25
55-65
35-45
5-15
25-35
45-55
Attenuation, dB
18
16
14
12
10
8
6
4
2
0·001
0·01
0·1
1·0
10·0
Percentage of time attenuation exceeds ordinate

FIGURE 38

The minimum and maximum contributions come from the range (45-55) degrees and (5-15) degrees, respectively. For 0.01 percentage of time, the excess attenuation in the range (15-25) degrees is almost 3.5 times that of the range (45-55) degrees. For the same percentage, the error due to scattering for the range (15-25) is 4.0 times that of the range (45-55°). This suggests that the error due to scattering is more sensitive to elevation changes as compared to excess of attenuation, therefore, the radiometers operated in emission mode are stronger function of elevation. Communication links along Earth-space path will employ geostationary satellites at fixed elevations, usually (25-35)° of elevation. Such a satellite, (from present statistics) for 0.01% of time will experience 9.1 dB's of attenuation and an error due to scattering of 3.2 dB's.

In order to show explicitly how scattered radiation behaves with elevation angle, a polar plot Fig. (39) was also obtained from the total observations. The maximum elevation one can obtain from our Sun tracking radiometer is 62.5 degrees, therefore, the polar plot is limited to the range (5-62.5°). The plot for 0.005% of time of observation shows a maximum scattering at 20° elevation and a minimum at 50° elevation. The magnitude of main and side lobes decrease for higher percentage of time of observations.

10.3 Seasonal Variability

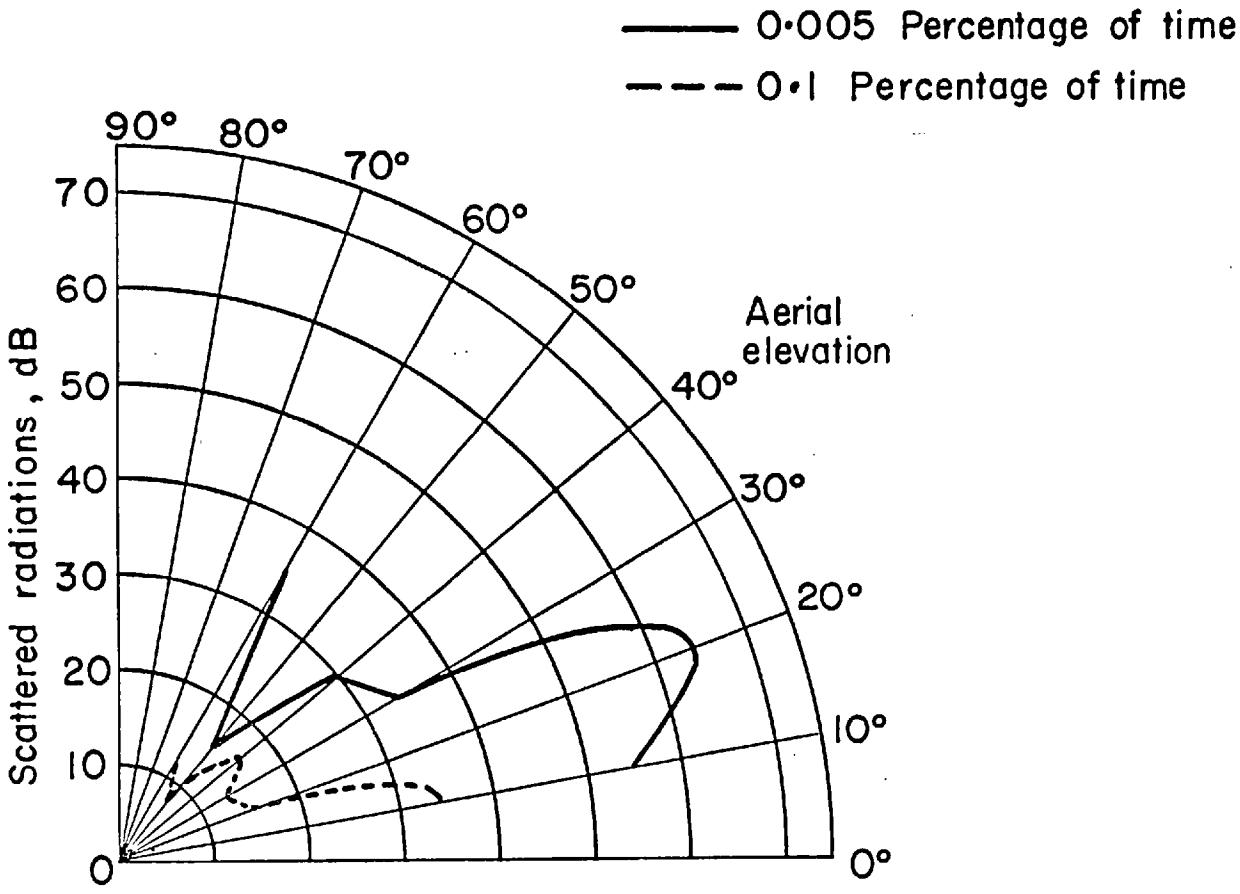
The one year of observations presented in Figure (40) is not enough to reach a conclusion regarding seasonal variability. However, we divide the whole year into three categories.

Category I December, January, February, March.

Category II April, May, June, July.

Category III August, September, October and November.

The percentage plot was obtained by dividing the total attenuation measurements into 0.5 dB steps(attenuations less than 0.5 dB were ignored) and



Polar Diagram of Scatter Radiation

FIGURE 39

NEG. NO. REF NO. 2249/2

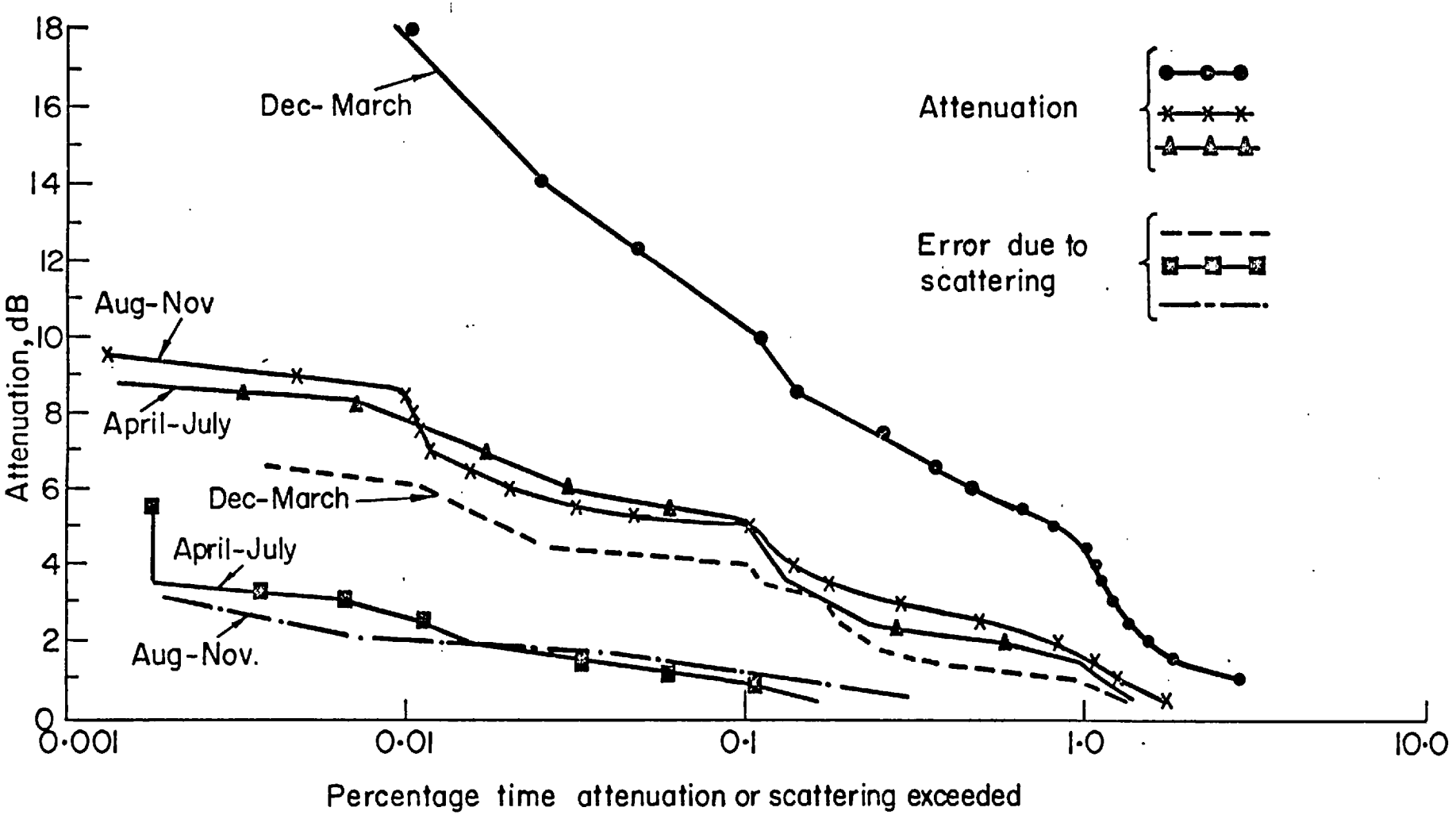

18
16
14
12
10
8
6
4
2
0
Attenuation, dB
Dec- March
Aug-Nov
April-July
Dec-March
April-July
Aug-Nov.
Attenuation
Error due to scattering
0·001
0·01
0·1
1·0
10·0
Percentage time attenuation or scattering exceeded

FIGURE 40

0.05% of Time	Excess Att. dB	Error due to Scattering	Ratio K
Cat. I	13.7	4.4 dB	3.1
Cat. II	5.7	1.7	3.2
Cat.III	6.2	1.9	3.2

Table 9

the total observational hours during months under the various categories. It is interesting to note that the seasonal variability can be avoided by simultaneously using cumulative distribution curve of excess attenuation and error due to scattering. The excess of attenuation and error due to scattering for 0.05% of time is tabulated for the three different categories in Table 9 above. The ratio K of excess of attenuation to error due to scattering is constant with a mean value of 3.17, the maximum variation about the mean being 2.2%.

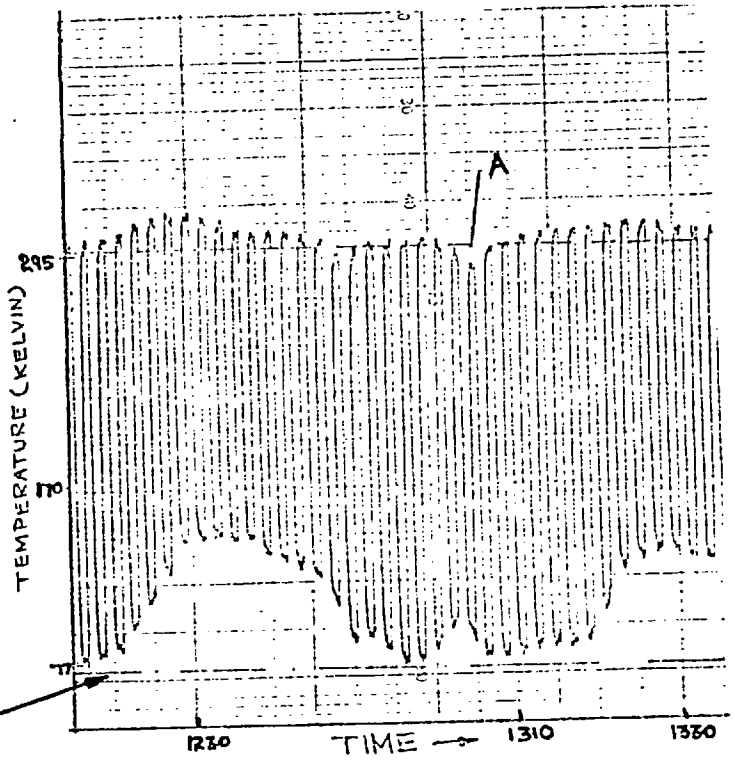
11. EXPERIMENTAL RESULTS ON POLARISATION EFFECTS BY RAIN

The cross-polarised radiometer in fixed angle thermal emission mode and in 'nodding mode' was operated during the months (February-April) and (May-July) respectively. Unfortunately because of an exceptionally dry summer not many recordings of intense storms in the nodding mode could be made and as such it is difficult to predict the long-term effect of polarised scattering on passive radiometer measurements.

Figure (41) shows the recording of the cross-polarised radiometer at a fixed elevation angle of 35.0 degrees during a rainy period on 30th April 1976. A maximum difference of 21.0 K between vertical and horizontal aerial temperatures is recorded for a horizontal aerial temperature of 180.0 K. These correspond

Clear Day Polarisation Difference _ _ _ _ _

Clear Day Reference for Horizontal polarizations ___ . ___ . ___



Clear Day Level

Recording of Cross-Polarised Radiometer on 30th April, 1976

FIGURE 41

to horizontal and vertical attenuations of 4.69 and 3.79 dB's at 273.0 K of mean atmospheric temperature. In general, horizontal aerial temperature has been greater than vertical aerial temperature but there were occasions when the reverse was noticed such as at A of Figure (41). The vertical aerial temperature at A is greater than the horizontal by almost 10.0 K and it can be explained either in terms of the canting angle of the falling drops or by a large portion of the scattered energy being transferred to the vertical beam by its surroundings. We rule out the latter possibility because the two beams are practically examining the same portion of rain, as well as being continually switched. Moreover it is more likely that a greater portion of energy will be scattered into the horizontal beam if thermally scattered energy is polarised. Therefore, we are left with the concept of canting angle. The study of the low horizontal attenuation, although corresponding difference of attenuation between polarisations is large, suggests that column of the rain must have tilted due to prevailing heavy wind giving rise to higher vertical apparent brightness temperature.

The horizontal recorded output during 1 min of intense rain observation could vary by almost 12.0 K. The overall experimental data obtained in this mode are plotted in Figure((42). A linear regression fit to the experimental points, by the least-squares method, gives the following equation

$$T_{AH} = 1.08\ T_{AV} \tag{91}$$

Goodness of fit to the experimental point is 0.95. The result shows that horizontal attenuation of 6.0 decibels corresponds to 5.17 decibels of vertical attenuation i.e. a difference of 0.83 dB's between polarisations. The experimental data points are also compared with dashed theoretical curve (Figure 42) and are in agreement for vertical brightness temperature less than 200 K. Unfortunately, we could not have observations greater than 200.0 K due to lack of intense storms during observational period so they could not be compared with theory. The

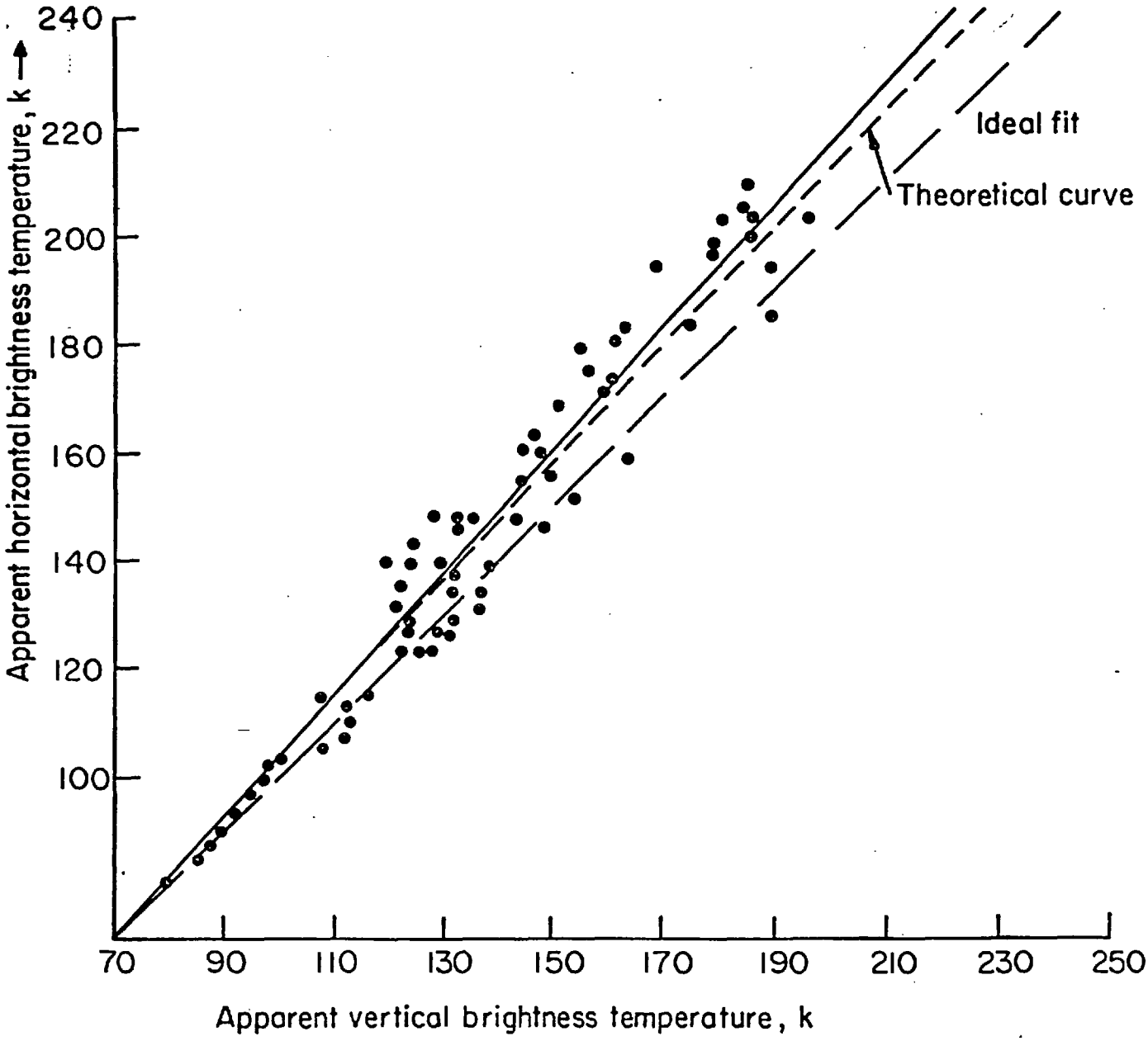


FIGURE 42

Ref. NO 2249/25 Neg. NO.

theoretical curve was evaluated for rain depth 3 kms, horizontal extent 10 kms and aerial elevation 18.0 degrees. Theoretically, vertical attenuation of 5.17 dB corresponds to horizontal attenuation of 5.72 dB's i.e. a difference of 0.55 dB.

The recorded output in Figure (41) also shows that in contrast to an actual transmitting-receiving system the radiometer is sluggish in studying the minute details of polarisation by rain. Therefore, a much smaller integration time constant of the radiometer is required.

The cross-polarised radiometer was operated in nodding mode for several months and few storms were recorded. Visual comparison of recorded output of polarised recievers during periods of rain shows that minute fluctuations in the horizontal Sun beam are greater in amplitude compared to vertical Sun beam. This is because of the horizontally polarised aerial being more subjected to scattered energy provided we assume that the system noise is the same in both receivers.

The experimental data for the observed months is plotted in Figure (43) and the best fit to the horizontal and vertical data is shown by continuous and dashed line. For 10.0 dB of apparent attenuation true horizontal and vertical attenuations are 13.5 dBs and 11.5 dBs respectively. The results were evaluated using Aerological records with the mean atmospheric temperature of the medium and varying from 273.0-280 K they correspond to aerial elevation ranges (10-35) degrees. Therefore for a meaningful comparison between theory and experiment more results need recording, especially at lower aerial elevations. The theoretical calculations based on model discussed in Section (2) give horizontal and vertical attenuations of 14.7 and 13.5 dB's respectively for 10.0 dB of apparent attenuation for aerial elevation less than 18.0 degrees.

12. FURTHER WORK

The equipment essentially requires development whereby all the three experiments can be performed simultaneously. Although it is possible to obtain measurements using the nodding cross-polarised radiometer, discussed in Section (5.1),

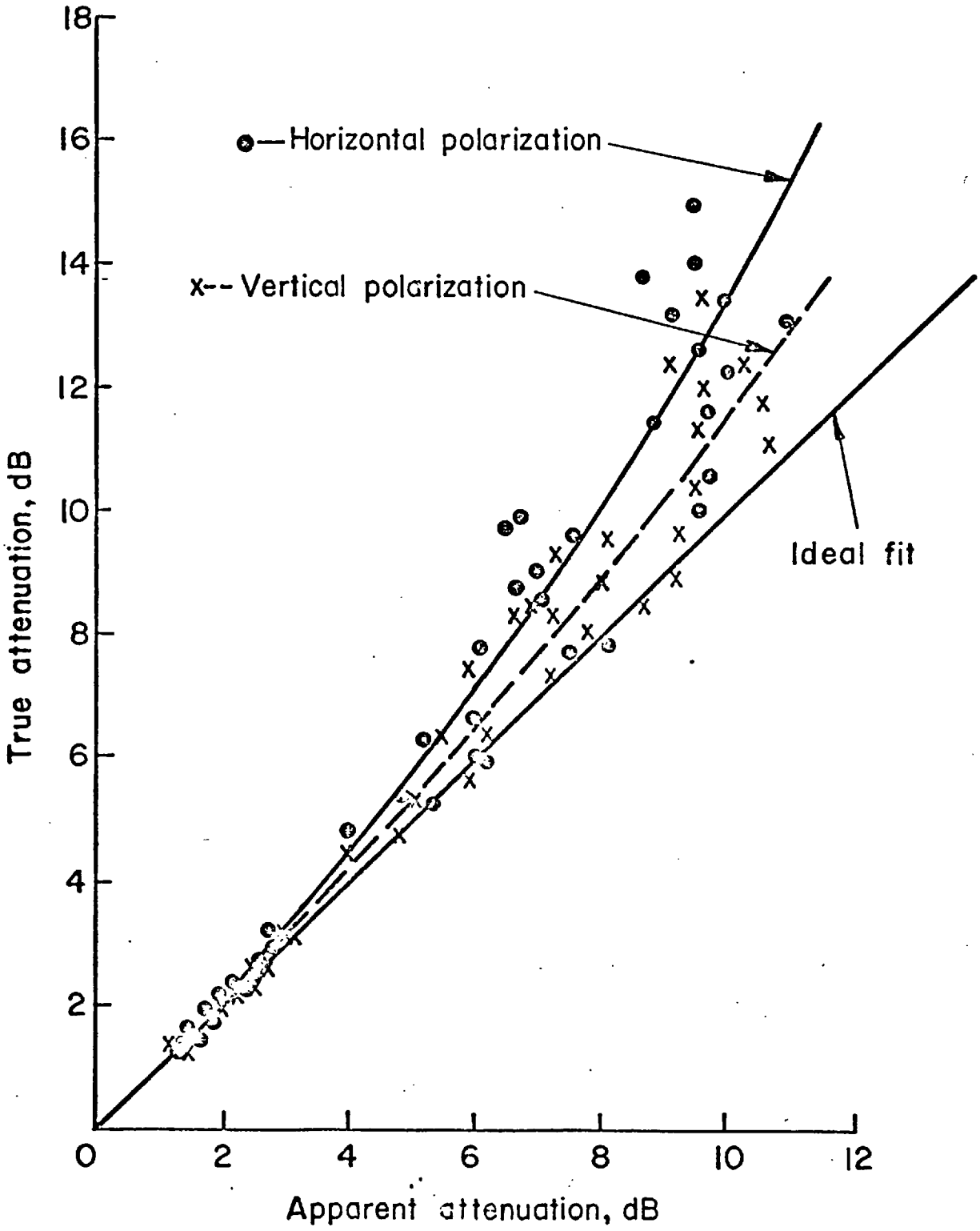


FIGURE 43

NEG. NO. REF NO 2249/31

the rather large nodding time taken by the nodder and the continuous change of radiation pattern of the polarised Sun-tracking aerial make it an unwelcome choice during intense stormy conditions.

A modified receiver in which the above conditions can be partially met would also monitor the tracking properly. It is proposed that the present microwave receiver should have a cassegrain antenna with a conical feed. The sub-reflector can be made to spin at audio frequency about its central axis in such a way that during off-set the beam is sufficiently off the Sun, and therefore the only contribution is from the atmosphere. The aerial feed is next connected to an orthomode transducer followed by a tapered mode transition. This would enable us to have dual linear polarisation simultaneously. Polarised incoming radiations then can be compared to that of the load using the Ferrite devices and receiving system discussed earlier. The polarised Sun and sky signals can be extracted using switching techniques. The output then can be fed to a four-channel data logger for final analysis by computer. The technique not only reduces feed waveguide attenuations, but hour angle and declination motors can be easily programmed to take into account any lateral-shift due to tracking error. The receiver must be modified to be capable of distinguishing 1.0 K change at much lower than present time constants of 1.0 second. This is important if the radiometric study is to be extended for studying the minute details of polarisation behaviour of thermally emitted energy and relating it to an actual transmitting-receiving system.

The calculations are done for zero canted raindrops and therefore it will be interesting to extend it for non-zero canting angles bringing about cross-polarisation effects.

It is not known by how many Kelvins the polarised aerial temperature is in error due to the thin water layer formed over the feeds. Work in this direction should be undertaken, and is discussed briefly in Appendix (A2).

There are times when our observational periods overlap with ATS-6 observations taken at Appleton Laboratory. The experiment is being conducted to study rain attenuation and polarisation effects of rain on transmitted linear polarisation (25^{o} to vertical) at 30 GHz. Various elevations data obtained using nodding and cross-polarised radiometer can be normalized* to ATS-6 observational elevation of 25.0^{o} and results compared to actual transmitting-receiving system. By doing this not only the effectiveness of the radiometer for studying rain attenuation can be proved but also an indirect method for studying polarisation effects of rain can be exploited. However one has to be extra-cautious in normalizing results to any elevation angle using the cosecant law. The factors which particularly affect the normalization are

(a) The angular dependence of the scattering and attenuation caused by a single heavy storm.

(b) The spatial distribution of the storm.

---

* The attenuation measured at some angle of elevation 'e' can be scaled to some other elevation 'V' by the 'Cosec Law' if the attenuating media is horizontally uniform.

Attenuation (dB) at V = Attenuation (dB) at e x $\frac{\sin e}{\sin V}$.

Elevation at which atten. was measured	$F=\frac{\sin e}{\sin V}$ for scaling to 'e'	
	10^{o}	40^{o}
90^{o}	5.76	1.56
60^{o}	4.99	1.35
45^{o}	4.07	1.10
30^{o}	2.88	0.77
10^{o}	1.00	0.27

13. CONCLUSIONS

The microwave radiometer technique has been applied to study the effect of scattering and polarisation by rain on millimetre wavelength propagation with reasonable success. It has been shown experimentally that the results obtained by a passive radiometer are grossly underestimated if the above effects are neglected, especially if condensed water droplets are present within the radio path.

Modified theoretical results were obtained using distorted raindrops based on Zavody's theory. This in turn led us to the polarisation behaviour of the emitted and scattered energy. Theoretically, at 37 GHz, the attenuation deduced from sky temperature measurements neglecting scattering and polarisation can be low for horizontal and vertical polarisations by as much as 3.7 dB and 2.5 dB in 10 dB respectively. It is also shown that thermally emitted energy (including scattering by rain and ground) by rain is polarised, and a difference of 0.55 dB in 5.7 dB of horizontal attenuation is possible. The polarisation behaviour of emitted and scattered radiation from ground becomes important for heavy rain and low aerial elevation.

One year's observations, using a single-beam horizontally polarised radiometer, verified the importance of scattering; and the measurements show that error even greater than 3.6 dB due to scattering can occur. The error increases with increasing attenuation and the measured results are given by the following relation,

$$S \text{ dB} = K(\alpha_{true} \text{ dB})^{c}$$

where $K = 0.11$ and $c = 1.51$

Results obtained correspond to a number of varying conditions of weather and include a number of intense stormy periods. The theory grossly underestimates (almost by a factor of 3) the error due to wet snow and therefore requires modification.

The statistical analysis show that for 0.01% of the time (corresponding to 14 minutes of observations in a year) 14.0 dB of attenuation is exceeded. The corresponding error due to scattering and rainfall rate is 4.3 dBs and 10 mm h^{-1} respectively. The error is more critical of elevation changes as compared to true attenuations. For 0.01 percentage of time the error due to scattering and the attenuation for the elevation range (15-25) is respectively 4.0 and 3.5 times greater than that of the range (45-55) degrees.

The higher error above 7.0 decibels for both summer and winter showers is explained in terms of the non-isotropic nature of thermal emission and scattering. A cross-polarised radiometer has been built and the observations at fixed angle during periods of showers confirm that energy emitted (including scattering) by rain is polarised, and the experimental results broadly agree with theoretical calculations. The cross-polarised radiometer is completely electronic and does not have any mechanical moveable parts, and the problem of contribution due to thin water-film formed over feeds during intense period of rain should be investigated further.

A few storms recorded by the nodding cross-polarised radiometer show that the error due to scattering is not the same for the two polarisations, and is higher for horizontally polarised passive-radiometers. Because of the limited number of storms recorded during an exceptionally dry summer the long-term assessment and comparison with theory has been made difficult. The experimental results give horizontal and vertical error of 3.5 dB and 1.5 dB in 10 dB in deducing attenuation from sky temperature.

Further work requires more recordings of intense storms using a lower time constant (< 1 sec) cross-polarised radiometer capable of measuring 1.0 K input change, and of the contribution to two polarisations from the water film formed over the feeds.

ACKNOWLEDGEMENTS

The author wishes to thank the Director of the S.R.C. Appleton Laboratory for providing facilities to carry out this research programme.

He wishes to thank his Supervisors, Dr. J. A. Lane and Dr. R. H. Clarke for their guidance and understanding throughout this work, and Dr. D. L. Croom, Dr. P. G. Davies and the Staff of Appleton Laboratory. Particular thanks are due to Dr. Croom and Mr. Zavody for much valuable discussion.

Thanks are also due to Government of India (Ministry of Education) for financial support.

BIBLIOGRAPHY

1. Tillotson, L. C., "A model of a domestic satellite communication system", B.S.T.J., 47 No. 10, pp. 2111-2137, 1968.

2. "Telecommunication aspects on frequencies between 10 and 100 GHz", NATO-AGARD Conference, Proc., No. 107, September, 1972.

3. Davies, P. G., "Radiometer measurements of atmospheric attenuation at 19 and 37 GHz along Sun-Earth paths", Proc., I.E.E. Vol. 120, No. 2, February 1973.

4. Chandrasekhar, S., "Radiative transfer" Dover Publication, N.Y.

5. Zavody, A. M., "Effect of scattering by rain on radiometer measurements at millimetre wavelengths" Proceeding I.E.E., Vol. 121, No. 4, April 1974.

6. Coates, R. J., "Measurement of solar radiation and atmospheric attenuation at 71.0 GHz" Proc. I.E.E., 1958, No. 6, pp. 122-126.

7. Davies, P. G., "Radiometric studies of atmospheric attenuation of solar emission at 19 GHz", Proc., I.E.E., Vol. 118, No. 6, June 1971.

8. Joss, J., Thomas, J. C. and Walg, E. A., "The accuracy of daily rainfall measurements by radar", Proceedings of the American Meteorological Societies 13th Radar Meteorology Conference, Montreal, 1968.

9. Bray, W. J., "Basic communication sciences", Proc. Roy. Soc. 1968, 308, pp. 183-198.

10. Wilson, W. R. "Sun tracker measurements of attenuation by rain at 16 and 30 GHz" B.S.T.J. Vol. 48 Nos. May-June, 1969, pp. 1383-1403.

11. Gordon-Smith, A. C. and Gibbons, C. J. "Simple overall absolute calibrator for mm wavelength for horn-radiometer measurement" Electronic Letters, 1972, p. 59.

12. Jonas, P. R., "Private communication".

13. Kraus, J. D., "Radio Astronomy".

14. Davies, P. G. and Lane, J. A., "Statistic of tropospheric attenuation at 19.0 GHz from observation of solar noise", Electronic Letters, 1970, pp. 522-523.

15. Dicke, R. M., Beringer, R., Khyl, R. L. and Vane, A. D., "Atmospheric absorption measurements with a microwave radiometer", Physocs, Rev., 1946, 70, pp. 340-348.

16. Harvules, G. G. and Brown, W. E., "The simultaneous investigation of attenuation and emission by the Earth's atmosphere at wavelengths 4 cm - 8 mm", J. Geophysc. Res., 1969, 74, pp. 4453-4471.

17. Croom, D. L., "Sun as a broad band source for tropospheric attenuation measurements at millimetre wavelengths", Proc. I.E.E., 1973, 120 (10) pp. 1200-1206.

18. Zavody, A. M., "Effect of scattering on radiometers measurements of attenuation in rain", Electron. Letters, 1973, 9, pp. 328-329.

19. Medhurst, R. G., "Rainfall attenuation of centimetre waves. Comparison of theory and measurement", I.E.E.E. Trans. AP., Vol. 13, pp. 550-564, July, 1965.

20. Crane, R. K., "Microwave scattering parameters for New England rain", M.I.T. Lincoln Lab., Lexington, Mass., Tech. Rep. TR426, October 1966.

21. Jones, D. M. A., "The shape of raidrops" Ibid, 1959, 16, pp. 504-510.

22. Hulst, Van de, "Light scattering by small particles".

23. Pruppacher, H. R. and Pitter, R. L., "A semi-empirical determination of the shape of cloud and raindrops", J. Atmos. Sci. Vol. 28, pp. 86-94.

24. Semplak, R. A., "Effect of raindrops on attenuation at 30.9 GHz". Radio Science, Vol. 5, No. 3, pp. 559-564, March 1970.

25. Oguchi, T., "Attenuation of electromagnetic waves due to rain with distorted raindrops", Journal of Radio Research Labs. (Tokyo) Part I, Vol. 7, pp. 467-485, September 1960 Part II, Vol. 11, pp. 18-44, January, 1967.

26. Saunders, M. J., "Cross polarisation at 18 and 30 GHz due to rain", I.E.E.E. Trans. AP-19, pp. 273-277, March 1971.

27. Setzer, D. E., "Anisotropic scattering due to rain", Ibid, 1971, 50, pp. 861-868.

28. Setzer, D. E., "Computed transmission through rain at microwave frequencies", B.S.T.J., 1970, 49, pp. 1873-1892.

29. Brooks, G. E. P., "The English climate", English University Press, 1954, pp. 41.

30. Blanchard, D. C. "The behaviour of water drops at terminal velocity in air", Trans. Amer. Geophys. Union, 31, 6, 836-842, 1950.

31. Magono, C., "On the shape of water drops falling in stagnant air", J. Meteor., 11, 1, 77-79, 1954.

32. Nelson, A. R. and Gokhale, N. R. "Oscillation frequencies of freely suspended water drops", J. Geophys. Res. 77, 15, 2724-2727, 1972.

33. Kumai, M. and Itagaki, K. "Shape and fall velocity of raindrops", J. Meteor. Soc. Japan, 32, 3, 69-76, 1954.

34. Jones, D. M. A., "The shape of raindrops" J. Meteor, 16, 504-510, 1959.

35. Pruppacher, H. R. and Beard, K. V., "A wind tunnel investigation of the internal circulation and shape of water drops falling at terminal velocity in air", Quat. J. R. Met. Soc., 96, 408, 247-256, 1970.

36. Spilhaus, A. F. "Raindrop size, shape and falling speed", J. Meteor., 5, 108-110, 1948.

37. Imai, I., "On the velocity of falling raindrops", J. Meteor. Soc. Japan, 28, 113-118, 1950.

38. Oguchi, T., "Scattering properties of oblate raindrops and cross-polarisation of radio waves due to rain; calculations at 19.3 and 34.8 GHz", J. Radio. Res. Labs. (Tokyo), 20, 102, 79-118, 1973.

39. Morrison, J. A. and Chu, T. S., "Peturbation calculation of rain induced differential attenuation and differential phase shift at microwave frequencies", B.S.T.J., 52, 10, 1907-1913, 1973.

40. Morrison, J. A. and Cross, M. J. "Scattering of a plane electromagnetic wave by axisymmetric raindrops", B.S.T.J., 53, 6, 955-1019, 1974.

41. Oguchi, T. and Hosoya, Y., "Scattering properties of oblate raindrops and cross-polarisation of radiowaves due to rain (Part II), calculation at microwave and millimetre wave region", J. Radio Res. Labs. (Tokyo) 21, 105, 191-259, 1974.

42. Humphrey, W. J., "Physics of the air".

43. Stutzman, L. W. and Ko, H. C., "On the measurement of antenna beamwidth using extraterrestrial radio sources", I.E.E.E. Trans. AP Vol. AP-22, No. 3, pp. 493-495, May 1974.

44. Watson, P. A., "Working group Report III of the IUGRM Colloquium, Microphysics of hydrometeors and polarisation", Journal de Recherches Atmospheriques (Proceedings of IUGRM Colloquium), 8, 1-2, 477-484, 1974.

45. Conway, R. G., "Measurement of radio sources at centimetre wavelengths", Nature, Vol. 199, p. 1177, September 21, 1963.

46. Gibbins, C. J., Gordon-Smith, A. C. and Croom, D. L., "Atmospheric emission measurements at 85 to 118 GHz", Plant. Space Sci., 1975, Vol. 23, pp. 61-73.

47. Wulfesberg, K. N. and Altshuler, E. E., "Rain attenuation at 15 and 35 GHz", Trans. I.E.E.E. AP. Vol. AP 20, No. 2, March 1972.

48. Croom, D. L., Davies, P. G. and Powell, R. J., "Anomalies in attenuation and emission by rain at 37 GHz", Electronics Letters, Vol. 8, March 1972.

49. Strickland, I. J., "The measurements of slant path attenuation using radar, radiometers and a satellite beacon", in I.U.C.R.M. Colloquium Proc., pp. 111.6-1 to 111.6-9, October 1973.

APPENDIX A1

OPERATING CHARACTERISTICS OF 37.0 GHz NODDING RADIOMETER

(Horizontally Polarised)

	CHARACTERISTICS	37.0 GHz RADIOMETER
(a)	ANTENNA	Parabolic direct feed type
	Diameter	18 inches
	Gain	39.5 dB
	Antenna efficiency i.e.	
	Gain 3 dB/main beam gain	~ 0.86
	Beam width	1.49^{o}
	Side lobes	Below 40 dB and are not measurable with the system.
(b)	WAVE GUIDE SWITCH	
	Type	4 port, cross-polarised
	Isolation	> 62 dB
	V.S.W.R.	1.04 : 1
	Insertion Loss	< 0.05 dB
(c)	MODULATOR	
	Type	Electronic modulator (Ferrite switch)
	Mod. Frequency	Sq. modulation 3.0 kHz
	Isolation between on and off position	> 30 dB

	CHARACTERISTICS	37.0 GHz RADIOMETER
(d)	ISOLATOR	
	Isolation	> 31 dB
	Loss	~ 0.4 dB
	V.S.W.R.	~ 1.1
	H.P.B.W.	1.0 GHz
(e)	IF AMPLIFIER	
	Bandwidth ($25^{\circ}C$)	(80-400) MHz
(f)	LOCAL OSCILLATOR	Gunn-diode
	Frequency	37.0 GHz
	Power Output	~ 30 MW
	Power Temp Coefficient	- 0.02 dB/C°
	Freq Temp.Coefficient	~ - 1.0 MHz/C°
(g)	SENSITIVITY OF RADIOMETER $= K \frac{T_{SYS}}{\sqrt{BT}}$	1.0 K
(h)	TIME CONSTANT	1 sec
(i)	NOISE TEMP. OF SYSTEM INCLUDING TRANSMISSION LINES (Assuming ΔT Fluctuation in Atmosphere = 0)	8950 K
(j)	AMBIENT TEMP. OF RADIOMETER (IF Mixer etc.)	$22^{\circ}C \pm 1^{\circ}C$
(k)	NOICE FIGURE OF THE RADIOMETER	14.96 dB
(l)	BEAM OVERLAPPING WHEN ANTENNA IS 3° AWAY	No overlapping
(m)	NODDING TIME	1 Minute
(n)	NORMALISED GAIN CHANGE OF RADIOMETER WITH TEMPERATURE	$0.003^{\circ}C^{-1}$

APPENDIX A2

Before the receiving system was finally commissioned a number of checks on its performance were made.

(1) Radiation Pattern (Beam width measurement)

(2) Gain Stability

(3) Noise temperature of systems

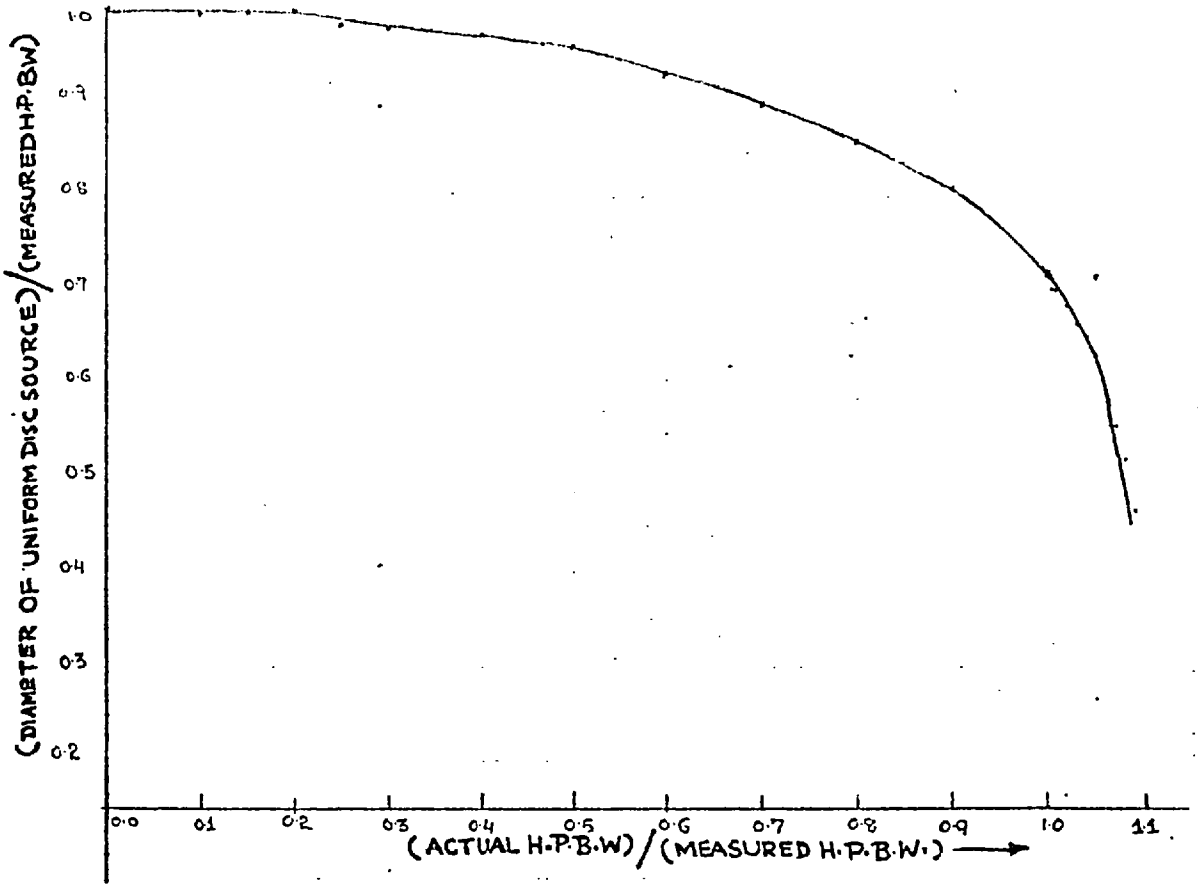
(4) Sensitivity

(5) Effect of water layer over feeds.

Radiation Pattern

Because of non-availability of an anechoic chamber it was easier to consider the Sun as a point source and the radiation pattern of the overall aerial was measured. The aerial was pointed ahead of the Sun and locked in position, the radiometer output was recorded continuously as the Earth's rotation carried the Sun through the antenna beam. After the Sun was past the antenna and the sky radiations have been recorded for a few minutes, 40 dB of attenuation was inserted with the attenuator to give zero reference reading. The receiver was next calibrated using (i) Noise tube, Liquid nitrogen and ambient temperature. After the gain check, the receiver was switched back to the antenna, the antenna was switched ahead of the Sun, locked and the sequence was repeated. The half power beam width for the single beam is 1.49 degrees.

It is to be noted that beam width measured by the method is an overestimated value because the Sun is not a point source (the Sun subtends an angle of 0.5^{o}). The error arising in the measured pattern because of convolution of the Sun's radiation pattern is treated by H.C.KO (43). Two dimensional convolution integral was reduced to a single integral through the use of two dimensional Fourier transform and the integral is evaluated. The measured antenna pattern is recovered by finding the inverse transformation. The results are presented in Figure (44) and are applicable for the measured antenna HPBW θM, the source diameter W and


(DIAMETER OF UNIFORM DISC SOURCE)/(MEASURED H.P.B.W)
1·0
0·9
0·8
0·7
0·6
0·5
0·4
0·3
0·2
0·0
0·1
0·2
0·3
0·4
0·5
0·6
0·7
0·8
0·9
1·0
1·1
(ACTUAL H.P.B.W)/(MEASURED H.P.B.W.)

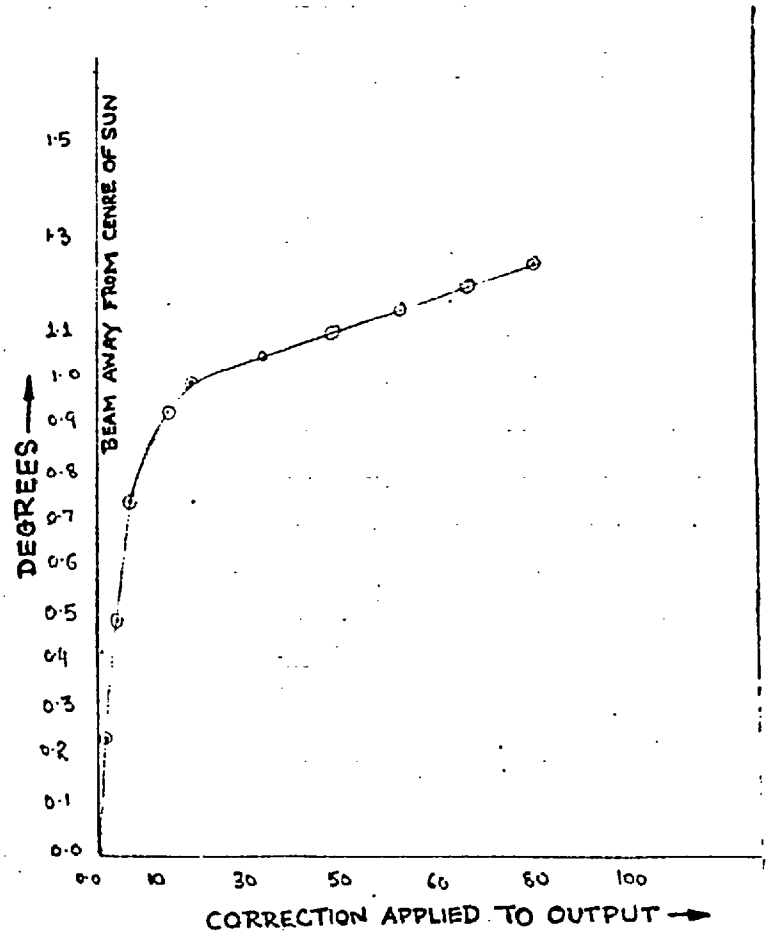

DEGREES
BEAM AWAY FROM CENRE OF SUN
1·5
1·3
1·1
1·0
0·9
0·8
0·7
0·6
0·5
0·4
0·3
0·2
0·1
0·0
0·0
10
30
50
60
80
100
CORRECTION APPLIED TO OUTPUT

FIGURE 44

and true antenna HPBW θA.

A similar technique was applied to obtain and correct the HPBW of the vertical and horizontal polarised aerial. The corresponding beam width is 1.17 and 1.27 degrees respectively.

GAIN STABILITY

To give some idea of the short term gain stability the receiver was run for a period of 48 hours with a noise tube replacing the aerial feed, the output being monitored on a chart recorder. After an initial warming up period of about 6 hours the gain did not vary by more $\pm$ 1.0 percent, of which an unknown proportion may be attributed to low noise amplifier shift.

Because the whole receiver was to be placed just behind the aerial being carried by the mount in open air it was important to determine the effect of changes in ambient temperature. The complete mixer and IF pre-amplifier assembly was put in a temperature controlled chamber, and its gain measured over a temperature range of + 15.0^{o}C to + 39.0^{o}C. The result of the test reveals a change in gain relative to that at 15.0^{o}C of about 0.3 percent/^{o}C.

SENSITIVITY

No attempt was made to increase the system gain to permit resolution of very small changes in output, but it was noticed that a change in input temperature of 1.0^{o}K was easily detectable with a time constant of 1.0 seconds.

$$\text{Sensitivity of Radiometer} = K \frac{T_{SYS}}{\sqrt{BC}}$$

RECEIVER NOISE TEMPERATURE

The antenna, transmission line and receiver contribute to the overall system temperature. In a Dicke radiometer the receiver noise temperature do not appear in the final results provided the gain and noise temperature of the receiver remain the same in the switched positions. The receiver noise temperature of a Dicke

radiometer can only be calculated indirectly by measuring the sensitivity and known predetection bandwidth and integration time.

We consider a case in which the receiver is switched between two ports, one connected to a load and the other to a vertically polarised aerial. The receiver will be essential cross-polarised if the port is connected to a horizontally polarised aerial instead of to the load.

When the receiver is connected to the antenna, T_A, the d.c. output voltage is

$$V_A = C_1 \, G_{HF} \, k(T_A + T_{SYS}) \, \Delta V_{HF} \tag{92}$$

when the receiver is connected to the comparison load, T_C, the dc output voltage is

$$V_C = C_1 \, G_{HF} \, k(T_C + T_{SYS}) \, \Delta V_{HF} \tag{93}$$

where

G = constant

G_{HF} = predetection power gain

ΔV_{HF} = Predetection bandwidth.

Hence, the output voltage from the multiplier is

$$V = C_2(V_A - V_C) = C_1 C_2 \, G_{HF} \, k(T_A - T_C) \, \Delta V_{HF} \tag{94}$$

For $T_A = T_{AH}$ and $T_C = T_{AV}$

$$V = C_1 \, C_2 \, G_{HF} \, k(T_{AH} - T_{AV}) \, \Delta V_{HF} \tag{95}$$

Therefore the output voltage is proportional to the difference of polarised aerial temperatures. For $T_{AH} = T_{AV}$, the receiver sensitivity of the cross-polarised receiver is determined by the system noise only, and the same is true of a single beam Dicke radiometer for $T_A = T_C$. By measuring sensitivity the following equation is used to obtain the value of receiver temperature due to the overall system

$$T_{min} = \frac{k\ T_{SYS}}{\sqrt{\Delta V_{HF} \tau}}$$

For a Dicke receiver k = 2, because the signal is connected to the receiver half of the time only. ΔT_{min} was 1.0 K, τ = 1 sec and ΔV_{HF} = 320 MHz

$$T_{SYS} = 8950\ K$$

The noise figure 'F' for a two port net-work

$$T_{SYS} = (F - 1)T_0$$

$$F_{DB} = 10\ Log_{10}F = 14.65\ dB.$$

EFFECT OF WATER LAYER OVER THE FEEDS

The performance of the aerial is degraded during periods of intense rain because of a thin layer of water being formed at the end of feeds. The thin film can act as an absorbing material being placed in front of the feeds. This can not only obstruct the incoming radiation but can also contribute its own noise temperature to two polarisations. Wilson[10] has measured an attenuation of 3.0 dB for water fall rate of 15 inches/hour at 30 GHz.

To protect the antenna performance during intense periods of rain, feeds were covered with a plastic hood of diameter 6 cms and depth 3 cms. The plastic hood was coated with a thin layer of Teflon because Teflon is a strong water repellant. We try to determine how this panel reacts to different rain intensities in the most ideal situation.

We assume

(1) The rain falls perpendicularly on the curved surface of the cylindrical hood.

(2) The thin layer of water formed in front of the feed is uniform.

(3) The effect of gravity does not distort the thin film.

If 'D' is the diameter of the cylindrical hood in metres then the amount of rain coming down is confined to the area given by $\frac{1}{4}.\pi.D^2$. If it rains P_{mm}/hr, the water falls off at the equator of the cylinder and the total water collected per running metre i.e. θ CC/min/metre is given by

$$\frac{\frac{1}{4}\pi D^2.P \times 10^{-3}\ 10^6}{60\ \pi D} = 4.17\ P.D \qquad (96)$$

The thickness dw of the water layer is related to diameter and rain intensity by the following relation,(60)

$$dw = C(\tfrac{1}{2}\ D\ P)^{7/12}$$

where

C = constant

For $D = 0.06$ metres

$$dw = 0.0007 \times P^{7/12} \qquad (97)$$

From equation (a) and (b)

$$dw = 0.0007 \times \left(\frac{\theta}{4.17\ D}\right)^{7/12} \text{mm} \qquad (98)$$

The above relation suggests that thickness of the water layer can be measured by measuring the water fall off at the equator. 100 mm h^{-1} rain can give a layer of approximately 0.01 mm thickness for the present cylindrical hood over the feeds.

A simple experiment can be done by spraying water from a fine nozzle on the radiometer focussed 'on' Sun and 'off' Sun. Both the readings can be combined to give excess of attenuation. A similar experiment for a cross-polarised radiometer can also be done and the difference of attenuation gives an indication of the polarised contribution due to the layer of water.

APPENDIX A3

ELECTRONIC ON/OFF ATTENUATOR DRIVER

TRG Ferrite switch was used as an ON/OFF attenuator in the vertical beam of the cross-polarised radiometer. The maximum attenuations introduced in the path, are 30.0 dB and 0.4 dB during 'ON current mode' and 'OFF current mode' respectively.

The electronic Driver circuit is basically a modified Smith* adjustable oscillator formed by T_{R1} and T_{R2}, Figure (45). At test point (A) the output waveform is a square wave between + 2.5 V and + 12.5 V. T_{R3} and T_{R4} convert the D.C. level and amplitude to give a square wave between 0 and + 6 volt (point B) which is used to switch T_{R5}. The switching time is determined by capacitors C. A switching time of the order of 1 minute was obtained.

When T_{R5} is switched on, a drop of about 5 volts is established across V_{R3}, and a fraction of this is fed to the base of T_{R6}, which with T_{R7} and R_1 forms a conventional constant current source. (The magnitude of the current can be carried by V_{R3}).

When T_{R5} is switched off, the base of T_{R6} goes to + 15 V and the current source is thus switched off. Since the output is a current driver, the output voltage is defined by the load. A ten ohm resistor is included in series with the load to facilitate monitoring of the output current on an oscilloscope. The circuit will not be damaged if the load is removed and replaced either by an open circuit or a short circuit.

---

* [Smith, H. J. Multivibrator CCTS, Electronic Engineering, 35, 46 (1963)]

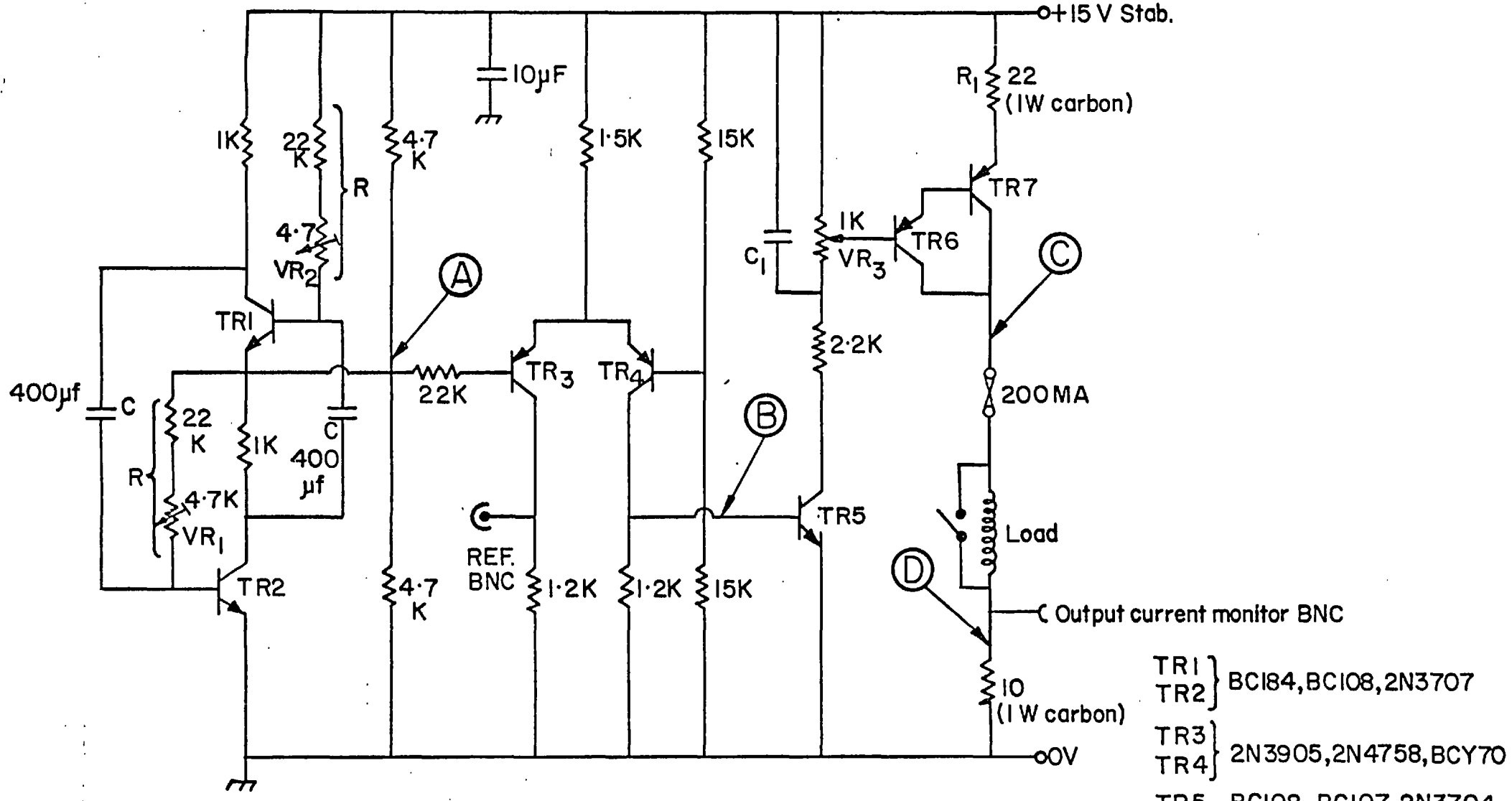

+15 V Stab.
10µF
1K
22 K
R
4·7 K
1·5K
15K
R1 22 (1W carbon)
TR7
4·7 VR2
TR6
1K VR3
C1
A
C
TR1
2·2K
400µf C
22 K
1K
R
4·7K VR1
C 400 µf
22K
TR3
TR4
200MA
B
TR5
Load
REF. BNC
1·2K
1·2K
15K
4·7 K
TR2
D
Output current monitor BNC
10 (1W carbon)
0V
TR1 TR2 BC184, BC108, 2N3707
TR3 TR4 2N3905, 2N4758, BCY70
TR5 BC108, BC107, 2N3704
TR6 2N3702 2N3906
*TR7 MJE 371

FIGURE 45

APPENDIX A4

DESIGN REQUIREMENTS OF MOUNTING AND DRIVE

The mechanical requirements of the mounting are summarised as follows :-

(i) It must provide stable and rigid support to the reflector and feed assembly.

(ii) It must be able to achieve the required pointing accuracy.

(iii) It must be easily set to any desired position.

(iv) It must have enough driving torque to be capable of carrying microwave receiver and aerial together.

(v) All necessary power inputs and signal outputs to be routed without hindrance to the drive and must be proof against adversities such as bad weather and strong winds.

All the above requirements are easy to achieve by careful design of the mount. The most important of all is the accuracy with which the wheel is divided into equal parts and also how accurately pulses are supplied by the pulse generator from the control chassis. The design of hour angle wheel and pulse rate to motor is derived as follows.

Hour Angle wheel is divided so that 1.0 rev. corresponds to 1.0 degree i.e. 0.0006944 rev. per min.

Therefore, worm is being driven at 360 x 0.0006944 = 0.25 rev. per min. Since there is a reduction of 1.250, therefore, the stepper shaft is being driven at 0.25 x 250 rev. per min.

Now the stepper shaft rotates at 7.5^{o} per pulse or 1.0 rev. per 48.0 pulse. Pulse rate to motor = 0.25 x 250 x 480 = 3000 ppm = 50 pulses per sec.

APPENDIX A5

DERIVATION OF ELEVATION FROM LOCAL TIME

The aerial elevation of the Sun-tracking radiometer was obtained from the Sun's co-ordinate and the Local Time. The various equations involved are as follows.

Latitude of Slough = $51^{o}29.3'$

Longitude of Slough = $00^{o}33.8' = \varphi L$

UT = G.M.T. (hours)

ET = Equation of Time (hours)

S = Declination of Sun in degrees

H = Hour angle

From spherical astronomy[13], we can write

$$\text{Sin } E = [\text{Sin } S \text{ Sin } \varphi + \cos S \cos \varphi \cos H] \qquad (99)$$

where

E = Elevation of the Sun

$$H = \frac{(UT - 12.0 + ET) \times 60 \times \pi}{4 \times 180} - \frac{\varphi L \times \pi}{60 \times 180}$$

or

$$H = \left\{0.2618 \ [UT - 12.0 + ET] - 0.00983\right\} \qquad (100)$$

The above value of hour angle is applicable to Slough only and the corresponding elevation of the Sun and therefore of the aerial can be obtained by substituting values of S, φ and H in equation (99).